***IN VIVO* GENOME-WIDE ANALYSES OF THE *DROSOPHILA* P53**

TRANSCRIPTIONAL NETWORK

APPROVED BY SUPERVISORY COMMITTEE

John M. Abrams, Ph.D. (Mentor)

Beatriz Fontoura, Ph.D. (Chair)

Helmut Kramer, Ph.D.

W. Lee Kraus, Ph.D.

DEDICATION

To my mother Glória,

the first geneticist to inspire me and

the strongest woman I know.

ACKNOWLEDGEMENTS

I want to thank my mentor Dr. John M. Abrams, your guidance was pivotal for my growth as a scientist. My committee members Drs. Beatriz Fontoura, Lee Kraus and Helmut Kramer, and previous member Dr. Michael Buszczak for providing their unique perspectives to my projects and enriching my training. Former Abrams lab member, Dr. Nichole Link, who was a bench mentor to me. Abrams lab members, who have supported me in times of frustration and shared my enthusiasm in science; collaboration with Dr. Amanda E. Jones was essential for bioinformatics analyses of high throughput datasets.

I also want to thank my parents. Glória and Roberto, who have taught me to think critically and supported my choices. My partner in life Brad, you make me a better person.

IN VIVO GENOME-WIDE ANALYSES OF THE *DROSOPHILA* P53 TRANSCRIPTIONAL NETWORK

by

PAULA S KURTZ

DISSERTATION

Presented to the Faculty of the Graduate School of Biomedical Sciences

The University of Texas Southwestern Medical Center at Dallas

In Partial Fulfillment of the Requirements

For the Degree of

DOCTOR OF PHILOSOPHY

The University of Texas Southwestern Medical Center at Dallas

Dallas, Texas

August, 2017

***IN VIVO* GENOME-WIDE ANALYSES OF THE *DROSOPHILA* P53 TRANSCRIPTIONAL NETWORK**

Publication No._____

PAULA S. KURTZ, Ph.D.

The University of Texas Southwestern Medical Center at Dallas, Graduation Year

Supervising Professor: John M. Abrams, Ph.D.

p53 is the most commonly mutated gene in human cancers. Despite decades of p53 studies we do not fully understand how p53 suppresses tumors. Similar to human p53, the *Drosophila* counterpart is a transcription factor that can respond to genotoxic stress and promote adaptive responses at the cellular level. Our lab has leveraged the powerful genetics of *Drosophila* to study p53 functions *in vivo*. In the context of the developing fly, p53 robustly activates important apoptotic genes in response to DNA damage to promote cell death. In the embryo model, we discovered an important p53 enhancer that forms chromatin contacts through long genomic distances and enables p53 to activate various genes. How p53 programs are adapted in different cellular contexts is poorly understood. In my dissertation work I examined two layers of p53

regulation, long-range enhancer looping and p53 DNA occupancy. To further examine enhancer looping, I exploited the established embryo model and the well characterized p53 *reaper* enhancer. At the single cell resolution, I demonstrated that the p53 enhancer can contact multiple targets simultaneously; however these multigenic complexes appear in low frequency. I also have preliminary genome-wide data suggesting in embryos this p53 enhancer contacts additional p53 targets. In addition, through genome-scale analyses I dissected novel p53 programs in a postmitotic model (the *Drosophila* head). Interestingly, postmitotic p53 programs are distinct from networks described in developing cells. I found that the canonical p53 apoptotic program is unresponsive in *Drosophila* heads, establishing this system as an ideal *in vivo* model to study alternate functions of p53. To determine how p53 differential programs are specified, I tested two distinct mechanisms for tissue specific target activation, p53 enhancer looping and DNA binding. Interestingly, I observed no change in enhancer looping to cell death targets in heads. However, I did detect loss of p53 enhancer binding. Lastly, I integrated genome-wide analyses of p53 DNA occupancy and transcriptional control in embryos and heads. Interestingly, I found that at the genome-scale p53 binding landscapes poorly correlate with nearby transcriptional effects, indicating that p53 enhancers could be generally acting through long distances.

TABLE OF CONTENTS

PRIOR PUBLICATIONS

Kurtz, P, Jones, A.E., Abrams, J.M. Dynamics of the p53 regulatory network in *Drosophila* postmitotic tissue. *In preparation*

Tiwari, B., **Kurtz, P**., Jones, A.E., Wylie, A., Abrams, J.M. (2017). Retrotransposons mimic germ plasm determinants to promote transgenerational inheritance. *Current Biology*. *(In review)*

D'Brot, A., **Kurtz, P**., Regan, E., Jakubowski, B., & Abrams, J. M. (2016). A platform for interrogating cancer-associated p53 alleles. *Oncogene*. doi: 10.1038/onc.2016.48

Wylie, A., Jones, A. E., D'Brot, A., Lu, W. J., **Kurtz, P**., Moran, J. V., . . . Abrams, J. M. (2016). p53 genes function to restrain mobile elements. *Genes Dev*, 30(1), 64-77. doi: 10.1101/gad.266098.115

Link, N., **Kurtz, P.**, O'Neal, M., Garcia-Hughes, G., & Abrams, J. M. (2013). A p53 enhancer region regulates target genes through chromatin conformations in *cis* and in *trans*. *Genes Dev*, 27(22), 2433-2438. doi: 10.1101/gad.225565.113

LIST OF FIGURES

LIST OF TABLES

LIST OF APPENDICES

LIST OF DEFINITIONS

3C-	chromosome conformation capture
4C-	circular chromosome conformation capture
AO-	Acridine orange
BAC-	Bacterial artificial chromosome
Bp-	base pair
ChIP-	chromatin immunoprecipitation
CTD-	carboxyl terminal domain
DBD-	DNA binding domain
eGFP-	enhanced Green fluorescence protein
eRIPD-	Embryo RIPD
FISH-	fluorescence in situ hybridization
GO-	Gene Ontology
GOrilla-	Gene Ontology enRIchment anaLysis and visuaLizAtion tool
hRIPD-	Head RIPD
IHC-	immunohistochemistry
IR-	Ionizing radiation
Kb-	Kilo bases
kDa-	Kilo Daltons
mCh-	mCherry
MiMIC-	Minos-Mediated Integration Cassette
NHEJ-	Non-homologous end joining
OD-	oligomerization domain
$p53RE^{rpr-}$	p53 response element upstream of *rpr*
PCR-	Polymerase chain reaction
PRD-	Proline rich domain
RIPD-	Radiation induced p53 dependent
RMCE-	Recombination-Mediated Cassette Exchange

RT-ddPCR- Reverse transcriptase droplet digital PCR

TAD- Transactivation domain

TSS - Transcription start site

WT- Wildtype

CHAPTER ONE

THE P53 TUMOR SUPPRESSOR PROTEIN

TP53 is the most frequently mutated gene in human cancers. Consistent with its pivotal role in tumor suppression programs, p53 loss leads to cancer growths with complete penetrance in mice (Donehower et al., 1992; Jacks et al., 1994; Kenzelmann Broz & Attardi, 2010). Furthermore, in humans, inherited p53 mutations underlie the familial cancer syndrome, Li-Fraumeni syndrome (F. P. Li et al., 1988; Olivier et al., 2003). Despite almost 40 years of research since p53's discovery (DeLeo et al., 1979; Kress, May, Cassingena, & May, 1979; Lane & Crawford, 1979; Linzer & Levine, 1979; Melero, Stitt, Mangel, & Carroll, 1979), and close to 30 years since its characterization as a tumor suppressor (Baker et al., 1989; Finlay, Hinds, & Levine, 1989), the precise mechanisms by which p53 confers tumor suppression are not completely understood.

p53 was discovered in mouse cells transformed with SV40 virus, several groups detected a ~53 kDa protein that was co-precipitated with SV40 T antigen (Kress et al., 1979; Lane & Crawford, 1979; Linzer & Levine, 1979; Melero et al., 1979). Shortly after its discovery, it became evident that p53 was important in tumorigenesis; p53 protein levels were incredibly high in malignant transformed cells (50-100 fold). Furthermore, this upregulation occurred in cells transformed by various stimuli, from many tissue-types and species (Jay et al., 1980; V. Rotter, 1983; V Rotter, Witte, Coffman, & Baltimore, 1980). This was also an early indication that p53 genes were evolutionarily conserved throughout species.

Initially p53 was mistakenly classified as an oncogene, based on observations that p53 and known oncogenes cooperated to transform normal embryonic cells (Eliyahu, Raz, Gruss, Givol, & Oren, 1984; Parada, Land, Weinberg, Wolf, & Rotter, 1984). Furthermore, overexpression of cDNA cloned p53 led to cellular immortalization *in vitro*

(Jenkins, Rudge, & Currie, 1984). However, observations that cancer cell lines from mice and humans contained rearrangements in the p53 gene began to call into question whether p53 was inducing tumorigenesis (Masuda, Miller, Koeffler, Battifora, & Cline, 1987; Mowat, Cheng, Kimura, Bernstein, & Benchimol, 1985). Then, it was determined that transformed cell lines used to make the first p53 cDNA clones contained mutant p53 (Hinds, Finlay, & Levine, 1989; Pennica et al., 1984).

Several studies contributed to switching the status of p53 from oncogene to tumor suppressor. First, p53 was identified as the gene residing in the short arm of chromosome 17, a region commonly deleted in various kinds of human cancers (Baker et al., 1989). Then, while surveying cancers containing allelic deletions of chromosome 17, Nigro et al. determined that the retained copy of p53 in these cancers were mutant, usually containing missense mutations in four hotspots (Nigro et al., 1989). Lastly, Finlay et al. demonstrated that p53 suppresses transformation of rat embryonic fibroblasts (Finlay et al., 1989).

p53 was then characterized as a transcription factor that coordinates cellular adaptive responses to stress such as apoptosis, cell cycle arrest and senescence (Vousden & Prives, 2009). Under non-stressed conditions, p53 protein levels are kept low by physical association to negative regulators such as the E3 ubiquitin ligase MDM2. After stimuli post-translational modifications activate p53, disrupting the interaction with negative regulators (Momand, Zambetti, Olson, George, & Levine, 1992; Oliner et al., 1993; Shieh, Ikeda, Taya, & Prives, 1997). Interestingly, p53 binds the MDM2 gene to promote an autoregulatory feedback loop (Wu, Bayle, Olson, & Levine, 1993).

The p53 protein contains five key regulatory domains (from N to C terminus): transactivation domain (TAD), proline rich domain (PRD), DNA binding domain, oligomerization domain (OD) and the carboxy-terminal domain (CTD) (Joerger & Fersht, 2010). Interaction between the TAD domain and transcriptional coactivators p300/CBP as well as components of the transcription machinery confer gene regulation by p53 (Lill, Grossman, Ginsberg, DeCaprio, & Livingston, 1997; Teufel, Freund, Bycroft, & Fersht, 2007; Thut, Chen, Klemm, & Tjian, 1995). In addition, p53 protein-protein

interactions can be mediated through the PRD (Olsson, Manzl, Strasser, & Villunger, 2007). The DNA binding domain, which is the most mutated domain in cancers, enables sequence specific binding to two decameric motifs (half sites) of the sequence RRRCWWGYYY (R=A,G; W= A,T; Y=C,T) separated by 0-13 base pairs (el-Deiry, Kern, Pietenpol, Kinzler, & Vogelstein, 1992; Funk, Pak, Karas, Wright, & Shay, 1992). The OD allows the formation of the active p53 tetramers (Weinberg, Veprintsev, & Fersht, 2004) and the CTD contains nuclear localization signals (Olsson et al., 2007). Post-translational modifications have been detected in all domains with varying effects in protein stability and function (Gu & Zhu, 2012; Olsson et al., 2007). These post-translational modifications can be specified by many proteins, including Check Point Kinase 1 and Check Point Kinase 2 (Lakin & Jackson, 1999).

Initially, the findings that p53 can regulate genes to promote apoptosis, cell cycle arrest and senescence, seemed to explain its potent ability to suppress tumor growth. However, as the p53 targets which conferred each of these adaptive responses were identified and tested in mouse models, it became clear that although these pathways contribute to tumor suppression, they could not completely account for aggressive cancer phenotypes observed upon loss of p53 (Bieging, Mello, & Attardi, 2014). In addition, two independent studies examined phenotypes in mice that had combined loss of apoptosis, cell cycle arrest and senescence (T. Li et al., 2012; Valente et al., 2013). In one model, a p53 variant was generated containing mutations in three lysine residues; these animals had compromised apoptosis, cell cycle arrest and senescence. Surprisingly, these mice did not phenocopy early onset lethal cancers observed by loss of p53 (T. Li et al., 2012). Likewise, knock out mice lacking three pivotal p53 targets p21, Puma, and Noxa efficiently suppress the typical tumor development detected in p53 null animals, despite defective apoptosis, cell cycle arrest and senescence (Valente et al., 2013). Therefore, unappreciated functions of p53 are crucial in tumor suppression. Interestingly, in these two studies, it was noted that p53-mediated DNA repair and p53-controlled metabolism were functional in the mutant mice (T. Li et al., 2012; Valente et al., 2013).

One hypothesis is that specific p53 programs are important for tumor suppression in different cellular contexts. p53 has been reported to respond to a wide variety of stresses, from DNA damage, to hypoxia, starvation, telomere attrition, etc (Bieging et al., 2014). It has been observed that different kinds of stimuli activate specific p53 regulatory networks (Zhao et al., 2000). In addition, tissue-specific p53 responses have also been reported (Fei, Bernhard, & El-Deiry, 2002). Furthermore, it has been clear from many reports that regulation of p53 context specific effects relies on multiple layers of control; DNA binding specificity, post translation modifications, cofactors, enhancer epigenetics and looping, to name a few (Andrysik, Kim, Tan, & Espinosa, 2013; Gomes & Espinosa, 2010; Knights et al., 2006; Lidor Nili et al., 2010; Link, Kurtz, O'Neal, Garcia-Hughes, & Abrams, 2013; Mellert & Espinosa, 2013; Melo et al., 2013; Oda et al., 2000).

Most studies of p53 are performed in cell culture systems; this has limited our ability to fully understand how distinct cellular environments modulate p53 adaptive responses. In my dissertation work, I establish an *in vivo* model to study tissue-specific functions of p53, while uncovering novel p53 target genes. Using *in vivo* models, I also examine p53 DNA binding landscapes as a mediator of context specific p53 responses. Lastly, I explored how p53 enhancer chromatin looping transmits regulatory signal to p53 targets.

CHAPTER TWO

IN VIVO GENOME-WIDE ANALYSES OF THE *DROSOPHILA* P53 REGULATORY NETWORK IN POST MITOTIC TISSUE

INTRODUCTION

Early studies suggested that p53's ability to direct different cell fates can be uncoupled from one another. For example, $p53^{175P}$ point mutation abolishes apoptotic responses but has no effect in p53 mediated cell cycle arrest (Rowan et al., 1996). Furthermore, recent studies identified three key lysine residues that are crucial for p53 mediated apoptosis, cell cycle arrest and senescence. Strikingly, the combined abrogation of these three pathways, through p53 lysine mutations or combined knock out of p53 downstream targets, is not sufficient to recapitulate early onset tumor formation found in p53 null mice (T. Li et al., 2012; Valente et al., 2013). Together these observations challenged conventional models and established that non-canonical p53 programs are crucial for tumor suppression.

Mutations in the DNA binding domain of p53 are the most frequent allele class found in human cancers, suggesting that p53 DNA binding and associated gene regulation is important in tumor suppression (Hainaut & Hollstein, 2000). It is very clear that p53 can activate cellular fates such as apoptosis and cell cycle arrest through transcriptional activation of upstream effectors of those pathways (Valente et al., 2013). Numerous groups have characterized p53 networks through DNA binding and gene expression at the genome-scale and, in a comprehensive literature survey, I found a total of 31 peer-reviewed studies (K. C. Akdemir et al., 2014; Bandele, Wang, Campbell, Pittman, & Bell, 2011; Botcheva & McCorkle, 2014; Botcheva, McCorkle, McCombie, Dunn, & Anderson, 2011; Ceribelli, Alcalay, Vigano, & Mantovani, 2006; G. S. Chang et al., 2014; Idogawa et al., 2014; Janky et al., 2014; Jen & Cheung, 2005; Kenzelmann Broz

et al., 2013; Kirschner et al., 2015; K. H. Lee et al., 2010; M. Li et al., 2012; Y. Li et al., 2013; McDade et al., 2014; Menendez et al., 2013; Merlo et al., 2014; Nikulenkov et al., 2012; Rashi-Elkeles et al., 2014; Sammons, Zhu, Drake, & Berger, 2015; Sanchez et al., 2014; Schlereth et al., 2013; Shaked et al., 2008; Smeenk et al., 2011; Smeenk et al., 2008; Su et al., 2015; Tonelli et al., 2015; Wei et al., 2006; Younger, Kenzelmann-Broz, Jung, Attardi, & Rinn, 2015; Zeron-Medina et al., 2013). Many of these studies were performed in immortalized/cancer cell lines, despite findings that p53 can be activated by a variety of stresses, including extended cell culture (Botcheva et al., 2011; Shaked et al., 2008). Furthermore, as with the lesson learned in the discovery of p53, transformed cell lines often have a disabled or deranged allele of p53 (Millau, Mai, Bastien, & Drouin, 2010). Finally, only two studies included p53 null counterparts as controls for biologic validation of binding sites (Kenzelmann Broz et al., 2013; Tonelli et al., 2015). Although we have gained crucial insights in general p53 biology, these models are not ideal to learn context-specific p53 functions. Recently, three *in vivo* genome-wide p53 network studies have been published (Y. Li et al., 2013; Merlo et al., 2014; Tonelli et al., 2015). Only one of these investigates the stress-response p53 programs in different cellular contexts (B cells and non-B cells from spleen) (Tonelli et al., 2015). Understanding how p53 instructs context-specific cell fates can shed light into how different cancers escape tumor suppression programs. *In vivo* models to study these tissue specific p53 functions are lacking.

Drosophila has proven to be a powerful *in vivo* model for investigating p53 biology (Link et al., 2013; W. J. Lu, Chapo, Roig, & Abrams, 2010; Lunardi et al., 2010; Merlo et al., 2014; Wylie et al., 2016). In addition to the array of genetic tools which allow for rigorous *in vivo* studies, p53 function is highly conserved in *Drosophila*, and it is the only gene of its family present in the fly genome (no p63 or p73) (Belyi & Levine, 2009; W. J. Lu, Amatruda, & Abrams, 2009; Sutcliffe & Brehm, 2004). In this chapter, I characterize p53 programs in a postmitotic tissue, the *Drosophila* head. This context likely exerts distinct pressures to modulate p53 adaptive responses, given the specialized environment necessary to retain postmitotic neurons in a terminally differentiated non-dividing state. Corroborating this idea, recent studies have found that p53 prevents

neurodegeneration in postmitotic neurons (Merlo et al., 2014). Interestingly, I found that canonical apoptotic networks are unresponsive in postmitotic tissue and distinct programs are activated. To understand how p53 promotes alternate programs I mapped genome-wide p53 DNA occupancy in both the developing and postmitotic context. These studies constitute the first *in vivo* comparison of p53 genome-wide binding and expression regulation in a postmitotic versus a proliferative tissue. Finally, these analyses constitute the first integrated profile of p53 genome-wide binding and transcriptional genome-scale regulation in *Drosophila melanogaster*.

MATERIAL AND METHODS

Fly Stocks

Flies were kept at 18 to 25°C and fed standard medium. The wildtype strains used are *yw* and w^{1118} (Bloomington). The p53 mutant alleles used were $p53^{5A\text{-}1\text{-}4}$ (Xie & Golic, 2004) and $p53^{ns}$ (Sogame, Kim, & Abrams, 2003). The deletion of the p53RE upstream of rpr is $p53RE^{rpr-}$ (Link et al., 2013).

Reverse Transcription PCR (RT-PCR)

For ionizing radiation stimulus, flies were treated with 40Gy of γ-radiation. Total RNA was extracted from tissue of interest using TRIzol reagent (cat#15596018) according to manufacturer's protocol. Next, samples were treated with TURBO DNA-free kit (cat#AM1907). cDNA synthesis was performed with Bio-Rad's iScript Reverse Transcription Supermix for RT-qPCR (cat#1708840). ddPCR was performed using Bio-Rad Evagreen system. Alternatively, goTAQ PCR was used to check products through gel electrophoresis. For IR studies in heads, tissue was acquired 3 hours after treatment (time point was chosen based on induction of ku80 in a time course). Embryo tissue was acquired 1.5 hour after IR treatment as previously published (F. Akdemir, Christich, Sogame, Chapo, & Abrams, 2007; Link et al., 2013). All graphs containing error bars constitute 2-3 biological replicates; each biological replicate represents 15-30 animals homogenized together.

Target	Primer sequence
rp49 FWD	ATG ACC ATC CGC CCA GCA TAC A
rp49 REV	CGT AAC CGA TGT TGG GCA TCA GAT ACT
hid FWD	GAT GGG GAT TCG AGT TCG GAT TCG GAT
hid REV	CAC TGC CCA CCG ACC AAG TGC TAT A
rpr FWD	GTG TGC GCC AGC AAC AAA GAA CTA
rpr REV	TTG CGA TGG CTT GCG ATA TTT GCC
skl FWD	GAG AGA ATG AGC GAG ACA GTG ACA GAG A
skl REV	TCG ATT TGA AAA CTA GCG ACT GCT TAC A
xrp1 FWD	CAT TAC CAA CAT CAA GCG TTC TGC TCC G
xrp1 REV	TGT TGC TGG TGC TGG TAC TGG TAC TT
ku80 FWD	TGT GTG GCG GAG ATT CTT AAG GA

ku80 REV	ATC CTC GCA GGC TGT CTT ATT CAC A
ku70 FWD	AGG GCA AGG AGT TCG AGT TT
ku70 REV	GGA AGG CGT CCA GTT CGA TA
RnrL FWD	TAA GAG AGA TGG CAG GCA GG
RnrL REV	CCA TTG ATG ACT TGC AGG GTG
CG3448 FWD	ACT TCA ACG CTC TCA GCT CTC
CG3448 REV	CGT CGT CCA TCC ATT TGC TTC
BetaTry FWD	CCT CCT ATG GCT ACG GAA ACC
Beta Try REV	CAG CAC ATC CGT ATC CCC AG
Yip7 FWD	CCA TCA TCG GAA ACG AGT GGG
Yip7 REV	CTT GGG TGA ACT CGG GGC TA
AttB FWD	AAA GCG GTC CAG TCA CAA CT
AttB REV	AAG ACA TCC TTC ACT CCG GG
Dro FWD	CTG CTT GCT TGC GTT TTT GC
Dro REV	GGC AGC TTG AGT CAG GTG AT
IM23 FWD	TTC GTC TTG CAC GCA GAT TG
IM23 REV	CTG GCA TAC TCC GCC GAT AA
PGRP-SC2 FWD	GCT CAC GCC ACT AAC TGG AA
PGRP-SC2 REV	CAT CGG AGA GCA GAC CCT TG
TotM FWD	GAA AGC CAA GCC TGC ACT ATG
TotM REV	AGG CGC TGT TTT TCT GTG AC

RNA-seq

About 50-100 fly heads were homogenized together per condition. RNA was extracted following the same protocol described above. After inactivation of DNase an additional isopropanol precipitation was performed. Samples were quality controlled through cDNA synthesis followed by PCR for bench mark genes. Next, 10 µg of RNA were sent for library preparation and NGS (next generation sequencing) at the McDermott Center NGS Core at UT Southwestern Medical Center. Poly(A) enrichment and strand specific RNA sequencing was performed, pair ended.

Sequencing read pairs were pre-processed to remove adapters using Cutadapt (Martin, 2011) and low quality reads or bases with Prinseq (Schmieder & Edwards, 2011). Sequence alignment was to the *Drosophila* genome ‘dm6’ using Tophat2 and the parameters: -p 10 --mate-inner-dist=200 --mate-std-dev=40 --library-type fr-firststrand --no-coverage-search (Kim et al., 2013). The open-source Picard toolkit was used to mark PCR duplicates which were removed using SAMtools along with low quality

alignments (quality score below 25) prior to downstream analyses (H. Li et al., 2009; Picard, 2017).

Differential gene expression analyses were performed using the Cuffdiff program (Trapnell et al., 2010) through UT Southwestern Medical Center's BioHPC Galaxy Service (galaxy.biohpc.swmed.edu) (Afgan et al., 2016). The library normalization method was geometric with blind dispersion estimation and bias correction was performed. For analyses of p53 target activation, genes with expression values below 2 in all datasets were excluded as well as non-coding RNAs. A pseudocount of 1 was added to all gene expression values. The fold change was calculated between IR and no IR samples and a cutoff "2" fold change was used.

Gene Ontology enRIchment analysis (GOrilla)

We performed GO analyses in the "two unranked lists of genes" mode of GOrilla. Below is the description from results provided by the GOrilla web tool:

'P-value' is the enrichment p-value computed according to the mHG or HG model (not corrected for multiple testing of 6948 GO terms).

'FDR q-value' is the correction of the above p-value for multiple testing using the Benjamini and Hochberg (1995) method. Namely, for the i^{th} term (ranked according to p-value) the FDR q-value is (p-value * number of GO terms) / i.

'Enrichment' = (b/n) / (B/N), where:

N is the total number of genes

B is the total number of genes associated with a specific GO term

n is the number of genes in the top of the user's input list or in the target set when appropriate

b is the number of genes in the intersection

Akdemir's Microarray re-analyses (F. Akdemir et al., 2007)

Affymetrix DrosGenome1 probe set sequences and ID was downloaded from Affymetrix and aligned to dm6 using bowtie2 to assign updated genes. GEO datasets were downloaded (GSE2780) for expression values of each probe in the tested conditions.

To match RNA-seq analyses, a pseudocount of 1 was added to all genes to calculate fold change, and genes with low expression (below value of 2) were excluded. To determine radiation responsive genes, I followed similar parameters described in Akdemir et al. I considered responsive p53 dependent, genes that on WT the replicates average IR fold change was equal or above 2 and no change was detected in the p53 null. Similar to the published list, I excluded genes that were only induced in one replicate out of the three WT. To determine the basal p53 target list, we took genes with at least 2 fold change value up or down in both replicates of $p53^{ns}$ over WT^{w1118}.

Chromosome Conformation Capture (3C)

Tissue preparation: Starting with 5 ml of whole flies, *Drosophila* heads were separated from bodies by flash freezing on liquid nitrogen followed by vigorous vortexing and sieve sorting (sieves from Hogentogler, number 30 on top and number 40 on the bottom). The intact heads were crosslinked in 1 ml of the following buffer: 2%formaldehyde, 50 mM HEPES pH 7.6, 100 mM NaCl, 0.1 mM EDTA and 0.5 mM EGTA during 15 minutes at room temperature in the vortex (gentle mixing). Formaldehyde was quenched by rinsing tissue in 1 ml of 1XPBS, 0.01% Triton X-100 and 0.125 M glycine, two times. Next, tissue was incubated on ice for 15 minutes in lysis buffer (10mM Tris pH 8.0, 10mM NaCl, 0.2% NP40, fresh protease inhibitors). Then mechanical lysis was performed with glass homogenizer, loose pestle (A), 10 strokes. Lysate was spun down for 5 minutes at 4000g in 4°C to recover nuclei. Supernatant discarded.

Digestion: Nuclear pellets were resuspended in 1ml of 1.2X HindIII digestion buffer. Then each sample was split in 4 tubes and final volume of each tube brought up to 350ul of 1.2X HindIII digestion buffer along with 0.3%SDS. Samples were incubated at 65C for 10 minutes while shaking at 1100 rpm. Then 2% Triton was added and samples

were incubated at 37°C for 15 minutes shaking at 1100 rpm. Digestion was performed with 700U of HindIII enzyme at 37°C overnight shaking at 1100 rpm. The following day, HindIII was inactivated using 1.6% SDS with incubation for 30 minutes at 65°C shaking at 1100 rpm.

Ligation: Ligation was performed in final volume of 16 ml of the following buffer: 1X T4 DNA ligase buffer, 1% triton-X100, water. Samples were allowed to stand at bench for 30 minutes before adding ligase to allow triton to sequester SDS. Next, 8000U of T4 DNA ligase were added to samples, and incubation was performed at 16°C overnight.

Reverse Crosslinking: The following was added to reverse crosslink DNA: 0.2M NaCl, 20µg/ml RNase and 120µg/ml Proteinase K. Samples were incubated at 65°C for at least 4 hours.

DNA purification: To purify the 3C DNA, Phenol/chloroform extraction was followed by ethanol precipitation. Lastly, samples were put through Invitrogen PCR clean up columns to increase DNA purity. DNA quality was checked with gel electrophoresis and ddPCR dilution curves.

ddPCR: Interaction frequency between the p53RE^{rpr} and our previously characterized regions was assayed by droplet digital PCR according to our published protocol (probes and primers) (Link et al., 2013). Controls for normalization and background assessment spanned a gene desert genomic locus, also from our previously published assay (Link et al., 2013).

Chromatin ImmunoPrecipitation (ChIP)

We adapted previously published protocols (Chanas, Lavrov, Iral, Cavalli, & Maschat, 2004; Negre et al., 2006). Heads: starting with ~30 ml of adult whole flies, *Drosophila* heads were separated by flash freezing on liquid nitrogen followed by vigorous vortexing and sieve sorting. Sieves from Hogentogler, number 30 on top and number 40 on the bottom. Next, heads were homogenized while fixing in 10 ml of 1% formaldehyde in 60 mM KCl, 15 mM NaCl, 4 mM MgCl2, 15 mM HEPES (pH7.6), 0.5% Triton X-100 and fresh added 0.5 mM DTT, EDTA-free protease inhibitors (Roche). First, tissue was

mechanically disrupted in a ground glass homogenizer (5 strokes) and then in a Douncer with type A, loose, pestles (10 strokes). Fixation step together with homogenization totaled 15 minutes. Fixation was stopped with glycine to 225 mM incubated for 5 minutes on ice. Nuclei were recovered by centrifugation at 4000 g for 5 minutes at 4°C. Nuclei were washed three times with 3 ml of the same buffer used during fixation without formaldehyde. Next, nuclei were washed once with 3 ml of lysis buffer (140 mM NaCl, 15 mM HEPES pH 7.6, 1 mM EDTA, 0.5 mM EGTA, 0.1% sodium deoxycholate, 1% Triton X-100 and fresh added 0.5 mM DTT, and protease inhibitors). Then, nuclei were resuspended in 900 µl of sonication buffer (lysis buffer + 0.1% SDS and 0.5% N-lauroylsarcosine). Samples were incubated for 10 minutes while rotating at 4°C. Sonication was performed in three 1.5 ml Eppendorf tubes (300 µl of sample each) with the Diagenode Bioruptor for 45 minutes at high, 0.5 minute on/off. After sonication, samples were again incubated while rotating for 10 minutes at 4°C. Then, debris was spun down for 5 minutes, at 4000 g at 4°C. Supernatant was transferred to a clean tube. The pellet was resuspended in 900ul of sonication buffer and incubated while rotating for 10 minutes 4°C. Samples were pelleted again and supernatant was transferred and combined with previous. The combined supernatant was centrifuged two more times at max speed for 10 minutes each time. These spins were critical to decrease unspecific precipitation. Ten percent of the sample was kept for the input and the rest was split evenly for immunoprecipitation (usually igg, matching the concentration used for the experimental antibody). For p53, 2µg of *Drosophila* anti-p53 d200 from Santa Cruz was used. Immunoprecipitation was performed overnight on nutator at 4°C. The next day, 60 µl of Santa Cruz Protein A/G beads slurry (rinsed with lysis buffer) was incubated with samples for 4 hours on nutator at 4°C. Beads were washed three times with lysis buffer 5-10 minutes each and once with TE buffer on nutator at 4°C. Beads were eluted with 100 µl of elution buffer (20 mM Tris–HCl, pH 7.5, 5 mM EDTA, 50 mM NaCl and freshly added 1% SDS, 50 µg/ml Proteinase K and 20 µg/ml RNase A) for 10 minutes at 65°C in a thermoshaker at 900 rpm. Eluate was transferred to a clean tube and elution step repeated with 150 µl of elution buffer. Eluate was kept at 65°C in a thermoshaker at 900 rpm overnight for decrosslinking. The next

day a standard phenol/chloroform extraction was performed followed by isopropanol precipitation of the ChIP DNA. Glycine was used during nucleic acid precipitation for improved yield. This ChIP DNA was used for either ddPCR or NGS. Embryos were staged to four to six hours, collected and dechorionated with 50% bleach, followed by thorough wash with distilled water. Embryos were then prepared according to the ChIP protocol described above.

ChIP-ddPCR

We quantified protein-DNA binding to specific targets using Bio-Rad's droplet digital PCR with EvaGreen system, following manufacture's guidelines. Primers used are listed below:

Target	Primers sequence
p53 promoter FWD*****	CGCTTGTACTTGCATCATTCG
p53 promoter REV*****	GCGCCTTGGCTGGATAAAC
3′ UTR FWD*****	GTGGCAGCCGGTCGAA
3′ UTR REV*****	CAGCCAAAGCGGATGCA
p53RE^{rpr} FWD	CGGAAAACTGATATGGCGATAAG
p53RE^{rpr} REV	CGGTCCCTCAGTCTCCAAGTC
CG3967 FWD	GGC ATT GAA ATA CTT TTT GCG GTC
CG3967 REV	TCG TTT GCG ATC GTT CCG TT
corp FWD	TTG TTG CTC TAC GCC AAG CG
corp REV	ATT AAA CTC GTG CCA CCC CA
CG13204 FWD	GTG TGC ATG CAG CTC TCG
CG13204 REV	ATC GGA ATC TGC CAA CCG TC
Mhc FWD	GTT GTG TCG GAA CTC ATC CCT
Mhc REV	AGA TGA GCT GCG GTT GAT TGA
lok FWD	TTG AAA AGT GCG TTC CTA GCG
lok REV	AGT TCT TGA TGG CTC AGG CG
Tefu FWD	AGT GCA GGA GTC TGC CCA TA
Tefu REV	TTC TCT GTT GTG GGT GTC GC

*****From (Merlo et al., 2014).

ChIP-seq

ChIP DNA was quantified using Promega's QuantiFluor ONE dsDNA System according to manufacturer's protocol. Then, 10 ng of ChIP DNA was used to prepare NGS libraries following previously published protocols (Liu & Kraus, 2017; Quail et al., 2008).

Libraries were amplified with 8 PCR cycles. ChIP libraries were sent for sequencing on Illumina Next seq 500 at the McDermott Center NGS Core at UT Southwestern Medical Center.

Sequencing read pairs were pre-processed to remove adapters using Cutadapt (Martin, 2011) and low quality reads or bases with Prinseq (Schmieder & Edwards, 2011). Sequence alignment was to the *Drosophila* genome 'dm6' using Bowtie2 (Langmead & Salzberg, 2012). The open-source Picard toolkit was used to remove PCR duplicates and downstream analyses were performed on uniquely mapped reads (Picard, 2017). MACS2 was used to call peaks with the –nomodel and –ratio flags (Y. Zhang et al., 2008). The NCIS scaling ratio was calculated for each negative control and ChIP comparison using the NCIS R package (Liang & Keleş, 2012; R Core Team, 2017). Distance to nearest MACS2 peak was determined for all unique transcription start sites (TSS) of protein coding genes in the RefSeq annotation of the drosophila genome using BEDtools (Quinlan & Hall, 2010). Motif search was performed using Homer with the custom p53 motif matrix below (Heinz et al., 2010).

```
>GGACATGCCCAGACATGCCC    dp53(p53)        8
0.33    0.1736  0.33    0.1664
0.275   0.108   0.421   0.198
0.481   0.052   0.334   0.135
0.019   0.826   0.07    0.086
0.657   0.118   0.056   0.17
0.221   0.028   0.099   0.653
0.002   0.003   0.99    0.006
0.077   0.406   0.021   0.498
0.15    0.535   0.078   0.238
0.168   0.36    0.132   0.341
0.348   0.137   0.341   0.175
0.241   0.078   0.526   0.156
0.499   0.022   0.405   0.076
0.007   0.987   0.004   0.003
0.652   0.1     0.029   0.22
0.165   0.054   0.108   0.674
0.083   0.046   0.854   0.018
0.126   0.343   0.057   0.476
0.211   0.416   0.109   0.266
0.19    0.349   0.138   0.325
```

RESULTS

The canonical p53 apoptotic program is unresponsive in postmitotic tissue

Similar to its human counterpart, *Drosophila* p53 can upregulate a variety of genes in response to ionizing radiation (IR) (F. Akdemir et al., 2007; Brodsky et al., 2004). Among the radiation induced p53 dependent (RIPD) genes identified, are the pro-apoptotic genes Head Involution Defective, Reaper and Sickle. The genes *hid, rpr* and *skl* reside in a genomic region known as the H99 locus; when this locus is deleted most stress-dependent and programmed cell death is abolished (White et al., 1994). As expected, increased expression of these genes leads to massive p53 mediated cell death in both embryonic and larval tissues (F. Akdemir et al., 2007; J. H. Lee et al., 2003; Sogame et al., 2003). To determine whether p53 functions similarly in a postmitotic, specialized tissue, I measured upregulation of known p53 embryonic targets in irradiated *Drosophila* heads. I performed a time course RT-ddPCR assay in WT heads post irradiation, measuring target activation at 1, 3, 5 and 8 hours. I included the three cell death genes, *xrp1* (which is one of the most robust embryo RIPD genes) and *ku80* a DNA repair gene (figure 2-1A). Interestingly, the three cell death genes were unresponsive throughout the time points I tested post IR. However, at 3 hours, robust induction of *ku80* was observed. *Xrp1* transcript levels follow a bell shape trend, but no upregulation above two fold was observed; in embryos *xrp1* response is early after IR and very robust, reaching 10 fold changes. To test if p53 mediates activation of *ku80* in heads, I repeated the RT-ddPCR using the 3 hour time point in WT and $p53^{-}$ heads (figure 2-1B). Confirming the time course results, all cell death genes remain unresponsive in WT heads, similar to the p53 mutants. As expected, *ku80* induction is observed in WT animals only. Therefore, *ku80* induction is p53 dependent in postmitotic tissue.

p53 specifies alternate stress-responsive programs in post mitotic tissue.

The observations that p53 fails to activate canonical apoptotic programs in heads suggest that the postmitotic context could reveal p53 programs that are distinct from

previously described gene activity networks. To determine p53 stress responses in postmitotic tissue, I performed paired-end RNA-sequencing experiments in *Drosophila* heads of WT and p53 null animals, with and without IR exposure. Confirming the ddPCR results, neither *rpr, hid, skl* or *xrp1* are upregulated after stress in heads (figure 2-2). However, I did observe genome-wide p53 transcriptional effects in response to radiation, including the induction of *ku80*, which serves as a validating benchmark (figure 2-3A). Strikingly, nearly all stress-induced gene activation was p53 dependent (figure 2-3B). As previously reported in the embryos, I also detected p53 effects in basal gene expression in the postmitotic tissue (figure 2-4) (F. Akdemir et al., 2007). To identify p53 stress-responsive targets, I performed differential gene expression analyses and uncovered 92 novel head RIPD protein coding genes (hRIPD) (figure 2-5). The complete list of genes, annotated function and human ortholog is in appendix A. To validate the RNA-seq findings, I directly tested p53 mediated IR induction of five novel hRIPD genes by RT-ddPCR (figure 2-6A). These genes have predicted human orthologs (figure 2-6B). Confirming RNA-seq findings, p53 dependent gene upregulation was detected after IR in all five genes.

To better understand p53 stress responses in postmitotic tissue, I performed pathway enrichment analyses using the Gene Ontology enRIchment anaLysis and visuaLizAtion tool (GOrilla) (Eden, Navon, Steinfeld, Lipson, & Yakhini, 2009). Metabolism, proteolysis and DNA repair genes were significantly enriched among hRIPD genes (figure 2-7A). It is important to note that many of the genes in the metabolic and the proteolysis pathways were uncharacterized, and their association to these pathways is inferred through protein structure and phylogeny. In fact, only 16% of all head p53 IR targets have a tested function, while 37% have predicted functions and 47% have no annotated information about function (figure 2-7B) (biological process annotated using the “batch download” tool at flybase.org -FB2017_02-) (Gramates et al., 2017). DNA repair genes include two major components of NHEJ (non-homologous end joining), *ku80* and *ku70.* Interestingly, I identified a possible novel *Drosophila* DNA repair gene, *CG3448* which contains a *XRCC4*-like domain. In humans, *XRCC4* binds the NHEJ ligase, *Lig4,* and this complex is responsible for the ligation step of NHEJ. p53-regulated metabolic genes

include Adipokinetic hormone (*Akh*), a fly functional homolog of mammalian glucagon; *Akh* regulates metabolism of carbohydrates, lipids and glycogen (Galikova et al., 2015). Interestingly, mice studies demonstrated that upon starvation, p53 is required for gluconeogenesis and amino acid catabolism (Prokesch et al., 2017). Furthermore, p53 has been implicated in lipid metabolism in the mammalian system (Goldstein & Rotter, 2012). These observations establish the *Drosophila* head as an important *in vivo* model of postmitotic p53 stress responsive programs.

To comprehensively compare p53 transcriptional responses in heads and the previously described embryo program, I took advantage of published embryo microarray data (F. Akdemir et al., 2007). Since the microarray publishing in 2007, the *Drosophila* genome has been further sequenced and annotated. To properly compare datasets, the affymetrix probes were realigned and updated genes assigned (see methods). Next I combined the microarray updated gene expression data to the RNA-seq (note that the microarray does not cover all the annotated fly genes). After applying the same cutoffs and only examining genes represented in the microarray, I found minimal overlap of p53 targets in the two different contexts (figure 2-8A). In addition to *ku80,* two other DNA repair genes are common targets in the two tissues, *ku70* and RnrL (Ribonucleoside diphosphate reductase large subunit). Interestingly, *CG3448* (a predicted NHEJ gene) is also IR activated in both contexts (figure 2-8B). These observations suggest the DNA repair pathway is a conserved p53 program among the proliferative and postmitotic contexts.

Occupancy at the p53 *rpr* enhancer predicts activation of apoptotic program

To understand why the apoptotic genes are unresponsive in postmitotic tissue, I focused on a well characterized p53 response element ~ 5 kb upstream of *rpr* (hereafter referred to as $p53RE^{rpr}$) (Brodsky et al., 2000). Genetic ablation of the $p53RE^{rpr}$ eliminates stress-induced activation of *rpr* as well as *hid,* and *skl* (a genomic region spanning ~300kb) (Link et al., 2013). Strikingly, this enhancer is also required for activation of genes in *trans* such as *xrp1* and *ku80* (Link, 2011; Link et al., 2013). Long-range regulation of these p53 targets is accomplished through chromatin contacts that

link the p53RE^{rpr} and the cell death genes (Link et al., 2013). Therefore, I hypothesized that diminished p53 enhancer looping to the cell death genes prevents p53-mediated activation in this locus. To test this hypothesis I mapped p53 enhancer looping through the H99 locus of *Drosophila* heads, by adapting our published digital-3C assay for head tissue (Link et al., 2013). I found that the p53 enhancer maintains loops to H99 cell death genes despite lack of p53 gene activation (figure 2-9A). In fact, the looping pattern through the entire H99 locus is well conserved in heads when compared to the published embryo pattern (Link et al., 2013). Therefore, failure to activate cell death genes in heads is not explained by lack of p53 enhancer looping. In embryos, the p53RE^{rpr} is required for activation of *ku80,* which is located in *trans* to the p53RE^{rpr} (Link, 2011). To determine if the *rpr* enhancer is also important for the activation of *ku80* in heads, I measured activation of *ku80* in flies in which the p53RE^{rpr} was genetically removed (figure 2-9B). Confirming my previous observations, in heads of the p53RE^{rpr-} strain all three cell death genes were unresponsive. However, *ku80* induction remained unaffected in the flies lacking the p53RE^{rpr}. Therefore, the p53RE^{rpr} is not required for induction of *ku80* in postmitotic tissue.

The observation that the *rpr* enhancer is dispensable for p53 target activation in heads indicate that differential p53 DNA binding to the p53RE^{rpr} could explained the failure to activate the cell death locus. To test this hypothesis I measured p53 protein binding to the p53RE^{rpr} using ChIP-ddPCR in both embryos and heads. To quality control the ChIP samples, I quantified p53 binding to previously published positive and negative regions (p53 promoter and 3'UTR respectively) (Merlo et al., 2014). As expected, in embryos p53 binds the p53RE^{rpr}, but, in contrast, p53 binding was absent in heads (figure 2-10A). These ChIP experiments were performed under unperturbed conditions and, as seen in other systems, p53 was pre-bound to these response elements prior to stress-induced target activation in embryos (K. H. Lee et al., 2010; Merlo et al., 2014; Tonelli et al., 2015). To test if p53 protein binds to the p53RE^{rpr} in heads only after stimulus, I performed ChIP-ddPCR in heads after treating flies with IR. No significant increase in p53 binding to the p53RE^{rpr} was observed after IR (figure 2-10B). Combined, these

studies suggest that in postmitotic tissue a different enhancer network directs p53 tissue-specific transcriptional responses.

Genome-wide tissue comparison of p53 DNA occupancy

Based on the observation that occupancy of the p53RE^{rpr} predicts tissue specific gene regulation, I hypothesized that distinct enhancer networks enable p53 to direct tissue adapted responses. To characterize genome-wide p53 enhancer networks, I performed anti-p53 chromatin immunoprecipitation in embryos and heads, followed by high throughput sequencing (ChIP-seq). To ensure the biological validity of p53 enriched regions, I also performed ChIP-seq in p53 null tissue, processed in parallel. Therefore, p53 peaks were called through comparison of ChIP signal in WT and p53 null tissue. I confirmed the ChIP-seq quality by checking the previously published p53 binding site at p53 gene promoter (figure 2-11A) (Merlo et al., 2014). A total of 135 p53 enriched regions in embryos and 392 in heads were identified. Interestingly, 75 regions had p53 enrichment in both tissues (figure 2-11B). Additionally, a significant portion of called peaks contained the highly conserved p53 binding motif (in heads, 25.8%, embryos, 24.4%). To validate the ChIP-seq experiments, I directly tested six p53 peaks from varying enrichment scores using ChIP-ddPCR in heads (figure 2-11C). I observed p53 enrichment in all peaks by ChIP-ddPCR. Strikingly, when I compared the quantified enrichment of p53 peaks from the two ChIP methodologies, the peak heights trend in each ChIP method is remarkably similar (figure 2-11D), increasing the confidence in peaks uncovered by ChIP-seq not only qualitatively but also quantitatively. Next, I confirmed ChIP-ddPCR findings that p53 binds the p53RE^{rpr} in embryos but not in heads (figure 2-12A). Surprisingly, p53 enrichment was detected at *hid* and *xrp1,* both require the *rpr* p53 enhancer and are IR induced in embryos only (figure 2-12B-C). Therefore, p53 binding at each of the two genes is not sufficient to predict stimulus-induced gene activation. This corroborates the model that the p53RE^{rpr} is the p53 enhancer controlling the embryonic targets *hid* and *xrp1* (Link et al., 2013).

Basal p53 genome-wide DNA occupancy does not predict transcriptional programs in postmitotic tissue

The extent of basal p53 binding to stress response targets is not well established. Although studies conducted in cancer/immortalized cell cultures suggested p53 basally binds to most stress response targets, later studies conducted in primary normal cell lines and *in vivo*, uncovered significant stress dependent p53 DNA binding (Shaked et al., 2008; Tonelli et al., 2015). Both in embryos and heads, most p53 binding sites were found within 5 kb of a TSS (61.48% and 78.32% respectively) (figure 2-13A-B). To determine whether basal p53 binding predicts IR induced programs, all genes within 5 kb of a p53 enriched region were identified and pathway enrichment analyses performed using the GOrilla web tool (table 2-1) (Eden et al., 2009). The 5kb distance was chosen based on distance between the well characterized p53RE at *rpr*. As expected, in embryos the apoptotic pathway is enriched; p53 peaks are present at *rpr, hid, egr* (all known apoptotic p53 IR targets) and at two additional apoptotic genes (*Tao* and *Chrb*). Interestingly, *Tao* appears to be basally repressed by p53 as its gene expression is ~2.3 fold higher in p53 mutants by Akdemir's microarray and it is unaffected in heads (data not shown). *Chrb* is not affected by p53 in any of the conditions tested in our studies. In heads, p53 binding was not enriched in any of the p53 stress response transcriptional programs (DNA repair, metabolism and proteolysis) (table 2-2). Among the enriched pathways for p53 binding in heads are some developmental processes. This is interesting, as p53 function in developing neurons have been reported (Tedeschi & Di Giovanni, 2009). Strikingly, p53 was only bound within 5kb of one head RIPD gene, (*CG15456*, modestly induced at ~2.3 fold after IR). In flies, no annotated function for *CG15456* was found, however a predicted human ortholog is the gene *MIEN1* (migration and invasion enhancer 1). In humans *MIEN1* is a characterized oncogene associated with a variety of cancers, including breast, colorectal and oral cancers; it is highly implicated with tumor invasiveness (Dong et al., 2015; Katz et al., 2010; Rajendiran et al., 2015). Links between *MIEN1* and *TP53* appear to not have been reported.

To systematically associate the genome-wide p53 DNA occupancy and transcriptional effects, I examined the distance between p53 transcriptionally affected genes to a p53 binding site (these include genes basally and IR affected by p53). Strikingly, I observed very limited p53 transcriptional effects nearby p53 binding sites; even among basally p53 affected genes (figure 2-14A-B). Therefore, only a small portion of p53 peaks in both embryos and heads correlate with proximal p53 transcriptional effect. In embryos, 12.6% of peaks correlated with transcriptional effect within 5 kb (figure 2-15A) and as expected some of the top IR targets were pre-bound before stress. Strikingly, in heads, only 5.3% of peaks were associated with p53 transcriptional effects within 5kb (figure 2-15B); none of the top IR induced genes were pre-bound by p53. Next, I annotated genes transcriptionally affected by p53 loss in each tissue within 5kb of a p53 peak, as these are likely p53 direct targets. Gene functions and predicted human orthologs were annotated using flybase (Appendix B) (Gramates et al., 2017). Strikingly, 72.2% and 73.7% of embryo and head direct p53 targets have predicted human orthologs respectively. Therefore, there is great potential for evolutionary conservation of these p53 networks in higher animals.

Finally, based on recent p53 *in vivo* studies suggesting significant *de novo* recruitment of p53 binding in response to IR, I explored the possibility of stress-dependent p53 binding. Studies by Tonelli et al., conducted in B cells found that IR activated genes bound by p53 are more likely to contain the canonical motif with no spacer between the two decameric half sites (Tonelli et al., 2015). Therefore, I probed the promoters of both embryo and head RIPD genes for presence of the unsplit p53 consensus (within 5kb of TSSs) (figure 16A-B). I found that in embryos 30.5% of RIPD genes contain the p53 motif compared to 4.5% RIPD genes that are pre-bound by p53. In heads, 23.9% of RIPD genes have the motif versus 1.1% being pre-bound. These analyses suggest that *de novo* DNA binding may be the mechanism through which p53 drives most stress responses in the *Drosophila* model.

Loss of p53 is associated with strong inflammation in *Drosophila* heads

To characterize genes basally controlled by p53, I performed differential gene analyses using the RNA-seq datasets. I identified all protein coding genes that have increased expression in p53 null heads and performed GOrilla pathway analyses (2 fold and up) (Eden et al., 2009). Strikingly, immune response pathways were highly enriched and by far the most predominant pathways found (table 2-3). Next, I annotated genes associated with immune responses (table 2-4). Among the immunity genes, are many antimicrobial peptides (*IM23, IM2, IM1, TotM, Dro*). To validate our RNA-seq findings (figure 2-17A), I performed RT-PCR in WT and $p53^{-}$ fly heads (figure 2-17B). Similar upregulation of immune response genes was observed by gel electrophoresis. These analyses suggest loss of p53 leads to strong inflammation.

A simple explanation for the strong inflammation observed in $p53^{-}$ flies is that loss of p53 leads to chronic infection. To test this possibility, I performed bacterial load experiments. Briefly, I homogenized whole adult flies, WT and p53 mutants, and plated serial dilutions of the homogenates to detect the number of colony formation units per fly (figure 2-18A). I observed no significant difference between WT and $p53^{-}$ flies, suggesting that loss of p53 does not cause increased microbe growths. Furthermore, I examined the immune response genes for p53 binding in the ChIP-seq datasets and found no p53 enrichment at the immune genes' promoters (figure 2-18B). *Diedel* is the closest immune gene to a p53 peak (-4639bp from the peak). *Diedel,* is a negative regulator of the immune deficiency pathway; therefore, the upregulation of *Diedel* observed in p53 nulls cannot explain the upregulation of antimicrobial peptides.

Inflammation in p53 mutants correlates with dysregulated retroelement transcripts

Recent studies from our lab uncovered a novel function of p53. We demonstrated that p53 genes from invertebrates and vertebrates act to restrain retroelement expression (Wylie et al., 2016). Interestingly, retroelement dysregulation has been associated with upregulation of immune response pathways (Leonova et al., 2013; Mu, Ahmad, & Hur,

2016; Volkman & Stetson, 2014). To test if retrotransposons are dysregulated in *Drosophila* heads, I measured retroelement transcripts through our published RT-ddPCR assay. I found significant increase in transcripts of *Gypsy* in p53 mutant *Drosophila* heads that correlates with increased upregulation of *TotM* antimicrobial peptide (figure 2-19A). Previous studies have characterized the *Drosophila* RNA interference pathway as an important cellular mechanism to restrain retrotransposon expression in somatic and gonad tissues (Czech et al., 2008; Ghildiyal et al., 2008). One important RNAi components for retroelement repression in somatic tissue is Dicer-2. To further associate dysregulated mobile elements and inflammatory responses in heads, I measured *TotM* and *Gypsy* expression in *Dcr-2* mutants using RT-ddPCR assays. Interestingly, similar to p53 nulls Dcr-2 mutants are dysregulated for *Gyspy* retroelements which correlates with upregulation of the antimicrobial peptide *TotM* (figure 2-19B). Another cellular defense to restrain retroelement expression is the piRNA pathway. Although the piRNA pathway is traditionally associated with repression of germline retrotransposons, some components have been implicated in somatic repression of retroelements (Jones et al., 2016; Perrat et al., 2013). One of these components is Armitage, therefore I tested retrotransposon dysregulation and antimicrobial upregulation in armi mutant heads (figure 2-19C). Interestingly, armi mutants did not have significantly dysregulated *Gypsy* and also no upregulation of *TotM* is observed. However, the retroelement *TAHRE* is highly dysregulated. These observations suggest that if retroelements are the cause of inflammation in p53 null heads, not all retroelements provoke the upregulation of immune genes.

NF-kappaB-related proteins are not differentially activated in p53 mutant *Drosophila* heads

In *Drosophila* it is well known that activation of Relish, Dorsal and/or Dif (NF-kappa B related proteins) can activate a cascade of antimicrobial peptides (Ganesan, Aggarwal, Paquette, & Silverman, 2011; Hultmark, 2003; Valanne, Kallio, Kleino, & Rämet, 2012). A schematic of activation of these pathways is depicted in figure 2-20A. Briefly, Relish is cleaved and the nuclear portion is transported to promote activation downstream

targets. Dorsal and Dif are stabilized in the cytoplasm by interaction with Cactus, upon stimulus this interaction is disrupted and Cactus protein is degraded. Therefore, to test if these pathways are activated in $p53^{-}$ heads, I measured cleavage of Relish, as well as degradation of Cactus using Western blot experiments. I detected no evidence of increased activation of either Relish or Dorsal/Dif in p53 mutants (figure 2-20B).

In *Drosophila,* little is known about immunity pathways that sense nucleic acids. In the mammalian system, three defined pathways are nucleic acid sensors, cGAS, RIG-I and MDA5 (Barbalat, Ewald, Mouchess, & Barton, 2011). Therefore, mammalian models could shed light into whether retroelements are causing the inflammation observed in p53 mutants. To determine if this inflammation phenotype is conserved in higher animals, upregulation of interferon responsive genes was measured in the mouse brain, using RT-PCR (figure 2-21A-B). Preliminary data suggests that expression of IFIT-1, IFIT-3 and CXCL-10 is increased in hippocampus and cerebellum of the p53 mutants. Quantification of increased genes was measured in the hippocampus through ddPCR assays (figure 2-21C). This data is from RNA acquired from one mouse and therefore needs to be appropriately repeated before any conclusions can be made, together with measurements of retroelement dysregulation.

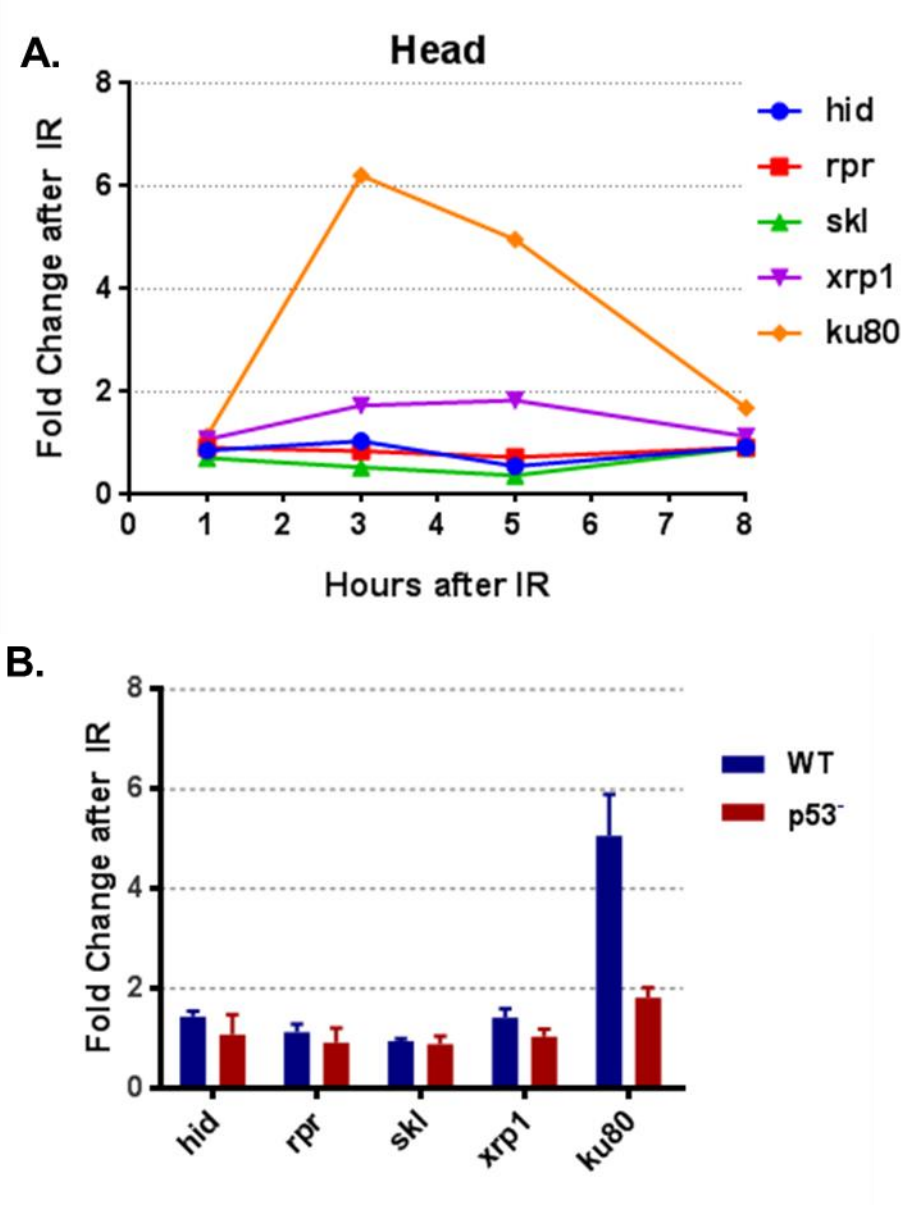

Figure 2-1: p53 apoptotic program is unresponsive in *Drosophila* postmitotic tissue

A. Time-course RT-ddPCR in WT *Drosophila* head tissue probing IR activation of published p53 targets. B. RT-ddPCR three hours after IR confirms *ku80* is activated in a p53 dependent manner; cell death genes *hid*, *rpr* and *skl* as well as *xrp1* remain unresponsive (*xrp1* is one of the most robust p53 targets in embryos).

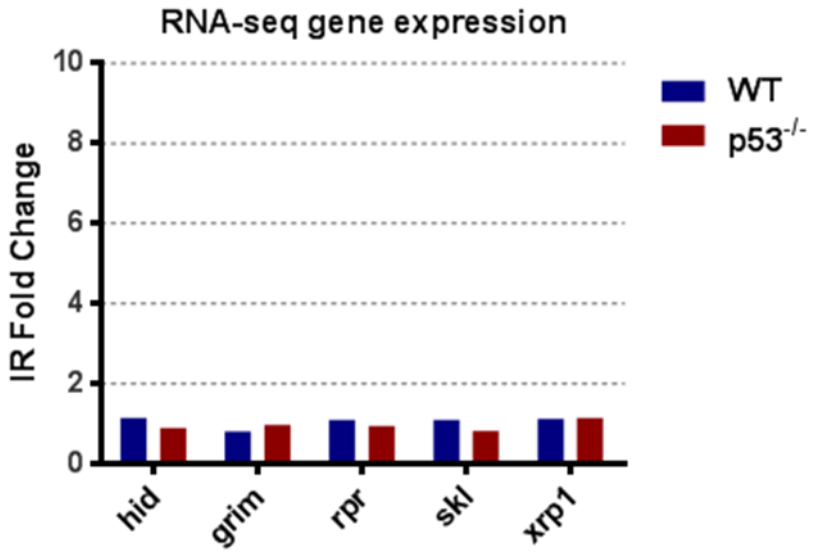

Figure 2-2: RNA-seq confirms p53 canonical embryo targets are unresponsive in heads.

RNA-seq was performed in WT and p53 mutant head tissue, with and without IR (3 hours post exposure).

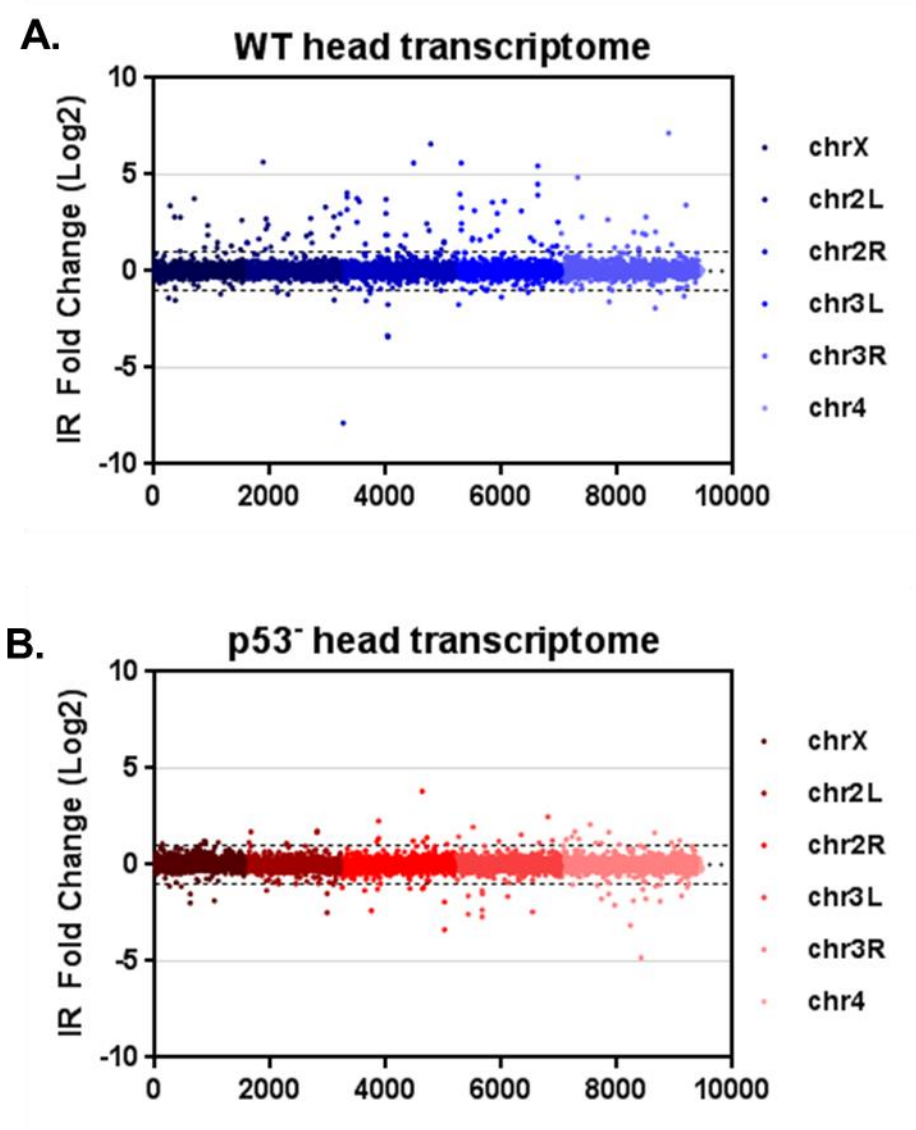

Figure 2-3: p53 promotes robust transcriptional responses in postmitotic tissue

A. WT gene expression changes after IR in heads. B. p53 null gene expression changes after IR in heads (dashed line represents cutoff of fold change equal to 2). Note that most genes activated by IR are p53 dependent. Genes with close to zero expression values in all conditions and non-coding RNAs were excluded (see methods for details).

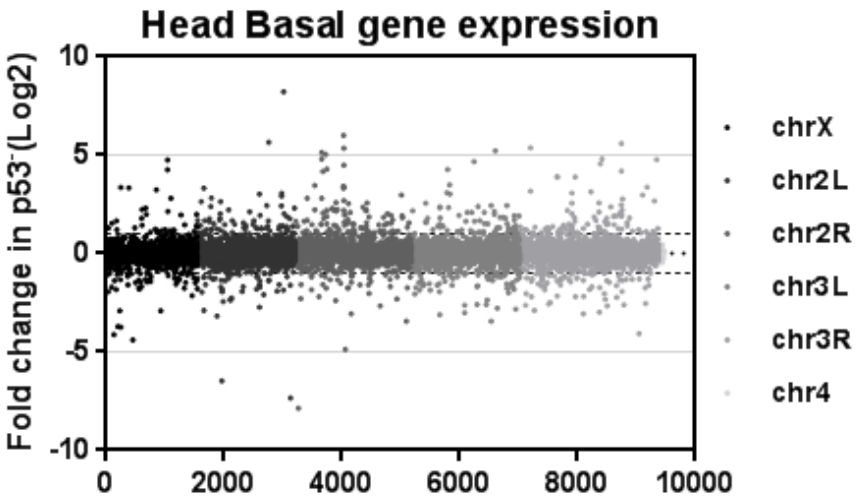

Figure 2-4: Basal gene expression is affected by p53 loss in postmitotic tissue

Basal gene expression changes in p53 mutants compared to WT (dashed line represents cutoff of fold change equal to 2). Note that p53 effects in basal gene expression have been reported in other systems. Genes with close to zero expression values in all conditions and non-coding RNAs were excluded (see methods for details).

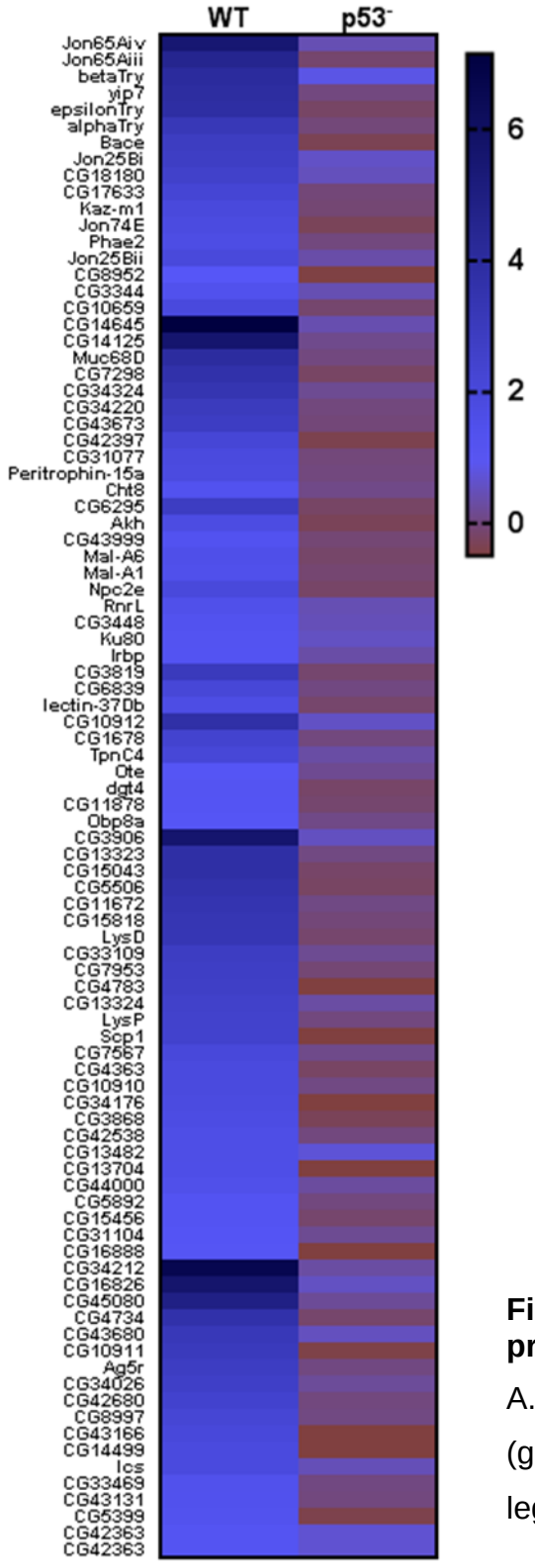

Figure 2-5: Novel p53 transcriptional programs in postmitotic tissue

A. Heat map of novel head RIPD genes (grouped by biological process). Colored legend is Log2 IR fold change.

A.

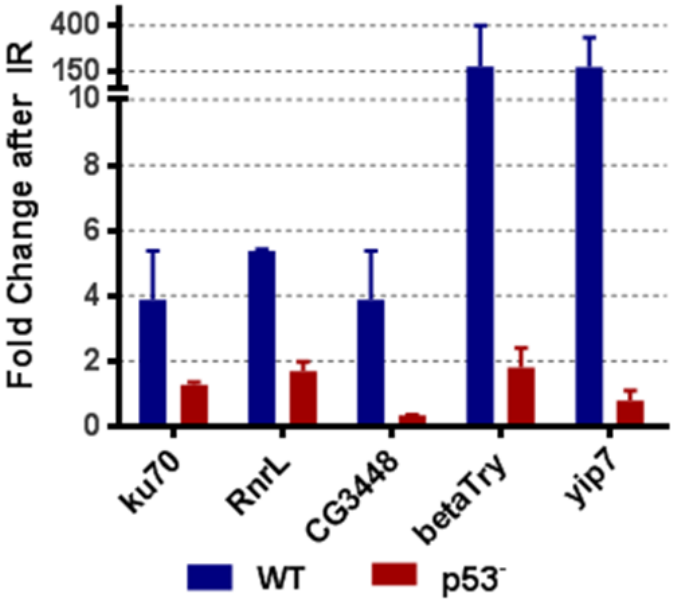

B.

hRIPD	H SAPIENS ORTHOLOGS
ku70	Hsap\XRCC6
RnrL	Hsap\RRM1
CG3448	Domain similarity to XRCC4
betaTry	Hsap\PRSS36
	Hsap\PRSS22
	Hsap\PRSS33
	Hsap\PRSS45
	Hsap\PRSS53
	Hsap\PRSS3
	Hsap\PRSS8
	Hsap\KLK15
	Hsap\PRSS27
	Hsap\TPSG1
	Hsap\PRSS38
	Hsap\PRSS1
yip7	Hsap\KLK3

Figure 2-6: RNA-seq validation

A. Five RIPD genes uncovered by RNA-seq were validated through RT-ddPCR assays. *Ku70* and *RnrL* are known DNA repair genes, *CG3448* is a predicted DNA repair gene. BetaTry and yip7 are serine proteases and their predicted human orthologs 'KLKs' are associated with carcinogenesis (Filippou, Karagiannis, Musrap, & Diamandis, 2016; Kryza, Silva, Loessner, Heuzé-Vourc'h, & Clements, 2016). B. All predicted human orthologs of validated postmitotic RIPD genes.

A.

P-value color scale				
$> 10^{-3}$	10^{-3} to 10^{-5}	10^{-5} to 10^{-7}	10^{-7} to 10^{-9}	$< 10^{-9}$

GO term	Description	P-value	FDR q-value	Enrichment
GO:0006030	chitin metabolic process	9.48E-11	6.58E-07	15.5
GO:1901071	glucosamine-containing compound metabolic process	1.78E-10	6.17E-07	14.6
GO:0006040	amino sugar metabolic process	2.11E-10	4.89E-07	14.4
GO:0006022	aminoglycan metabolic process	1.10E-09	1.91E-06	12.4
GO:1901135	carbohydrate derivative metabolic process	1.02E-05	1.41E-02	4.6
GO:0006508	proteolysis	2.79E-05	3.23E-02	3.3
GO:0043170	macromolecule metabolic process	1.63E-04	1.62E-01	1.8
GO:0006303	double-strand break repair via nonhomologous end joining	7.34E-04	6.37E-01	47.5

B.

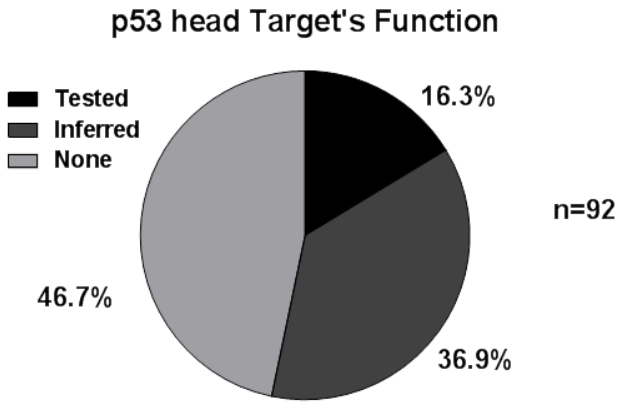

Figure 2-7: Functional annotation of p53 postmitotic programs

A. Pathway enrichment analyses results for p53 stress-responsive programs in postmitotic tissue (Eden et al., 2009). B. Flybase derived criteria for biological process annotation of RIPD genes in postmitotic tissue; only a small portion has a tested function.

A.

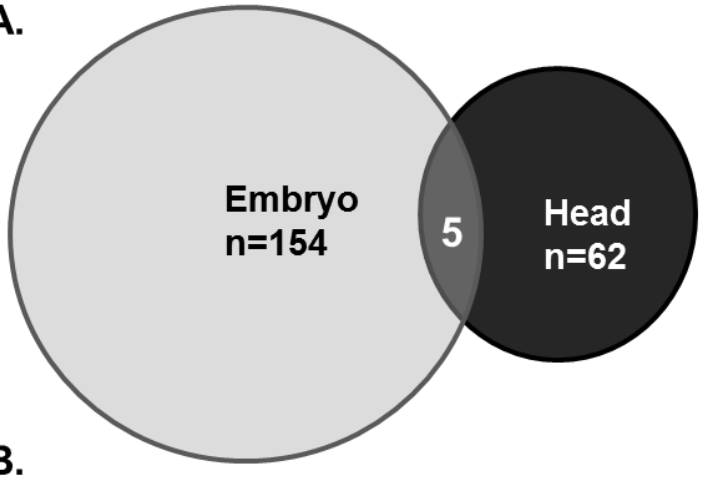

B.

Common RIPD genes between Embryos and Heads					
	IR Fold Change				
	Embryos		Heads		Biological Process
GENE	WT	$p53^{-ns}$	WT	$p53^{-k1}$	
RnrL	2.22	1.17	2.80	1.35	Tissue regeneration; DNA replication and repair
CheA7a	4.60	0.23	2.49	0.72	Sensory perception of chemical stimulus
CG3448	3.04	0.72	2.47	1.39	DNA recombination; DSB repair
Ku80	2.28	1.55	2.39	1.47	DNA recombination; telomere maintenance; NHEJ
Ku70	2.05	1.69	2.35	1.24	NHEJ

Figure 2-8: Comparison of p53 transcriptional regulation in embryos and heads

A. Venn diagram of overlapping p53 targets (RIPD) in embryos and heads. RNA-seq results were compared to published Microarray IR studies (F. Akdemir et al., 2007). Note that the number of RIPD genes in the diagram includes only genes represented in the Microarray. The total number of head RIPD genes in our studies is 92. B. The five common p53 targets in embryos and heads.

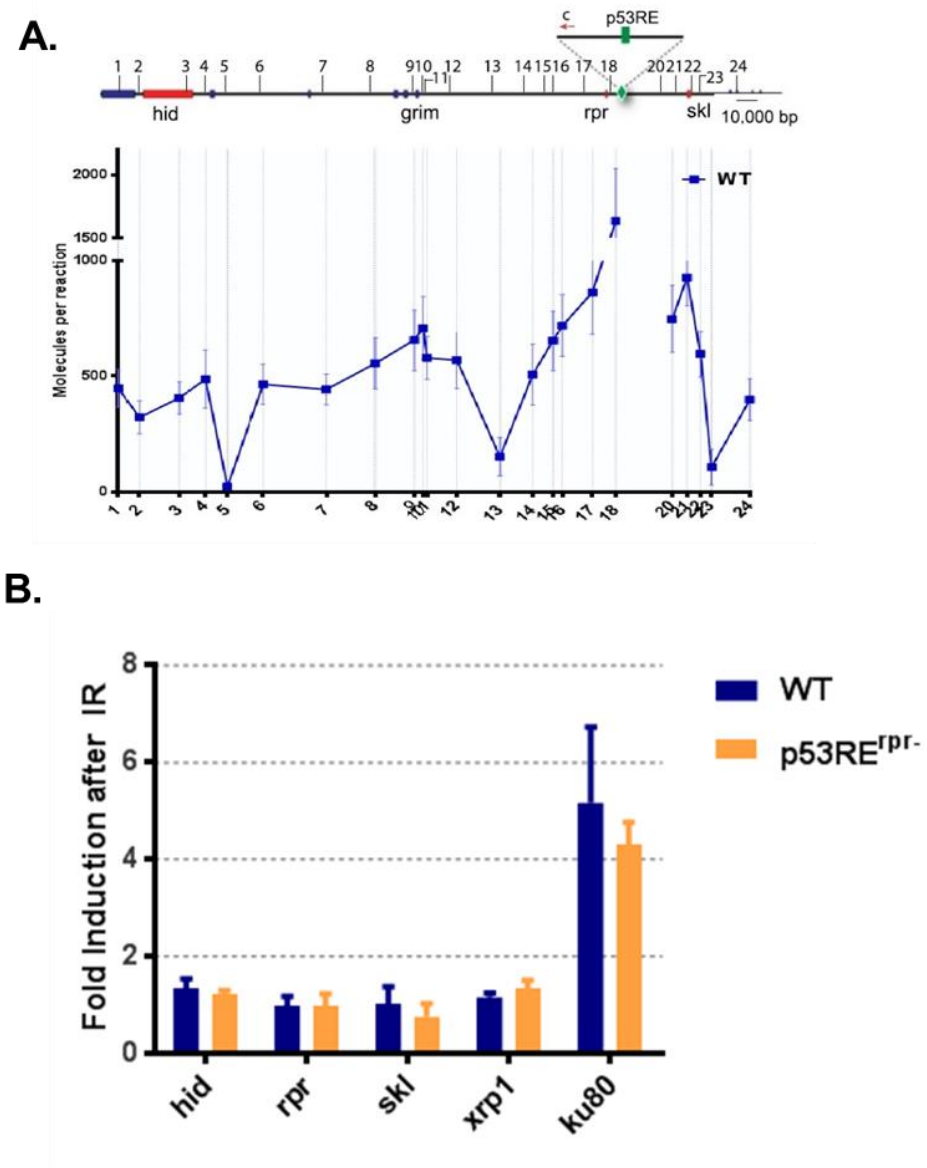

Figure 2-9: p53RE^{rpr} is not required for *ku80* induction in postmitotic tissue

A. 3C-ddPCR experiments in *Drosophila* head tissue. Interactions between the p53RE^{rpr}(green) and IR induced cell death p53 targets (red) were measured. H99 looping pattern is very similar to published patterns from embryos (Link et al., 2013). B. Genetic removal of the p53RE^{rpr} does not affect induction of *ku80* in postmitotic tissue. Note that previous studies determine this enhancer is required for *ku80* response in embryos (Link, 2011).

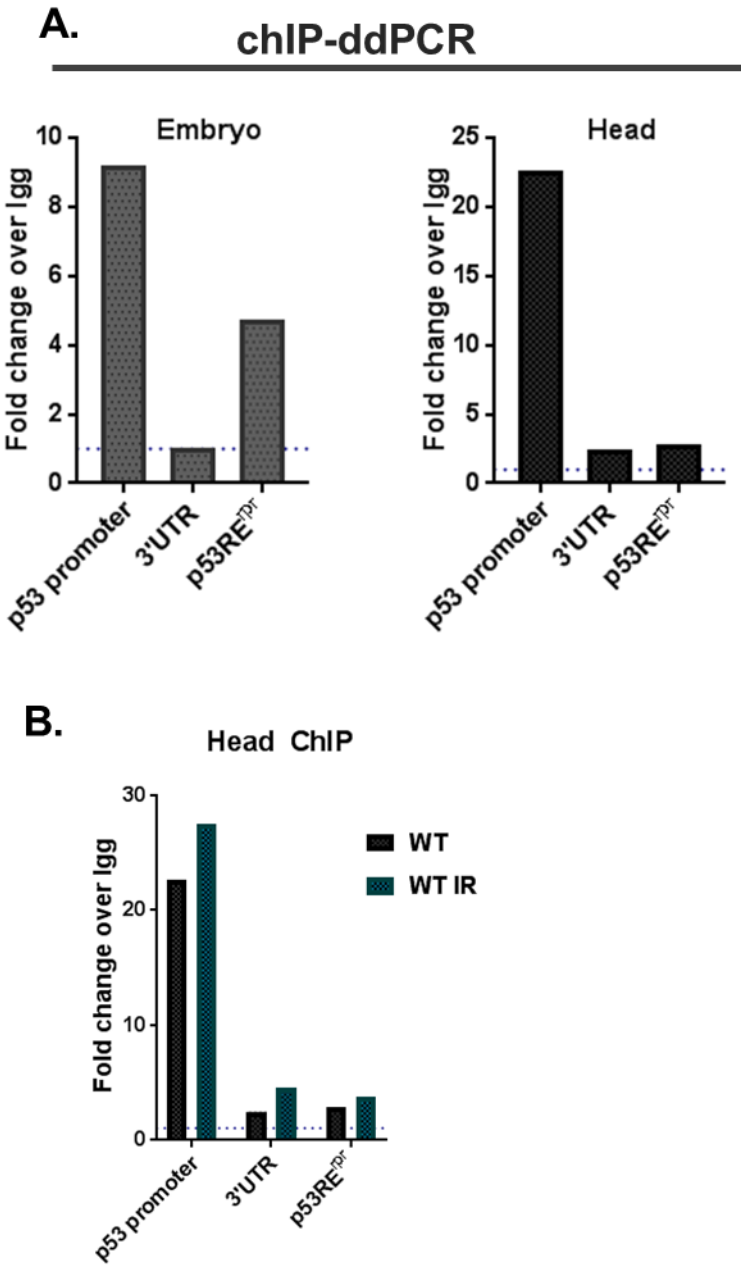

Figure 2-10: p53 binding to the p53RE^{rpr} predicts stress-responsive apoptotic program

A. ChIP-ddPCR performed with p53 and Igg antibodies. Published positive and negative control regions in the p53 gene were used (Merlo et al., 2014). p53 binds *rpr* enhancer in embryos only. B. ChIP-ddPCR in irradiated head tissue.

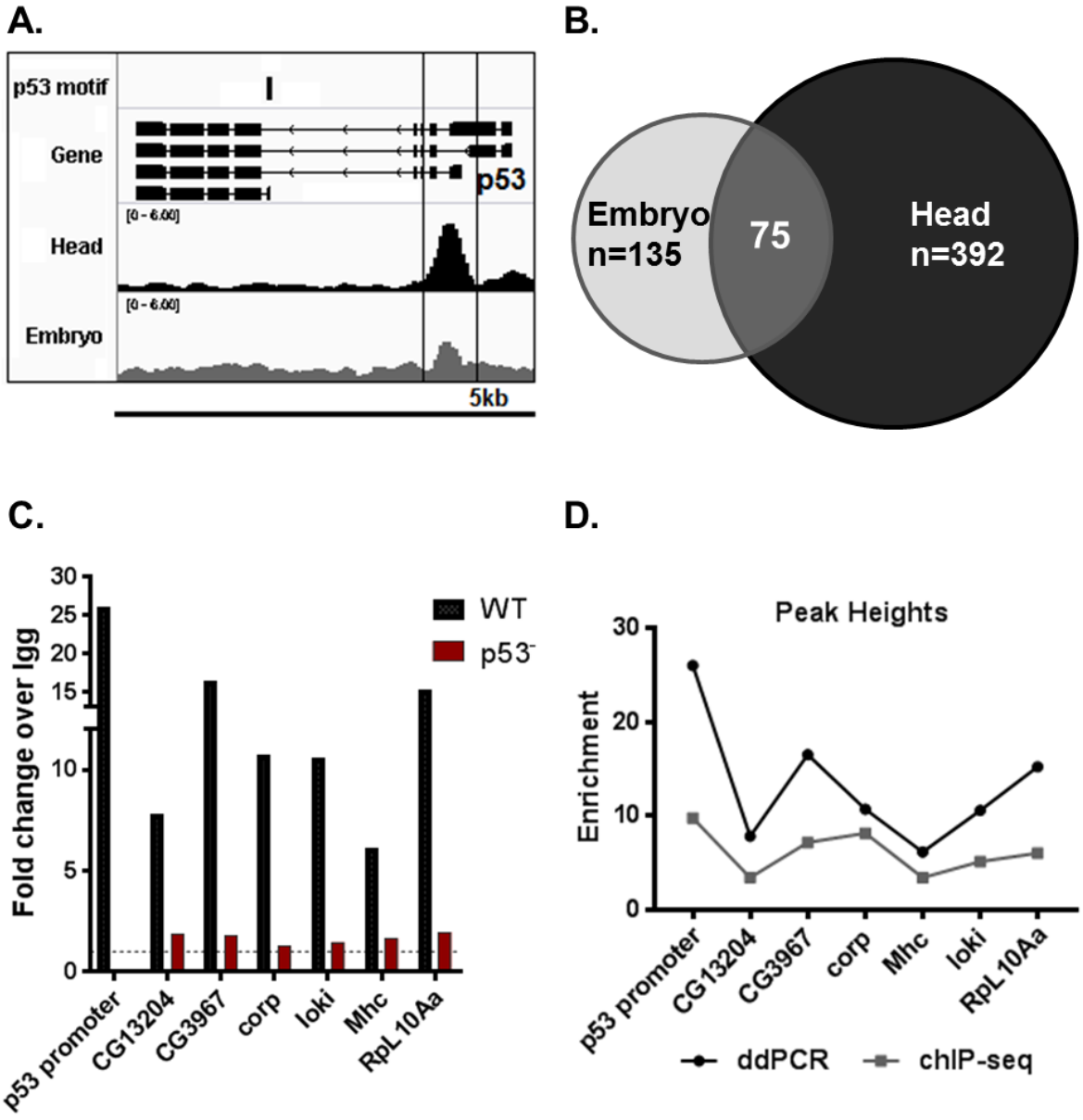

Figure 2-11: p53 genome-wide binding profiles in *Drosophila* embryos and heads
A. ChIP-seq detects published p53 enriched region at the promoter of p53 gene (Merlo et al., 2014). Graph displays fold enrichment over p53 null samples. B. ChIP-seq p53 peak distribution between tissues. C. ChIP-ddPCR validation of p53 binding sites uncovered by ChIP-seq. D. Peak height trends are similar in both ChIP methodologies.

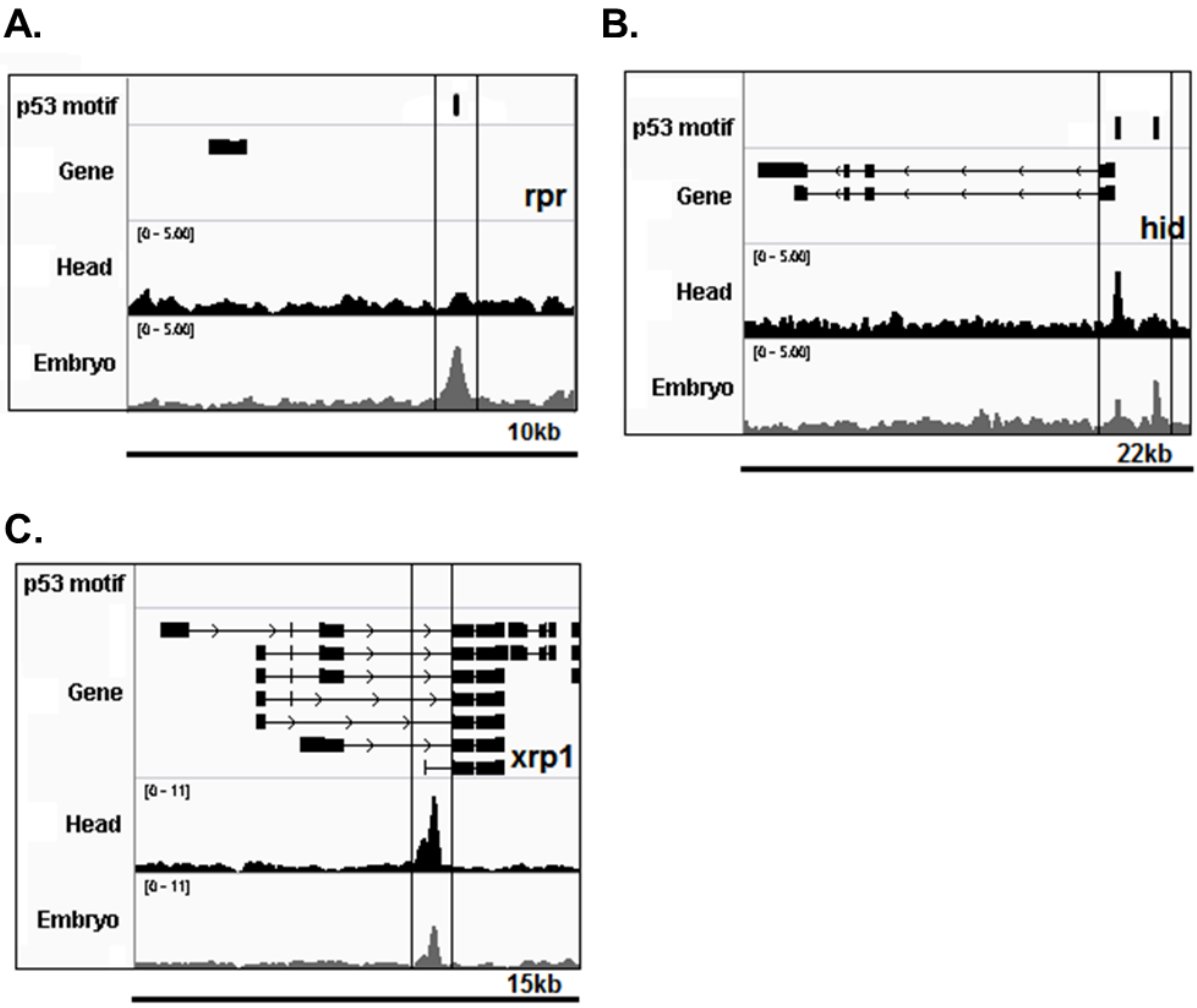

Figure 2-12: p53 is enriched at embryo targets in both embryos and heads.
A. ChIP-seq confirms that p53 occupies the canonical enhancer upstream of *rpr* in embryos only. B-C. p53 enriched regions in *hid* and *xrp1,* genes responsive only in embryos. Note that deletion of p53RE^{rpr} abrogates embryonic responses of *hid* and *xrp1* (Link et al., 2013). All graphs display fold enrichment over p53 null samples.

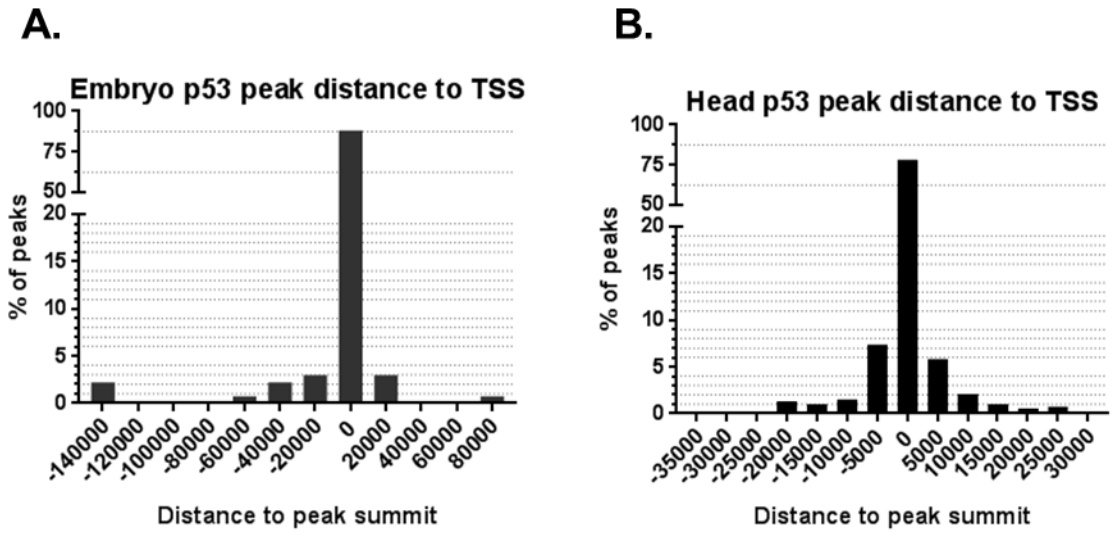

Figure 2-13: Most p53 binding sites are near a TSS

A-B. Distribution of the distance between p53 enriched regions and corresponding closest TSS in embryos and heads

Embryo Biological Process of genes within 5KB of a p53 peak				
GO Term	Description	P-value	FDR q-value	Enrichment
GO:0010646	regulation of cell communication	1.39E-06	9.68E-03	3.98
GO:0023051	regulation of signaling	1.39E-06	4.84E-03	3.98
GO:0048583	regulation of response to stimulus	8.39E-06	1.94E-02	3.46
GO:0009966	regulation of signal transduction	8.41E-06	1.46E-02	3.93
GO:0048518	positive regulation of biological process	1.62E-05	2.26E-02	2.85
GO:0006915	**apoptotic process**	**1.68E-05**	**1.95E-02**	**15.46**
GO:1902531	regulation of intracellular signal transduction	3.78E-05	3.76E-02	5.4
GO:0050789	regulation of biological process	6.97E-05	6.06E-02	1.82
GO:0050896	response to stimulus	7.92E-05	6.12E-02	2.38
GO:0050794	regulation of cellular process	1.01E-04	7.05E-02	1.85
GO:0097190	**apoptotic signaling pathway**	**1.59E-04**	**1.01E-01**	**27.83**
GO:1900119	**positive regulation of execution phase of apoptosis**	**1.70E-04**	**9.87E-02**	**92.78**
GO:2001272	positive regulation of cysteine-type endopeptidase activity involved in execution phase of apoptosis	1.70E-04	9.11E-02	92.78
GO:1902533	positive regulation of intracellular signal transduction	1.73E-04	8.62E-02	7.23
GO:0065007	biological regulation	1.94E-04	8.99E-02	1.7
GO:0048584	positive regulation of response to stimulus	1.96E-04	8.51E-02	4.36
GO:2001270	regulation of cysteine-type endopeptidase activity involved in execution phase of apoptosis	2.83E-04	1.16E-01	74.22
GO:0030431	sleep	3.77E-04	1.46E-01	8.07
GO:0010648	negative regulation of cell communication	5.56E-04	2.04E-01	4.86
GO:0023057	negative regulation of signaling	5.56E-04	1.93E-01	4.86
GO:0009896	positive regulation of catabolic process	5.68E-04	1.88E-01	10.45
GO:1900117	**regulation of execution phase of apoptosis**	**7.84E-04**	**2.48E-01**	**46.39**
GO:0043153	entrainment of circadian clock by photoperiod	7.84E-04	2.37E-01	46.39
GO:0009967	positive regulation of signal transduction	9.25E-04	2.68E-01	4.46

Table 2-1: GO analyses of Embryo genes within 5kb of a p53 ChIP peak.

Note that the apoptotic program is enriched.

Head Biological Process of genes within 5KB of a p53 peak				
GO Term	Description	P-value	FDR q-value	Enrichment
GO:0032502	developmental process	3.09E-14	5.38E-11	1.95
GO:0044767	single-organism developmental process	7.13E-13	7.09E-10	1.92
GO:0010646	regulation of cell communication	1.14E-10	7.21E-08	2.85
GO:0023051	regulation of signaling	1.14E-10	6.61E-08	2.85
GO:0048856	anatomical structure development	5.48E-10	2.93E-07	2.16
GO:0009653	anatomical structure morphogenesis	7.08E-10	3.51E-07	2.43
GO:0009966	regulation of signal transduction	1.48E-08	6.05E-06	2.72
GO:0009886	post-embryonic animal morphogenesis	2.56E-08	9.38E-06	3.3
GO:0048583	regulation of response to stimulus	2.76E-08	9.60E-06	2.43
GO:0060255	regulation of macromolecule metabolic process	3.64E-08	1.21E-05	1.96
GO:1902531	regulation of intracellular signal transduction	3.68E-08	1.16E-05	3.68
GO:2000112	regulation of cellular macromolecule biosynthetic process	5.31E-08	1.61E-05	2.24
GO:0019222	regulation of metabolic process	5.92E-08	1.71E-05	1.87
GO:0010556	regulation of macromolecule biosynthetic process	6.37E-08	1.77E-05	2.23
GO:0006355	regulation of transcription, DNA-templated	6.50E-08	1.74E-05	2.33
GO:2001141	regulation of RNA biosynthetic process	6.50E-08	1.67E-05	2.33
GO:1903506	regulation of nucleic acid-templated transcription	6.50E-08	1.61E-05	2.33
GO:0035107	appendage morphogenesis	8.89E-08	2.13E-05	3.93
GO:0031326	regulation of cellular biosynthetic process	1.08E-07	2.51E-05	2.17
GO:0009889	regulation of biosynthetic process	1.18E-07	2.65E-05	2.16
GO:0035120	post-embryonic appendage morphogenesis	1.49E-07	3.24E-05	3.98
GO:0007476	imaginal disc-derived wing morphogenesis	1.57E-07	3.31E-05	4.37
GO:0010468	regulation of gene expression	1.69E-07	3.46E-05	2.07
GO:0035114	imaginal disc-derived appendage morphogenesis	2.55E-07	5.08E-05	3.85
GO:0080090	regulation of primary metabolic process	2.79E-07	5.40E-05	1.88

Table 2-2: GO analyses of Head genes within 5kb of a p53 ChIP peak.

Only the top 25 biological processes are shown. p53 binding does not predict transcriptional programs. Hence, there is no overlap between GO terms detected by ChIP-seq and RNA-seq studies (figure 2-7A).

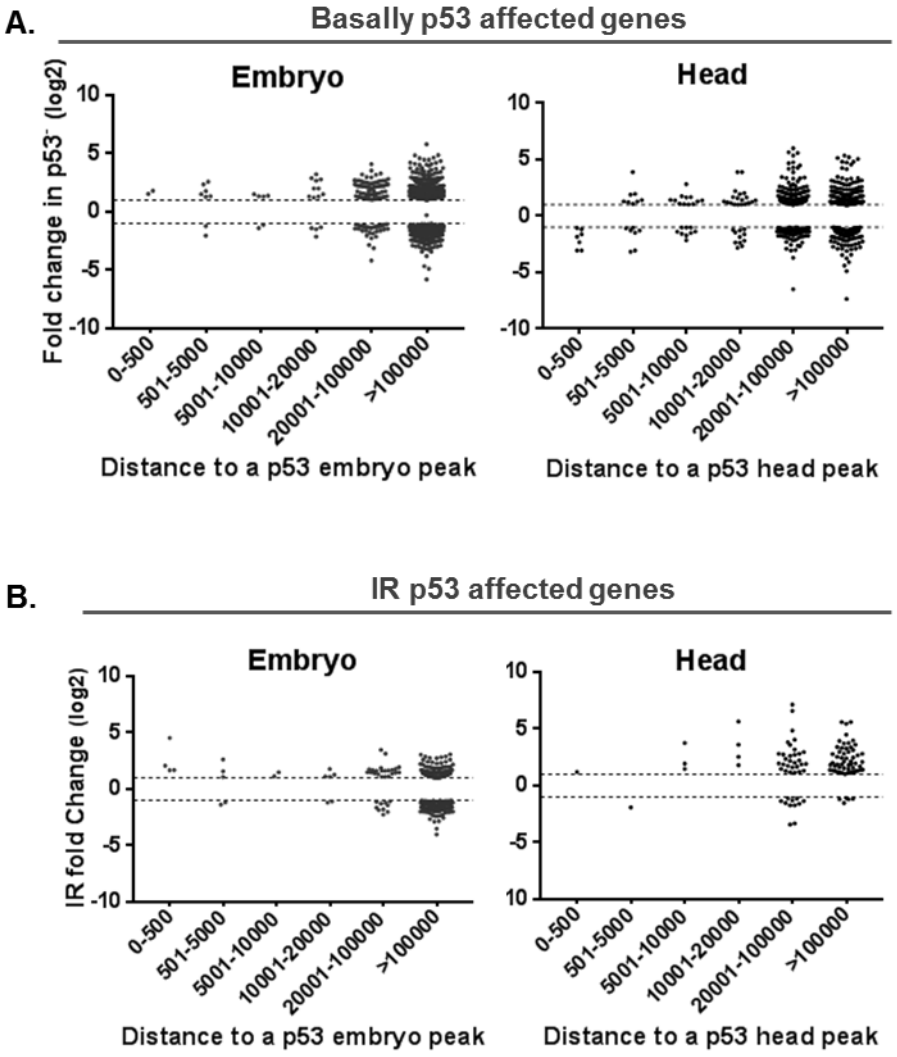

Figure 2-14: Most genes affected by p53 are not near p53 binding sites

A. Distance from TSS of genes basally affected by p53 loss to a p53 enriched region. B. Distance from TSS of genes p53-IR responsive to a p53 enriched region.

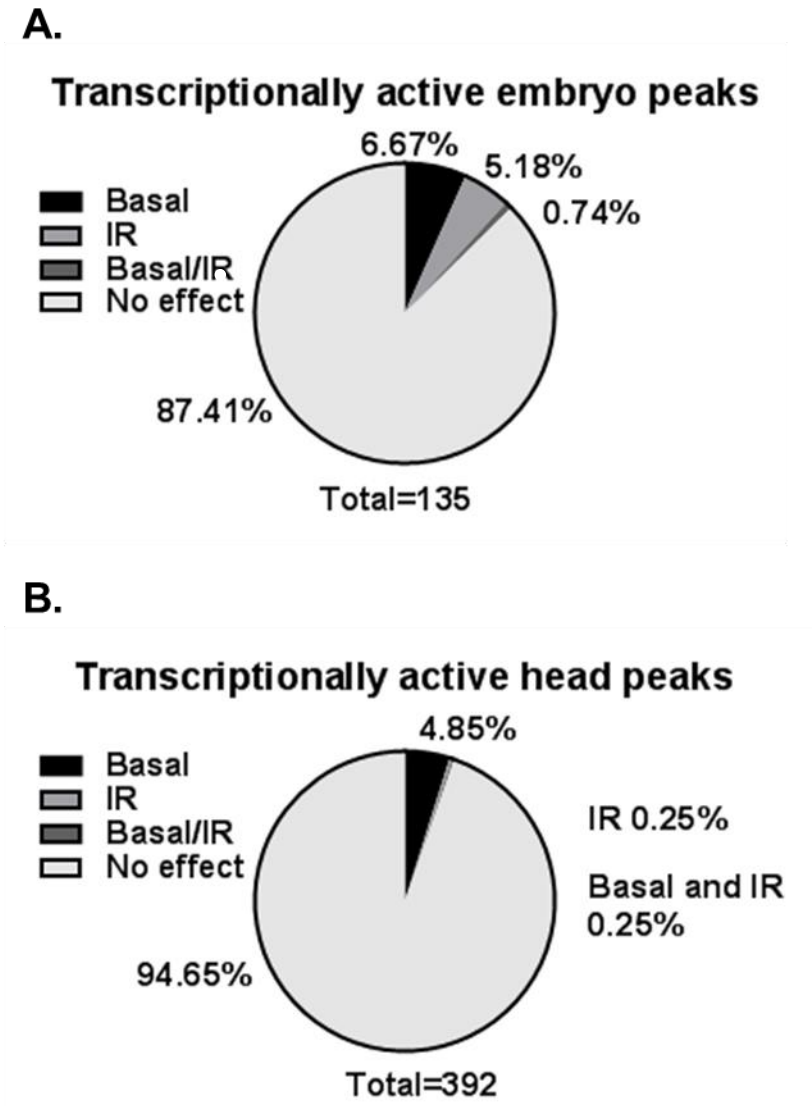

Figure 2-15: Very few p53 peaks exert transcriptional effects in near genes

A-B Percentage of peaks with transcriptional effects in genes within 5kb.

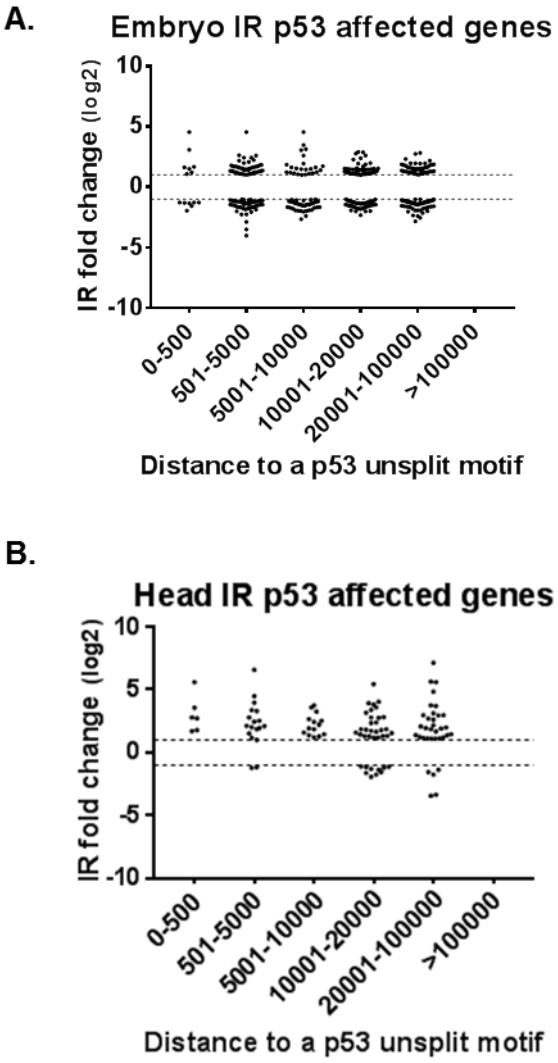

Figure 2-16: Many RIPD genes not basally bound by p53 contain a canonical p53 motif

A-B. Distance from TSS of genes p53-IR responsive to a canonical p53 motif with no space between decameric half sites, in embryos and heads (these unplist binding motifs are associated with IR activation in mouse models (Tonelli et al., 2015).

P-value color scale				
> 10^{-3}	10^{-3} to 10^{-5}	10^{-5} to 10^{-7}	10^{-7} to 10^{-9}	< 10^{-9}

GO term	Description	P-value	FDR q-value
GO:0050830	Defense response to Gram-positive bacterium	3.36E-13	2.11E-09
GO:0009617	Response to bacterium	7.54E-12	2.36E-08
GO:0051707	Response to other organism	3.40E-11	7.12E-08
GO:0043207	Response to external biotic stimulus	4.39E-11	6.88E-08
GO:0009607	Response to biotic stimulus	4.39E-11	5.50E-08
GO:0019731	Antibacterial humoral response	6.49E-11	6.79E-08
GO:0050896	Response to stimulus	5.95E-09	5.34E-06
GO:0006959	Humoral immune response	1.05E-08	8.23E-06
GO:0006952	Defense response	3.05E-08	2.13E-05
GO:0098542	Defense response to other organism	6.93E-08	4.34E-05
GO:0009605	Response to external stimulus	8.71E-08	4.97E-05
GO:0006950	Response to stress	1.17E-07	6.10E-05
GO:0042742	Defense response to bacterium	1.53E-07	7.37E-05
GO:0019730	Antimicrobial humoral response	2.93E-07	1.31E-04
GO:0009408	Response to heat	3.86E-06	1.61E-03
GO:0006955	Immune response	3.92E-06	1.54E-03
GO:0050829	Defense response to Gram-negative bacterium	8.04E-06	2.97E-03
GO:0009266	Response to temperature stimulus	2.36E-05	8.24E-03
GO:0002376	Immune system process	7.49E-05	2.47E-02
GO:0034605	Cellular response to heat	1.65E-04	5.19E-02
GO:0009628	Response to abiotic stimulus	2.45E-04	7.33E-02

Table 2-3: Immune response pathways are upregulated by p53 loss

Genes with expression increased by 2 and above in the p53 null heads were analyzed for GO enrichment (Eden et al., 2009).

Gene	WT	p53-/-	fold change
IM23	9.10	654.56	64.90
TotM	4.60	283.88	50.88
CecA2	13.61	703.62	48.23
AttB	14.58	549.05	35.30
Mtk	15.28	537.90	33.10
AttA	5.06	169.48	28.15
IM2	98.71	2252.43	22.60
edin	20.00	406.54	19.41
CecB	5.14	112.09	18.42
AttD	5.91	100.18	14.64
AttC	46.11	517.20	11.00
IM1	161.35	1624.07	10.01
TotC	79.84	678.24	8.40
Dro	153.88	1087.35	7.03
NimC1	4.26	31.94	6.26
TotB	0.83	9.79	5.90
CecA1	100.34	563.92	5.57
Drsl4	13.49	60.91	4.27
TotA	209.92	854.86	4.06
CecC	85.45	344.17	3.99
PGRP-SC2	59.41	229.22	3.81
Diedel	2.75	13.04	3.75
Drsl5	78.11	225.97	2.87
inaC	150.60	410.17	2.71
TotX	15.69	43.46	2.66
Swim	42.50	105.97	2.46

Table 2-4: Immunity-related genes with increased expression in p53 mutant. Genes associated with immune responses that have increased expression in p53 mutant head tissue.

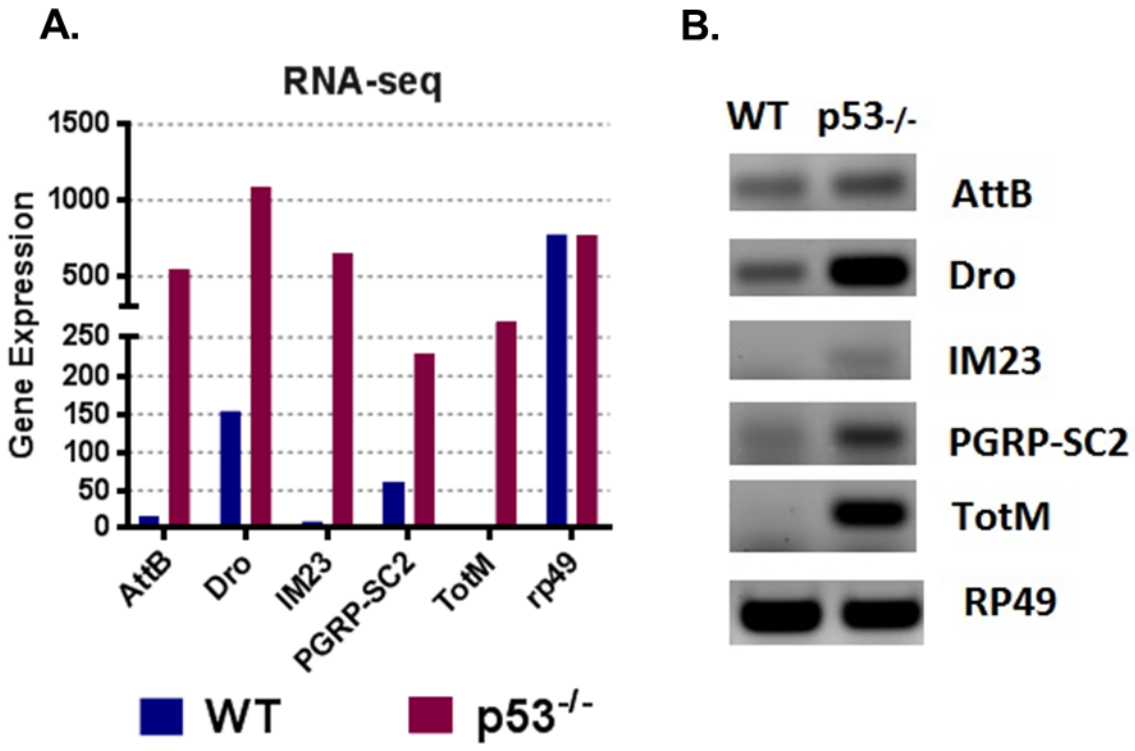

Figure 2-17: RT-PCR validation of increased immune response in p53 null

A. RNA-seq gene expression of immune response genes chosen for validation. B. RT-PCR show increased expression of immune response genes in p53 mutant heads.

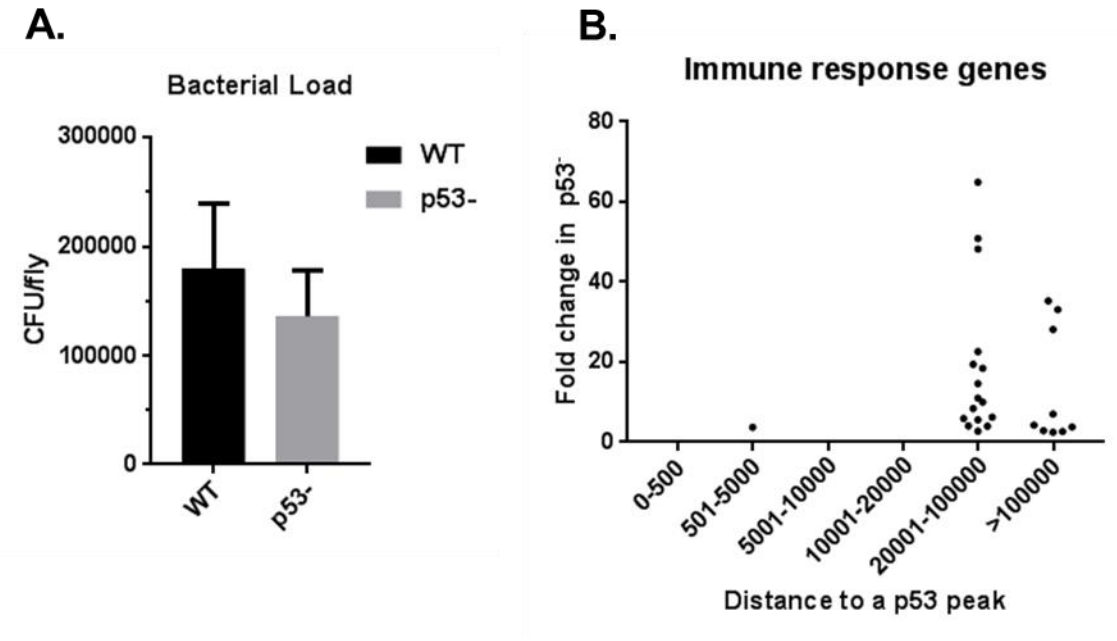

Figure 2-18: No increased microbe growth was detected in p53 null flies

A. Bacterial load assay detects similar levels of microbes in WT and p53 null whole flies. B. Immune response genes are evidently not bound by p53, with the exception of *Diedel* (negative regulator of immune response).

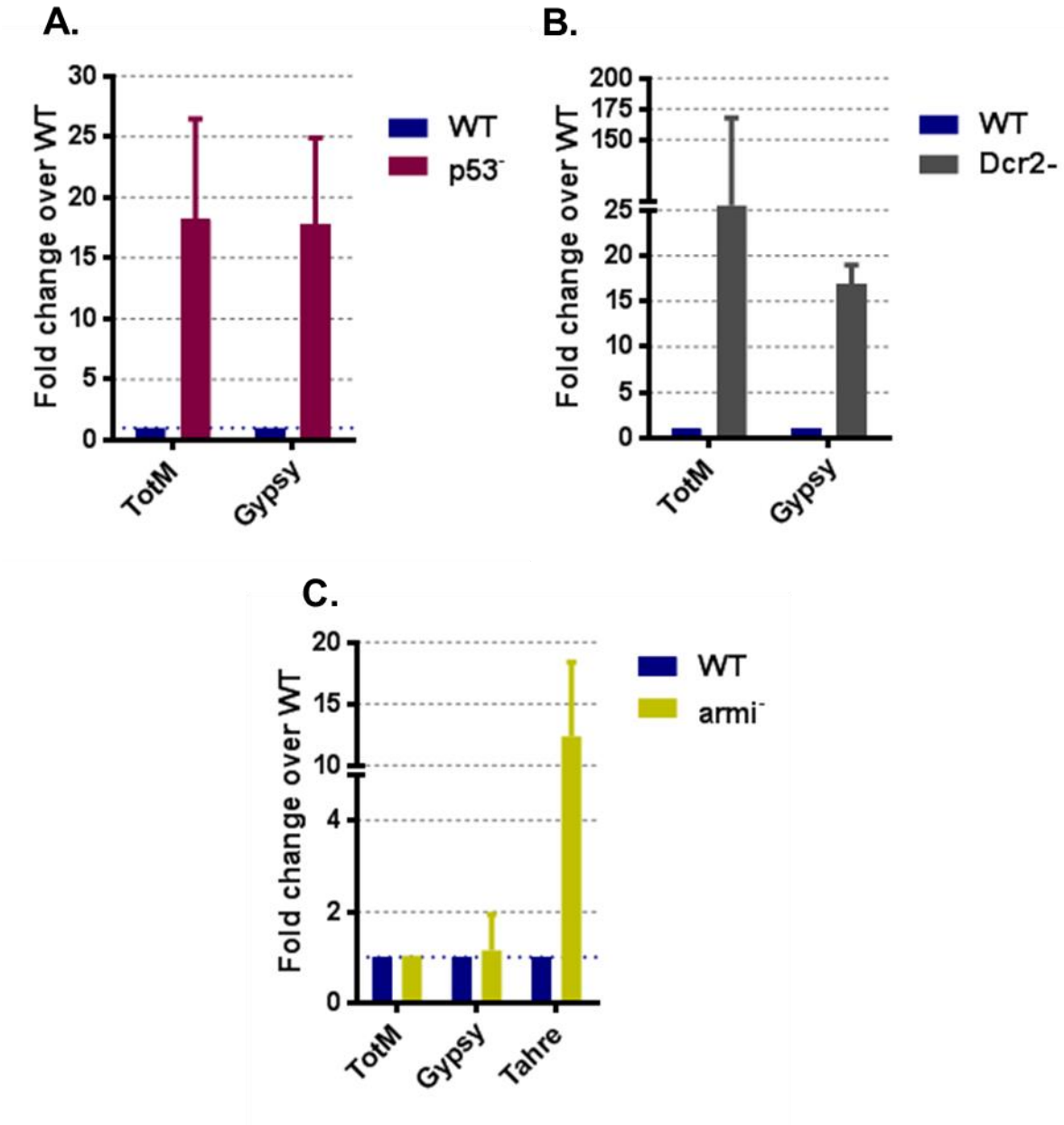

Figure 2-19: *Dicer-2* mutants phenocopy p53 mutants

A-B. RT-ddPCR quantification of dysregulated expression of retroelement *Gypsy* and immune gene *TotM* in p53 and Dicer-2 mutants. C. Armitage mutant does not exhibit dysregulated *Gypsy* or *TotM* but *TAHRE* retroelements are highly elevated in armi nulls.

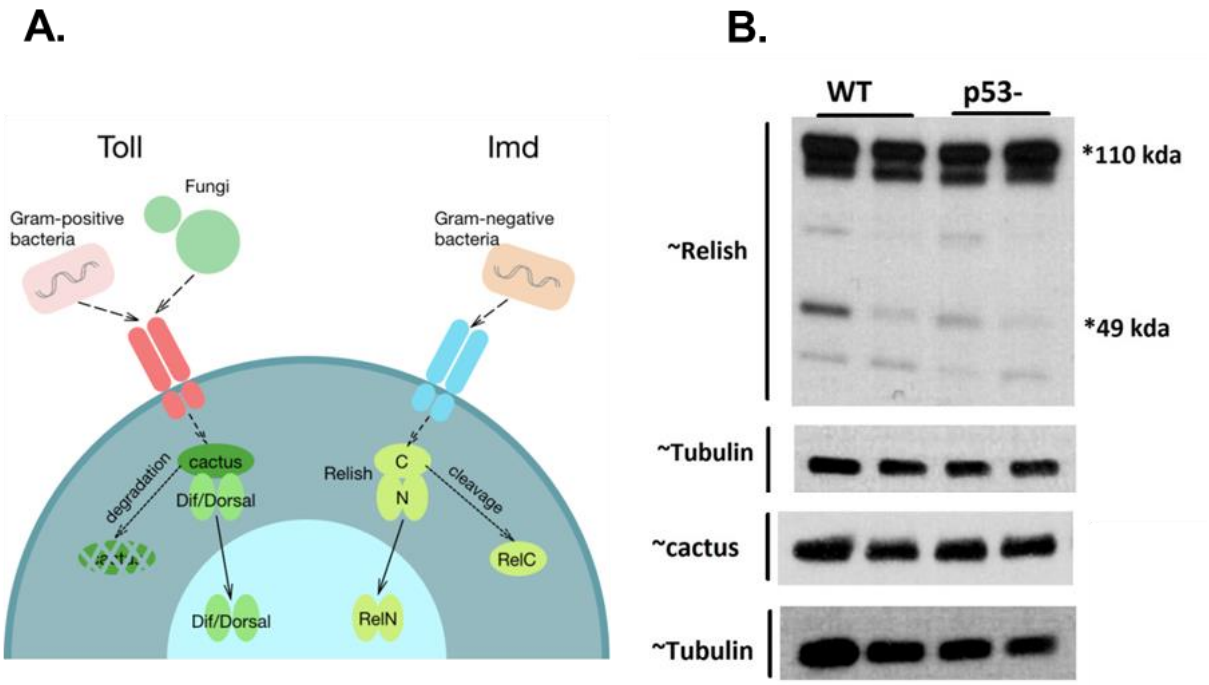

Figure 2-20: NF-kappaB-related proteins are not differentially activated in p53 mutant *Drosophila* heads

A. Schematic of activation of Dif/Dorsal through degradation of Cactus, and Relish activation by cleavage (dashed arrows indicate omitted steps). B. Western blots detected no increase in cleavage of Relish or degradation of Cactus in whole cell extracts from p53 mutants compared to WT heads.

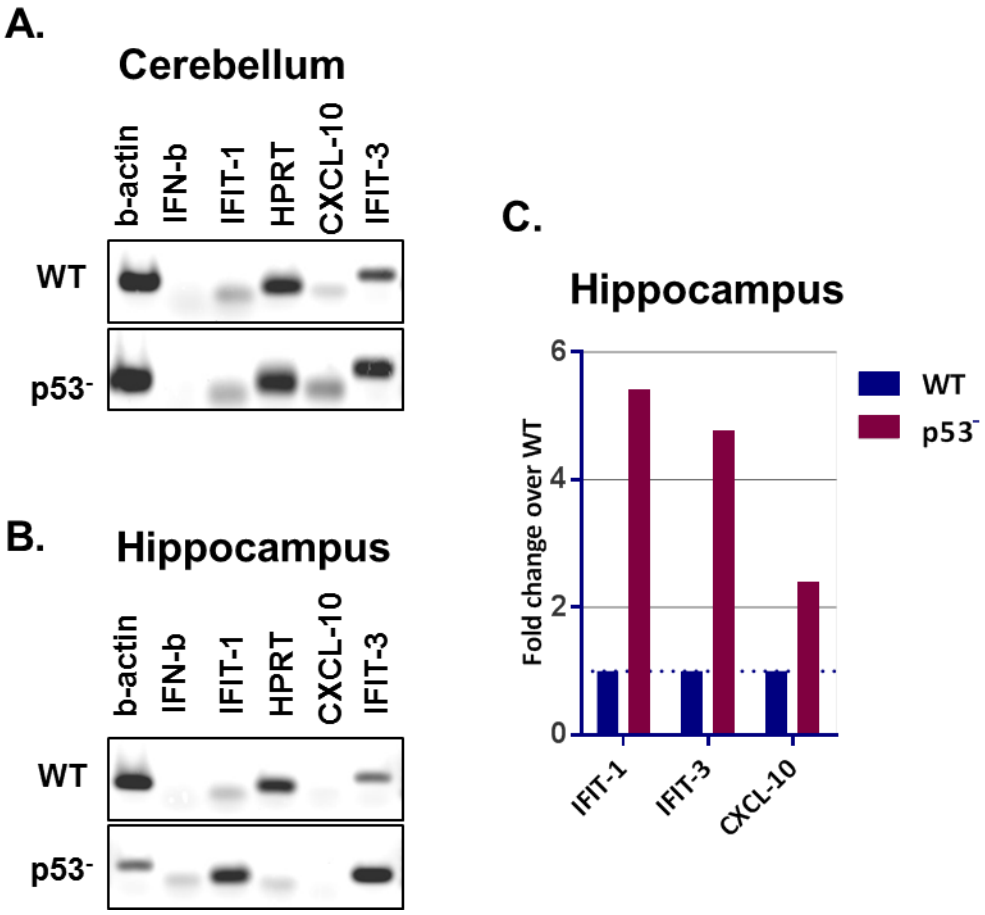

Figure 2-21: Interferon activated genes are elevated in p53 mutant mouse brain
A. RT-PCR detects elevation of interferon responsive genes in cerebellum and hippocampus of a p53 null mouse brain. B. ddPCR quantification of increased expression of interferon activated genes in hippocampus.

DISCUSSION AND RECOMMENDATIONS

p53 stress responses in postmitotic tissue

Here I characterized p53 transcriptional programs in a postmitotic context and contrasted to p53 networks in a proliferative tissue. I demonstrated that in *Drosophila* heads p53 does not activate the canonical stress-response apoptotic program upregulated in embryos. In postmitotic tissue, I observed p53 stress responses focused on DNA repair, metabolism and proteolysis. This is especially relevant considering recent findings that combined abrogation of apoptosis, cell cycle arrest and senescence is not enough to recapitulate early onset tumors observed in p53 mutant mice, indicating that alternate p53 programs are crucial in tumor suppression (T. Li et al., 2012; Valente et al., 2013). Interestingly, I observed conserved p53-mediated DNA repair in both tissues. Furthermore, many of the uncovered novel p53 postmitotic target genes have predicted human orthologs and some are associated with disease, including cancer.

Intriguingly, the predicted human orthologs of several p53 stress-responsive targets uncovered in the *Drosophila* postmitotic tissue are the Kallikrein (KLK) family of serine proteases (alphaTry, BetaTry, *yip7* and *Jon25Bi*). I did not find reports of KLKs being known p53 targets. KLKs dysregulated expression, activity or localization has been associated with carcinogenesis and other pathologies including neurological disease (Kryza et al., 2016). Strikingly, KLK3 (predicted *yip7* and *jon25Bi*) is one of the best known biomarker of prostate cancer, and it is thought to promote cancer evasion to apoptosis through interference in the p53 pathway (Filippou et al., 2016; Niu et al., 2008). Additionally, KLKs have been implicated with other hallmarks of cancer such as, energy metabolism, angiogenesis, cancer invasion and metastasis (Filippou et al., 2016). It would be interesting to test if KLKs are p53 targets in mammals, and furthermore, perhaps in gain of function p53 models KLKs are constitutively activated. Another interesting p53 postmitotic target uncovered by my analyses is *CG3448,* which contains a XRCC4-like domain. In mice, *XRCC4* loss leads to embryonic lethality associated with massive apoptosis of early postmitotic neurons (Yan et al., 2006). A fly

strain containing a p-element insertion in coding sequence of *CG3448* is available; therefore DNA repair function of *CG3448* could potentially be tested using this strain.

Tissue-specific p53 apoptotic response

Previously we had determined that genetic loss of a single p53 enhancer at the cell death gene *rpr* abrogates p53 IR activation of not only *rpr* but also genes far away such as*, hid, skl, ku80, xrp1* and *egr.* We had also shown that the *rpr* enhancer forms long-range chromatin contacts to its targets (Link et al., 2013). Interestingly, in embryos I found p53 binding sites not only at *rpr,* but also *hid, xrp1* and *egr.* Strikingly, in heads, where all of these genes are unresponsive, p53 binding is maintained in all of these sites with the exception of *rpr*. Therefore, p53 binding to *hid, egr* and *xrp1* in heads is not enough to induce p53 target activation at these genes. Interestingly, looping between $p53RE^{rpr}$ *hid* and *skl* are conserved in heads, despite lack of p53 protein binding to $p53RE^{rpr}$ as well as absent IR gene activation. Together, these observations suggest that p53 binding to the $p53RE^{rpr}$ is the tissue specific signal to induce the embryo p53 targets *hid, rpr, skl* and *xrp1*.

It is important to note that I cannot exclude that p53 mediates non-canonical apoptotic responses in *Drosophila* heads. It will be interesting to directly test if any cells undergo apoptosis in brains following IR. I performed pilot studies using acridine orange staining to probe for cell death post IR and determined this technique is difficult to perform in fly brains. Nonetheless, Merlo et al., conducted TUNEL studies in *Drosophila* brains following DNA damage induced by overexpression of *tau* and found that p53 is protective against apoptosis in postmitotic neurons (Merlo et al., 2014).

Basal genome-wide p53 DNA binding landscapes

I examined p53 DNA occupancy at the genome-scale to determine the extent of p53 pre-configured enhancer networks in tissue-specific transcriptional responses. I found that unlike the case study of the *rpr* enhancer, where tissue specific binding correlated with transcriptional regulation, little p53-mediated gene expression can be inferred from p53 DNA binding location. In the developing model, p53 was poised at the p53

apoptotic program, as well as a few top IR induced targets. Strikingly, in the postmitotic context no stress-responsive programs could be predicted from basal p53 binding; only one IR responsive gene was pre-bound by p53. However, genome-wide p53 motif search detected canonical p53 binding sites at ~24% hRIPD genes; therefore *de novo* p53 binding could promote some of the stress-responsive programs. One piece of evidence corroborating this idea, is the kinetics of *ku80* response. In embryos induction of *ku80* can be observed at 1 hour (Brodsky et al., 2004), while in heads *ku80* upregulation was first detected at 3 hours. Nonetheless, p53 DNA occupancy alone was a poor predictor of transcriptional effects in both contexts.

It has been demonstrated that p53 enhancers can act through chromatin looping to promote transcription both in mammalian cells (intra-chromosomal up to 430kb) (Melo et al., 2013), and *in vivo* in *Drosophila* (intra- and inter-chromosomal) (Link et al., 2013). Therefore, long-range p53 enhancer contacts could partly account for the discordance between DNA binding and nearby gene expression effects by p53. I also imagine that not all genes affected by p53 status are direct targets of p53. Finally, I did not examine association of p53 DNA binding and regulation of non-protein coding RNAs, given the established role of p53 in expression of microRNAs as well as lncRNAs (T. C. Chang et al., 2007; Chaudhary & Lal, 2017; Hermeking, 2012), this is an interesting venue to explore.

Interestingly, I detected p53 binding at two known p53 regulatory partners, *corp* and *loki*. *Corp* is a negative regulator of p53 (Chakraborty, Li, Zhou, & Golic, 2015) and it is IR induced in embryos only (data not shown). Intriguingly, modest *corp* upregulation is observed in heads of p53 null animals (~1.8 fold, data not shown), suggesting that perhaps p53 basally represses *corp* in the heads. This observation strengthens the similarity between *corp* and *mdm2. Loki* (check point kinase 2) is an upstream kinase that activates p53 in response to IR in embryos. Interestingly, mammalian *chk2* is negatively regulated by p53 (Tominaga et al., 1999). Reporter experiments suggest the *chk2* promoter contains p53 transcriptional activity, however direct p53 binding appears to not have been reported (Matsui et al., 2004). *Loki* expression is not altered by p53

status in the conditions tested in our studies. Of notice, in heads, gene expression of the other canonical p53 regulatory kinase, grp (chk1) is much higher than loki (data not shown), therefore chk1 could be important in modulating context specific p53 responses in the postmitotic tissue.

Together these genome-wide analyses establish the *Drosophila* head as a functional *in vivo* model for p53 stress responses in postmitotic tissue. It will be interesting to continue exploring these datasets to probe for patterns in chromatin epigenetic contexts for p53 enhancers in each tissue as well as p53 transcriptionally affected genes. There is currently many published ChIP datasets for a variety of histone modifications in *Drosophila* heads and embryos, as well as other regulatory DNA binding proteins (http://www.modencode.org/). Additionally, it will be interesting to contrast intrinsic properties of p53 protein that confer the tissue specific responses, such as post translational modifications and interaction with other proteins.

Inflammation in p53 null *Drosophila* heads

While investigating gene expression under non-stressed conditions, I detected a dramatic activation of immune response genes upon loss of p53 in *Drosophila* heads. Although I cannot completely exclude that these genes are directly repressed by p53, no p53 binding was detected at their promoters. I also have determined that p53 mutant flies are not overtly overgrown with microbes. Corroborating these results, I have data suggesting there is no increase in activation of the two major immune defense pathways against bacteria and fungi (Imd and Toll) in p53 null heads.

One possible explanation for the inflammation I observed in p53 mutant heads is increased expression of retroelements. Firstly, retrotransposon dysregulation is associated with immune responses in other organisms (Mu et al., 2016; Volkman & Stetson, 2014), and secondly, we have recently reported that loss of p53 leads to elevation of retroelement expression (Wylie et al., 2016). Supporting this model, I did detect dramatic increase in *Gypsy* transcripts in heads of p53 null flies (figure 2-17A). Furthermore, I observed that *Gypsy* dysregulation by loss of *Dcr-2* phenocopies

upregulation of the immune defense gene *TotM* detected in p53 null heads (figure 2-17B). Interestingly, upon loss of the piRNA component *armi, TAHRE* retroelement dysregulation was observed, but no *Gypsy* or TotM elevation was observed (figure 2-18). *TAHRE* retrotransposons are involved in telomere maintenance; hence these are co-opted for a beneficial cellular function. Therefore, it is reasonable to speculate that *TAHRE* elements could be less immunogenic. Nonetheless, no direct causative relationship between retroelement elevation and inflammation can be inferred from experiments presented here. *Drosophila* genomes contain dozens of different types of retroelements, and many copies of each are found throughout the genome. Therefore, directly testing if retroelements provoke the inflammation observed in p53 mutants by genetic loss strategies is unfeasible. I believe a more extensive analysis of *Dcr-2,* mutants could help shed light into whether retroelements cause inflammation, combined with studies in mammalian models where there is better characterization of intrinsic cellular responses to retroelements.

ACKNOWLEDGEMENTS

From the Abrams lab, I would like to thank Dr. Amanda E. Jones, for assistance in bioinformatics analyses of RNA-seq and ChIP-seq. Also from our lab, Dr. Annika Wylie, for discussions and protocols in retrotransposon related experiments; Dr. Bhavana Tiwari performed mouse experiment. From the Kraus lab, Dr. Lee Kraus, Dr. Yasmin Vasquez and Dr. Shino Murakami for great assistance in trouble shooting ChIP samples and sharing protocols/reagents for library preparation. From the McDonald lab, Dr. Ray McDonald and Dr. Ana Azevedo facilitated use of high quality equipment for chromatin shearing.

CHAPTER THREE

CHARACTERIZATION OF A P53 ENHANCER CHROMATIN LOOPS IN *DROSOPHILA* EMBRYOS

INTRODUCTION

It is known that regulatory elements can act across large genomic regions. Studies of genome organization have demonstrated that chromosomes arrange in defined territories inside the nucleus (Bolzer et al., 2005; Cremer & Cremer, 2006a, 2006b). Interestingly, microscopy analyses demonstrated that when active, genes loop out of their chromosome domains, (e.g. HoxB and uPA) (Chambeyron & Bickmore, 2004; Ferrai et al., 2010). Early studies of β-Globin mouse models suggested that regulatory elements could act across significant distances to activate genes. Many subsequent *in vitro* and microscopy studies indicated that non-neighbor sequences physically interact to transmit regulatory signal through chromatin looping. These observations instigated the idea that genomic three dimensional organizations are important for gene regulation. However, technical limitations prevented these early studies to conclusively demonstrate that distal genomic regions physically interact *in vivo* (reviewed in (de Laat et al., 2008)).

The development of chromosome conformation capture (3C) in 2002 enabled direct detection of chromatin physical interactions (Dekker, Rippe, Dekker, & Kleckner, 2002). 3C is a molecular approach to detect physical interaction of non-neighboring genomic sites and predict chromatin spatial organization at high resolution. Studies taking advantage of this technique have established at the single locus resolution that non-adjacent sequences can physically interact to mediate gene expression (de Wit & de Laat, 2012). Briefly, physical interactions are cross-linked, the DNA is digested and then ligation of cross-linked interactions is performed at very low concentrations to favor

ligation only between crosslinked complexes. The ligation frequency of two non-adjacent genomic regions can then be detected by quantitative PCR (Dekker, 2006; Dekker et al., 2002).

Recent *in vivo* studies in our lab determined that the well-characterized *Drosophila* p53 enhancer (p53RE^{rpr}) assembles chromatin conformations to directly activate genes in *cis* as well as in *trans* (Link et al., 2013). Strikingly, microarray data suggests deletion of this single enhancer abolishes activation of 75% of high stringency embryo RIPD genes throughout the genome (F. Akdemir et al., 2007; Link, 2011). This data suggests the p53RE^{rpr} is a major regulator of p53 DNA damage responses in embryos. Through 3C and FISH studies we have established that the p53RE^{rpr} physically interacts with three long distance targets, *hid* (~300kb away), *xrp1* (across the centromere) (Link et al., 2013) and *ku80* (different chromosome) (Link, 2011). Corroborating our findings, p53 enhancers in mammalian cells have also been shown to exert long-range function through chromatin looping (Melo et al., 2013). Combined these studies establish that the p53 network functions throughout the genome in three dimensions. This novel layer of p53-mediated gene regulation remains poorly understood and it significantly impacts the way we investigate genetic causes to human disease; mutations in regulatory elements could have effects anywhere in the genome.

In the studies presented in this chapter I sought to extend our understanding of the p53RE^{rpr} looping network and how it transmits multigenic regulation throughout the genome. My experiments were guided by three broad questions: First, can the p53RE^{rpr} form other functional physical interactions genome-wide? Second, is p53 required for genome-wide loop formation? Third, do p53RE^{rpr} target genes localize together in a hub to promote multigenic regulation?

MATERIAL AND METHODS

Fly stocks

Flies were kept at 18 to 25°C and fed standard medium. For 4C studies, two wildtype strains were crossed to produce heterozygous animals (*yw* and w^{1118}). The p53 mutant alleles were also crossed to generate heterozygous ($p53^{5A\text{-}1\text{-}4}$ (Xie & Golic, 2004) and $p53^{ns}$ (Sogame et al., 2003)). For FISH studies wildtype embryos of w^{1118} genotype were used.

Circular Chromosome Conformation Capture (4C)

We adapted a published 4C protocol to *Drosophila* tissue (Gondor, Rougier, & Ohlsson, 2008). A schematic of the 4C technique is depicted in figure 3-1. Four to six hour embryos were dechorionated with 50% bleach and crosslinked with equal amounts of heptane and fixative (2% formaldehyde, 50 mM HEPES pH 7.6, 100 mM NaCl, 0.1 mM EDTA and 0.5 mM EGTA) during 15 minutes at room temperature in the vortex (gentle mixing). Similar steps described in 3C (from chapter 2) were used with the following changes:

a. An aliquot of the sample was taken before and after adding the restriction enzyme to test digestion efficiency. (3C digestion efficiency had been previously optimized(Link et al., 2013))

   I. Digestion efficiency: Aliquots were treated with Proteinase K, at 65°C for two hours, DNA was purified with phenol/chloroform followed by ethanol precipitation. PCR was performed with primers spanning cutting sites around the p53RE bait fragment.

   II. Samples were optimized for at least higher than 70% digestion efficiency in the cut sites probed.

b. The restriction enzyme used with its corresponding buffer was the 4bp cutter HpaII

c. Ligation control: A sample was prepared in parallel in which reverse crosslinking was performed before ligation to control for random ligations.

d. Ligation was performed at 4°C for 3 days (ATP added everyday) with a room temperature incubation of 1 hour before reverse crosslink.

4C PCR amplification

After quality controlling 4C templates (digestion efficiency and PCR testing of known interactions) reverse PCR amplification from the p53RE^{rpr} bait fragment was performed. The first PCR was performed using 300ng of the 4C DNA with Iproof kit from Bio-Rad, in triplicates. Then a nested PCR was performed using column cleaned 1:5 dilution of product from first PCR as the published protocol (Gondor et al., 2008).

Primers:

1st PCR(annealing temperature 59.1°C):

FWD – GAG TAG ACA AAG TCA TCC TTC TCA GAT ACA TGG

REV – GTC CAA AGG CAA TCT TAT CGC CAT ATC AG

Nested PCR(annealing temperature 61.7°C):

FWD – CGT TAA CCA TTT CCT GCA TAG ATT ACT CGT GG

REV – ATC AGT TTT CCG TTC CCC ACC ACT TCA T

Templates were column cleaned and sent to McDermott Center where Illumina protocols were followed for library preparation and Next Generation Sequencing.

4C Bioinformatics

Sequencing read pairs were pre-processed to remove adapters and hpaII upstream sequence from ligation to the bait (p53RE^{rpr}) using Cutadapt (Martin, 2011) and low quality reads or bases removed with Prinseq (Schmieder & Edwards, 2011). Sequence alignment was to the *Drosophila* genome ‘dm6’ using Bowtie2 (Langmead & Salzberg, 2012). The open-source Picard toolkit was used to remove PCR duplicates and

downstream analyses were performed on uniquely mapped reads (Picard, 2017). The number of read pairs mapping to each predicted hpaII fragment were counted. HpaII fragments larger than 600 bp could not be captured by our experimental design, therefore only hpaII fragments within 600 bp were included in downstream analyses. Potential interacting regions were identified using the fourSig R program (window.size = 3, iterations = 1000, fdr = 0.001, fdr.prob = .01, only.mappable = TRUE) (Williams et al., 2014). Mappability was determined based upon hpaII fragment size (<600bp) and MODENCODE drosophila mappability data.

Fluorescence in situ Hybridization (FISH)

Bacterial artificial Chromosomes (BACs) spanning regions of interest were used to create DNA FISH probes using the Invitrogen FISH tag kit (cat# F32951). The manufacturer's protocol was followed using 10µg of input BAC DNA for nick translation (Quantified by Nanodrop) and 6 µl of DNase I. The labeling of Amine-modified DNA with fluorescent dye was extended from 1 hour to overnight, in the dark at room temperature. Probes specificity were validated by testing for single target hybridization sites on larval salivary glands. All BACs used were acquired through BAC PAC resources (https://bacpac.chori.org/) and are listed below:

BAC	Genomic Region
CH322-17A22	p53RE^{rpr}
CH321-80L05	*hid*
CH321-74N02	*ku80*
RP98-44N12	*xrp1*
CH321-63P04	*egr*
CH321-36G22	Control region downstream p53RE^{rpr}

Embryos were dechorionated with 50% bleach, fixed in equal volumes of 4% formaldehyde, 1x PBS solution and heptane during 15 minutes at room temperature in a vortex (gentle shaking). A methanol "cracking" step was preformed to remove vitelline

membrane, and embryos were hybridized with DNA probes according to Drosophila Protocols (Sullivan, 2000).

Microscopy

After hybridization, embryos were mounted in Invitrogen's SlowFade Gold antifade reagent and imaged on a Zeiss LSM 780 confocal microscope with 0.1-0.25µm z-sections. Images were deconvolved using the 3D Blind Deconvolution technique by AutoQuant (Media Cybernetics), and analyzed using Imaris Software. Briefly, the Coloc function was used to identify overlapping signal. Cells containing positive signal from all three probes were manually counted for colocalization using ImageJ cell counter tool.

RESULTS

Characterization of genome-wide chromatin interaction to the p53RE^{rpr}

Previously we exploited biased approaches to test physical interactions between the p53 enhancer at *rpr* and predicted p53 targets. These studies only included a few genes affected by the deletion of the *rpr* enhancer region (p53RE^{rpr}). Through microarray studies we have found that at least 75% of previously reported high stringency p53 IR-activated genes (RIPD) require the p53RE^{rpr} for proper stress response (F. Akdemir et al., 2007; Link, 2011). In addition, it is known that p53 loss affects basal expression of a wide range of genes (F. Akdemir et al., 2007). Interestingly, many of the genes basally affected by p53 loss are developmental, and flies lacking the p53RE^{rpr} have developmental defects (F. Akdemir et al., 2007; Link, 2011). Therefore, I hypothesized that the p53RE^{rpr} loops to additional p53 targets, both stress-response and basal. To determine the full scope of chromatin interactions to the p53RE^{rpr} in embryos I performed a genome-wide variation of the 3C technique, circular chromosome conformation capture (4C) followed by high throughput sequencing (4C-seq) (figure 3-1). Furthermore, I performed 4C-seq in p53 mutant embryos to ask whether p53 protein was necessary for the chromatin architecture assemble to the p53RE^{rpr}.

Looping interactions were determined using the FourSig R program (see methods for details). Briefly, regions with three consecutive mappable hpaII fragments were used to call “peaks” (fragments below 600bp). The average of reads from the three fragments was taken and if this number met the FDR cutoff 0.001 for that chromosome, a peak was called. Unfortunately, while analyzing the 4C data, serious concerns about the data quality came to light. First, the number of regions that were called interaction partners with the p53RE^{rpr} was extremely high, 4468 and 4943 regions in WT and p53 null respectively. When I included only high stringency interactions the number dramatically reduces to 228 in WT and 469 in p53 null (figure 3-2). The parameter for high stringency calls takes into consideration whether reads from one site alone out of the three fragments used to calculate average, accounts for that region meeting the FDR cut off. Second, due to the 4C strategy requiring restriction digestion instead of sonication, it

was difficult to determine reads that came from PCR duplication. Lastly, I was unable to use our benchmark genes that interact with the p53RE^{rpr} due to poor mappability at the known regions of interaction uncovered by 3C and FISH (figure 3-3A). Overall the H99 cell death locus where we have extensively mapped looping by 3C-ddPCR looked similar to what we profiled using 3C-ddPCR assay, however the critical looping region on the promoter of *hid* was not mappable (Link et al., 2013). Similarly, looping at the published p53RE^{rpr} *trans* target *xrp1* was not mappable by the 4C (figure 3-3B). Nonetheless, using only the high stringency interactions, I examined genes affected by p53 basally or in response to IR for interaction around the promoter region (within 2kb of TSS). I found a few potential p53RE^{rpr} looping partners among these p53 regulated genes (table 3-1-2). Most of the interactions were absent in the p53 mutant. While these analyses took place, updated versions of the 4C protocol were published, as I believe, others ran into similar problems; however we decided to hold off until this technique was better established.

p53RE^{rpr} interacts with targets in a pair-wise fashion at higher frequency

We observed a single p53 enhancer that enables p53 to activate gene expression of genes throughout the genome by physical association (Link et al., 2013). Given the multigenic regulation specified by a single p53 enhancer, I hypothesized that this regulation of multiple genes could be accomplished in a transcription factory-like compartment. To test this hypothesis, I conducted three-way DNA fluorescence *in situ* hybridization (FISH) experiments. I expected that if p53 targets associate in a hub, I would detect high levels of three-way physical interaction to the p53RE^{rpr}.

First, I confirmed specificity of the FISH probes by salivary gland hybridization (figure 3-4). One of the long-range p53RE^{rpr} *cis* target is the pro-apoptotic gene *hid.* This target is approximately 300kb from the p53RE^{rpr}. I performed FISH experiments using the p53RE^{rpr} and *hid* probes to test if the resolution of my FISH experiment was sufficient to resolve signal from probes less than 200kb apart. In addition, to establish three-way FISH, I generated a third probe for this pilot experiment. The control probe mirrored the *hid* probe length and distance to the p53RE^{rpr}, except it was downstream from the

p53RE^{rpr} (figure 3-5A). Note that at the single cell level, it is possible to distinguish all three genomic regions hybridized by the three distinct fluorescently labeled probes (figure 3-5B).

After validating the FISH reagents, I systematically measured three-way interactions between the p53RE^{rpr} and two targets at a time. Figure 3-6A shows a schematic of the fly genome and location of the probes I generated. In addition to the *cis* target *hid,* I tested three *trans* targets, *xrp1, ku80* and *egr.* Looping between the p53RE^{rpr} and *xrp1* and *ku80* had already been established (Link, 2011). Random regions of hybridized embryos were imaged by confocal microscopy (figure 3-6B). Detection of colocalization was automated by Imaris Software and only cells containing signal from all three channels were counted. Note that z-stacks taken in the confocal microscope allow detection of true interactions in the three-dimensional space within the nucleus.

Initially I tested p53RE^{rpr} colocalization with looping targets *hid* and *xrp1,* these results are published (Link et al., 2013). Strikingly, I observed that the p53RE^{rpr} can form simultaneous interaction to *hid* and *xrp1* (figure 3-7A). Next, I quantified pairwise interactions and three-way interactions (figure 3-7B). As expected p53RE^{rpr} associates at high frequency, in ~79% of cells, with the *cis* target *hid.* Similar to previous two-way FISH results, interaction between p53RE^{rpr} and *xrp1* were found on average in 38% of cells. Three-way associations were detected at lower frequencies, averaging at 23% of cells. Next, I performed three-way FISH using probes to *trans* targets. Given that *xrp1* is the most robust *trans* target, I kept *xrp1* in experiments with *ku80* and *egr.* Three-way interactions between the p53RE^{rpr} and two *trans* targets were very rare, and similar to frequencies observed with random probes (figure 3-7C-D) (Link et al., 2013). Together, these observations suggest that although the p53RE^{rpr} can form multiple interactions simultaneously, this conformation is not a stable constant chromatin structure.

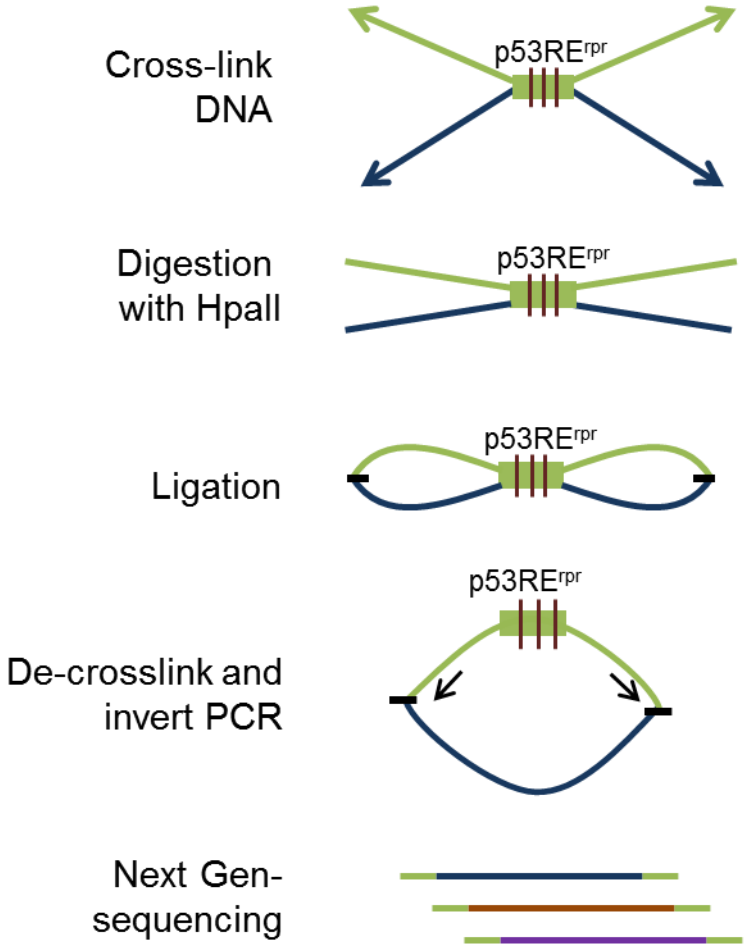

Figure 3-1: Schematic of the 4C-seq technique

Main steps in the 4C technique, I adapted a published 4C protocol to test genome-wide interactions to the p53RE^{rpr} (see this chapter's methods for details) (Gondor et al., 2008).

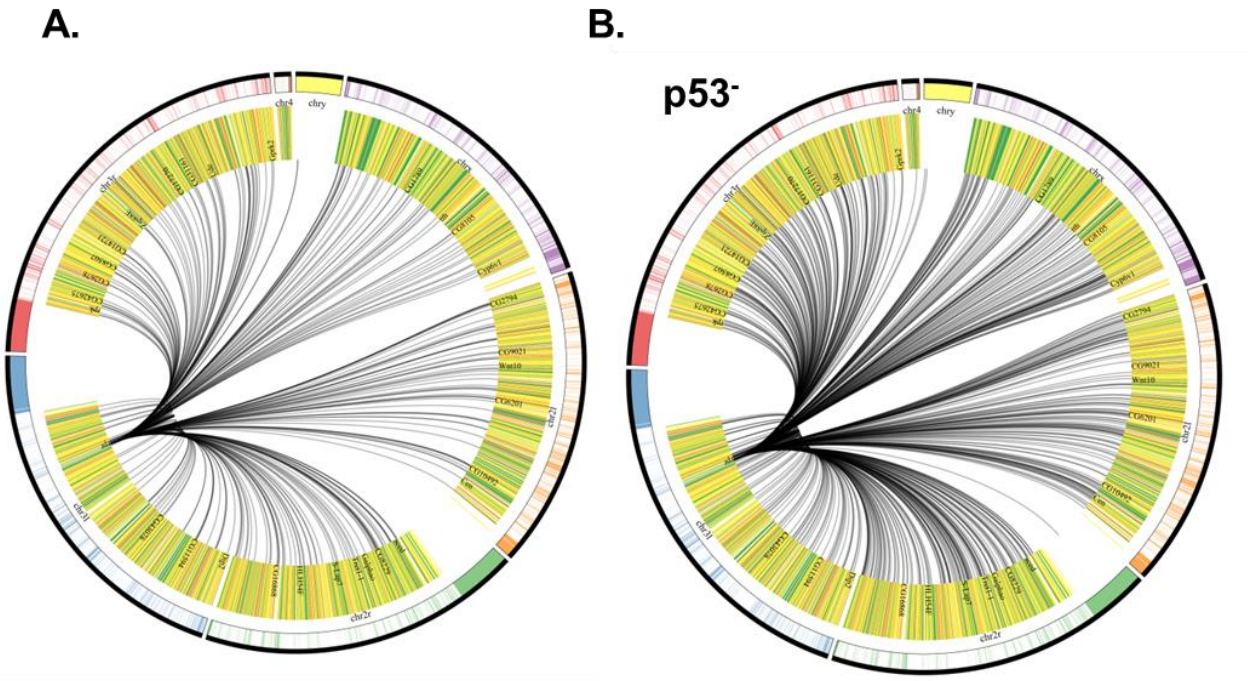

Figure 3-2: High-stringency loops to the p53RE^{rpr}

A-B. Genome-wide interactions uncovered by 4C-seq, in WT and p53 mutant embryos. Green lines represent genes that are p53-IR activated, yellow are unchanged and red genes that are p53-IR downregulated. These results are preliminary given concerns about 4C datasets quality (see results section for details).

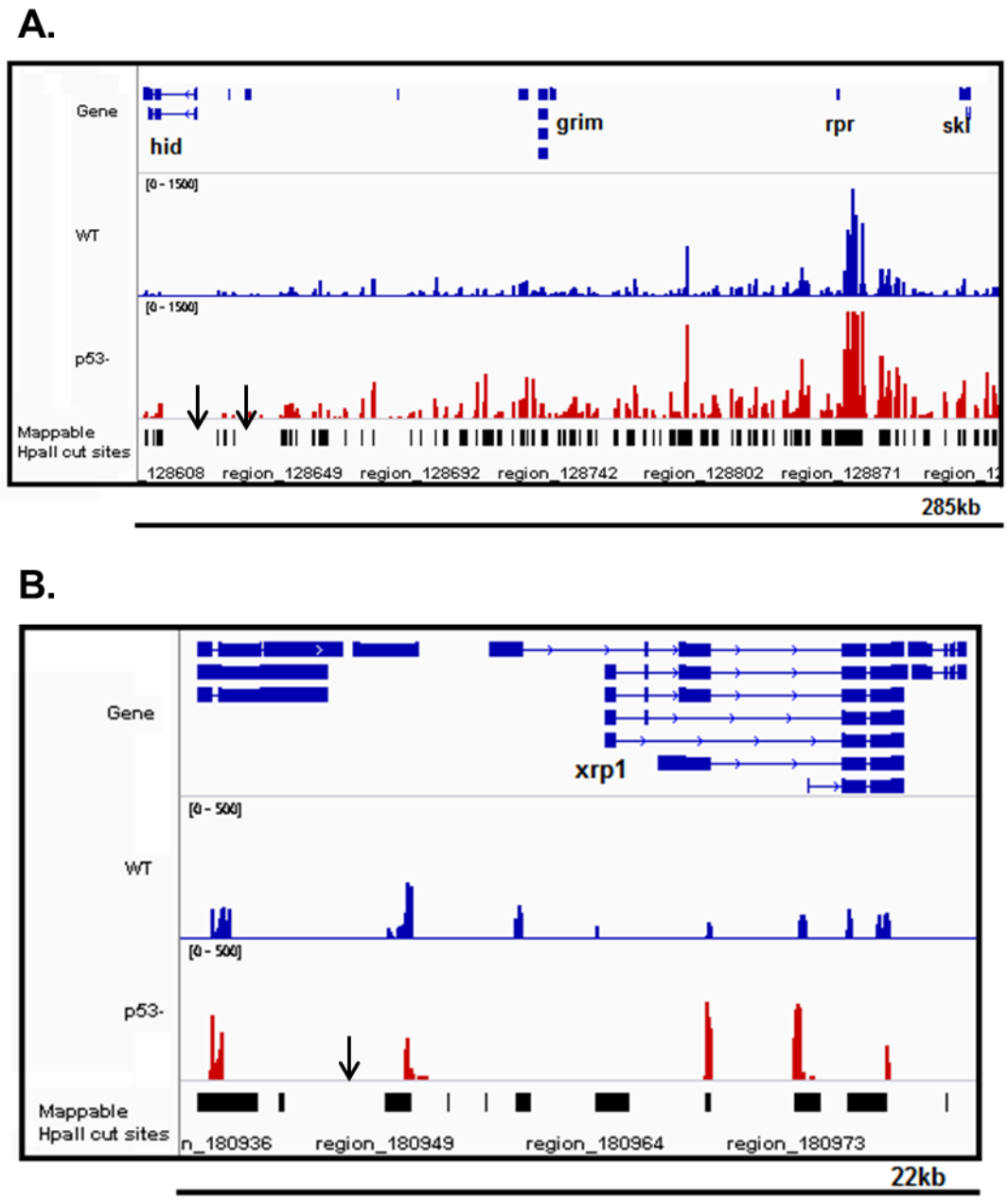

Figure 3-3: 4C profiles at published p53RE^{rpr} targets

A-B. Interaction frequencies determined by 4C-seq in the H99 cell death region and *xrp1* locus. Arrows indicate regions of no mappability where loops have been detected by our published 3C-ddPCR profiling (Link et al., 2013). These results are preliminary given concerns about 4C datasets quality (see results section for details).

	WT				p53-	Gene expression change
Gene Name	Peak Chr	Peak Start	Peak Stop	Peak Distance	Peak Distance	Basal
Zip88E	chr3R	15269422	15271934	761	NO PEAK	DOWN in p53-
Caf1-105	chr2R	10456297	10468238	302	NO PEAK	DOWN in p53-
c12.2	chrX	9319599	9320642	241	NO PEAK	DOWN in p53-
HLH54F	chr2R	17757149	17758546	0	-334	DOWN in p53-
wash	chr2R	12179565	12181369	0	NO PEAK	DOWN in p53-
Tret1-1	chr2R	11670091	11671550	-505	NO PEAK	DOWN in p53-
S-Lap7	chr2R	13781035	13783233	-790	NO PEAK	DOWN in p53-
CG6201	chr2L	11110999	11111372	1689	NO PEAK	UP in p53-
CG1789	chrX	8722071	8723420	1552	NO PEAK	UP in p53-
sced	chr2R	6658832	6660771	1507	NO PEAK	UP in p53-
ftz-f1	chr3L	18755479	18763621	1335	1182	UP in p53-
smg	chr3L	8994143	8995037	1212	NO PEAK	UP in p53-
CG8507	chr3R	9792211	9797187	729	NO PEAK	UP in p53-
rpk	chr3R	4646629	4651659	649	NO PEAK	UP in p53-
CG10492	chr2L	19054618	19059908	541	NO PEAK	UP in p53-
CG2678	chr3R	7914298	7917869	448	NO PEAK	UP in p53-
CG8105	chrX	15587884	15588557	152	0	UP in p53-
CG11594	chr3L	4024593	4025119	150	NO PEAK	UP in p53-
CG14721	chr3R	11735625	11738524	10	NO PEAK	UP in p53-
CG13380	chr3L	18592633	18621223	0	0	UP in p53-
CG8229	chr2R	8949509	8952985	0	0	UP in p53-
CG9021	chr2L	5899265	5905315	0	NO PEAK	UP in p53-
Cyp4p2	chr2R	9235113	9239814	0	NO PEAK	UP in p53-
Galphao	chr2R	10456297	10468238	0	NO PEAK	UP in p53-
Not1	chr2R	9575228	9579475	0	NO PEAK	UP in p53-
Pdk	chr2R	9425432	9428953	0	NO PEAK	UP in p53-
Ude	chr3R	24799076	24801091	0	NO PEAK	UP in p53-
Cyp4p1	chr2R	9235113	9239814	-226	NO PEAK	UP in p53-
c12.1	chrX	9319599	9320642	-376	NO PEAK	UP in p53-
Rme-8	chr2R	9177693	9178464	-432	NO PEAK	UP in p53-
CG16868	chr2R	20287529	20290023	-435	-653	UP in p53-
Cen	chr2L	20682380	20686428	-534	NO PEAK	UP in p53-
Dip2	chr3R	4646629	4651659	-974	NO PEAK	UP in p53-
Gprk2	chr3R	31402751	31404014	-1230	NO PEAK	UP in p53-
CG17270	chr3R	20820200	20821323	-1271	-1271	UP in p53-

Cyp6v1	chrX	20647164	20655394	-1727	NO PEAK	UP in p53-

Table 3-1: Potential p53 basally regulated genes that loop to the p53RE^{rpr}

High-stringency interaction regions (peaks) within 2kb of genes affected by p53 loss basally (from TSS). These results are preliminary given concerns about 4C datasets quality (see results section for details).

	WT				p53^{-}	Gene expression change
Gene Name	**Peak Chr**	**Peak Start**	**Peak Stop**	**Peak Distance**	**Peak Distance**	**IR response**
CG8507	chr3R	9792211	9797187	729	NO PEAK	UP
rpr	chr3L	18392564	18450215	0	0	UP
skl	chr3L	18392564	18450215	0	0	UP
Wnt10	chr2L	7360931	7364945	0	NO PEAK	UP
Prosbeta2R2	chr3R	5220054	5221902	-526	1021	UP
Lcch3	chrX	15916930	15924270	-834	NO PEAK	UP
Cyp6v1	chrX	20647164	20655394	-1727	NO PEAK	UP
Pph13	chr2L	578774	580840	1289	1018	DOWN
tth	chrX	13614666	13615237	1166	NO PEAK	DOWN
CG31161	chr3R	22617338	22619236	828	NO PEAK	DOWN
CG2794	chr2L	564400	565789	238	NO PEAK	DOWN
CG18231	chr3L	18592633	18621223	0	0	DOWN
CG42675	chr3R	5817929	5821117	0	NO PEAK	DOWN
CG43078	chr3L	8574797	8577516	0	NO PEAK	DOWN
Cpr47Ee	chr2R	11261252	11266140	0	NO PEAK	DOWN

Table 3-2: Potential p53 IR regulated genes that loop to the p53RE^{rpr}

High-stringency interaction regions (peaks) within 2kb of genes p53-IR responsive (from TSS). These results are preliminary given concerns about 4C datasets quality (see results section for details).

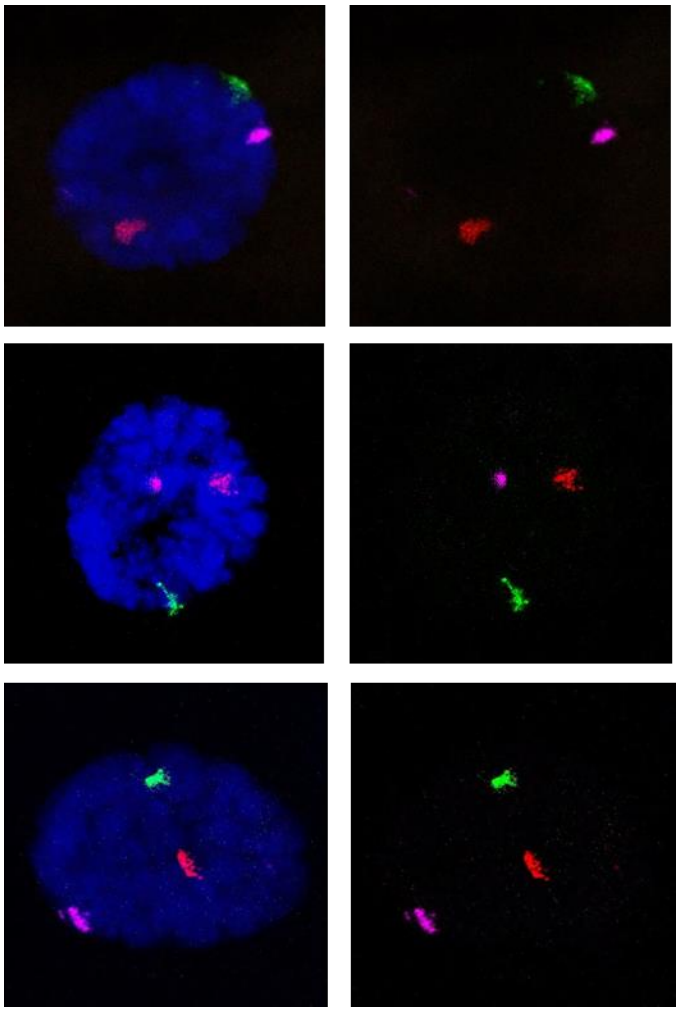

Figure 3-4: DNA FISH probes are unique

DNA FISH probes where hybridized to *Drosophila* larval salivary glands to confirm specificity.

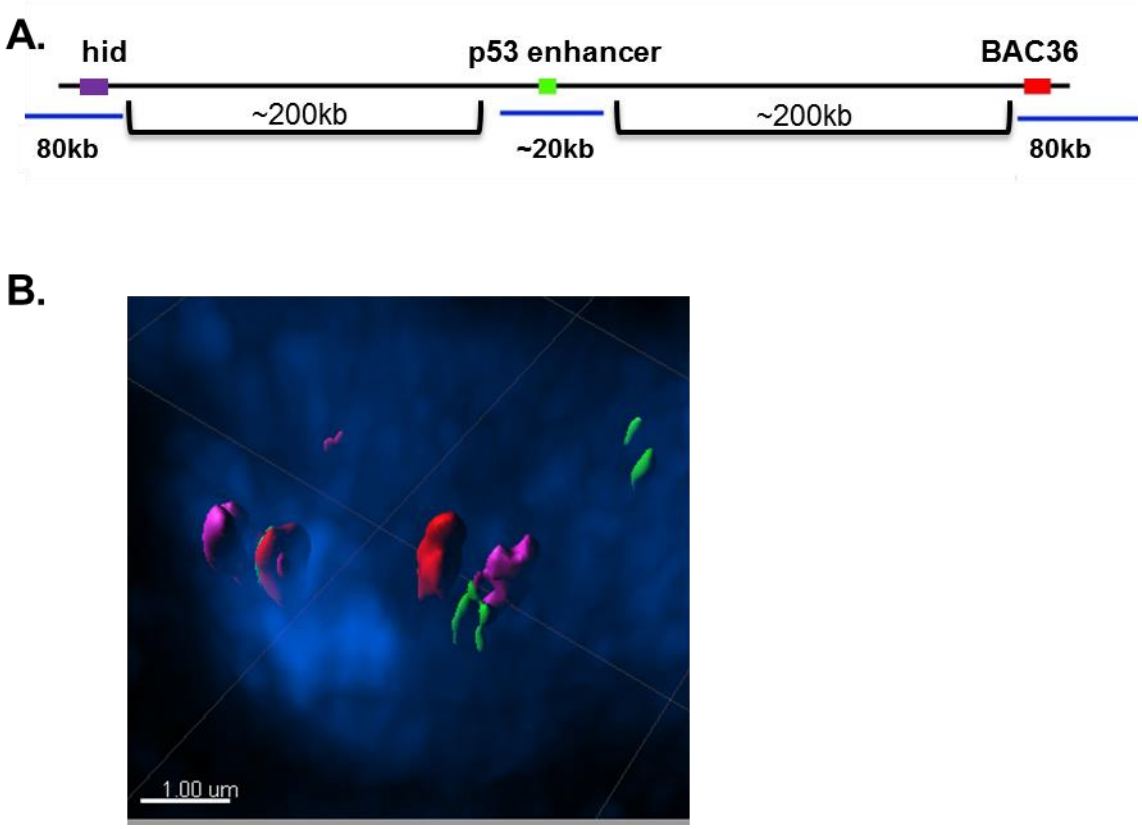

Figure 3-5: FISH probes within 200kb can be separated at the single cell resolution

A. Schematic showing FISH probes location, color and size. B. Nucleus from embryonic cells showing signal from the three probes can be resolved.

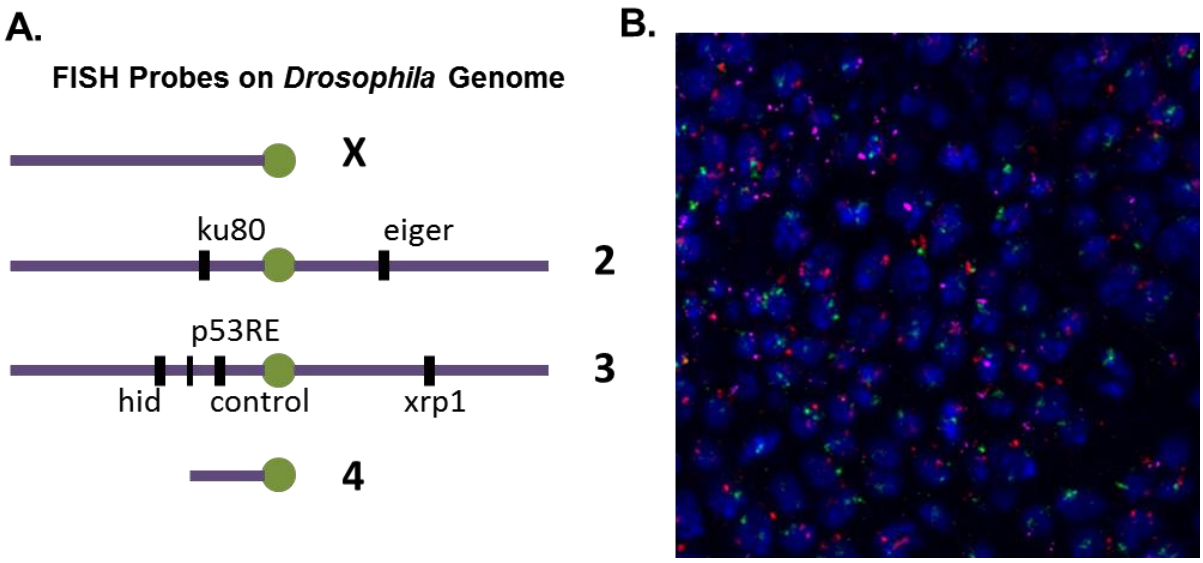

Figure 3-6: *In vivo* three-way FISH in *Drosophila*

A. Schematic showing FISH probes location in the *Drosophila* genome. B. Representative confocal image of *Drosophila* embryos used to quantify three-way interactions.

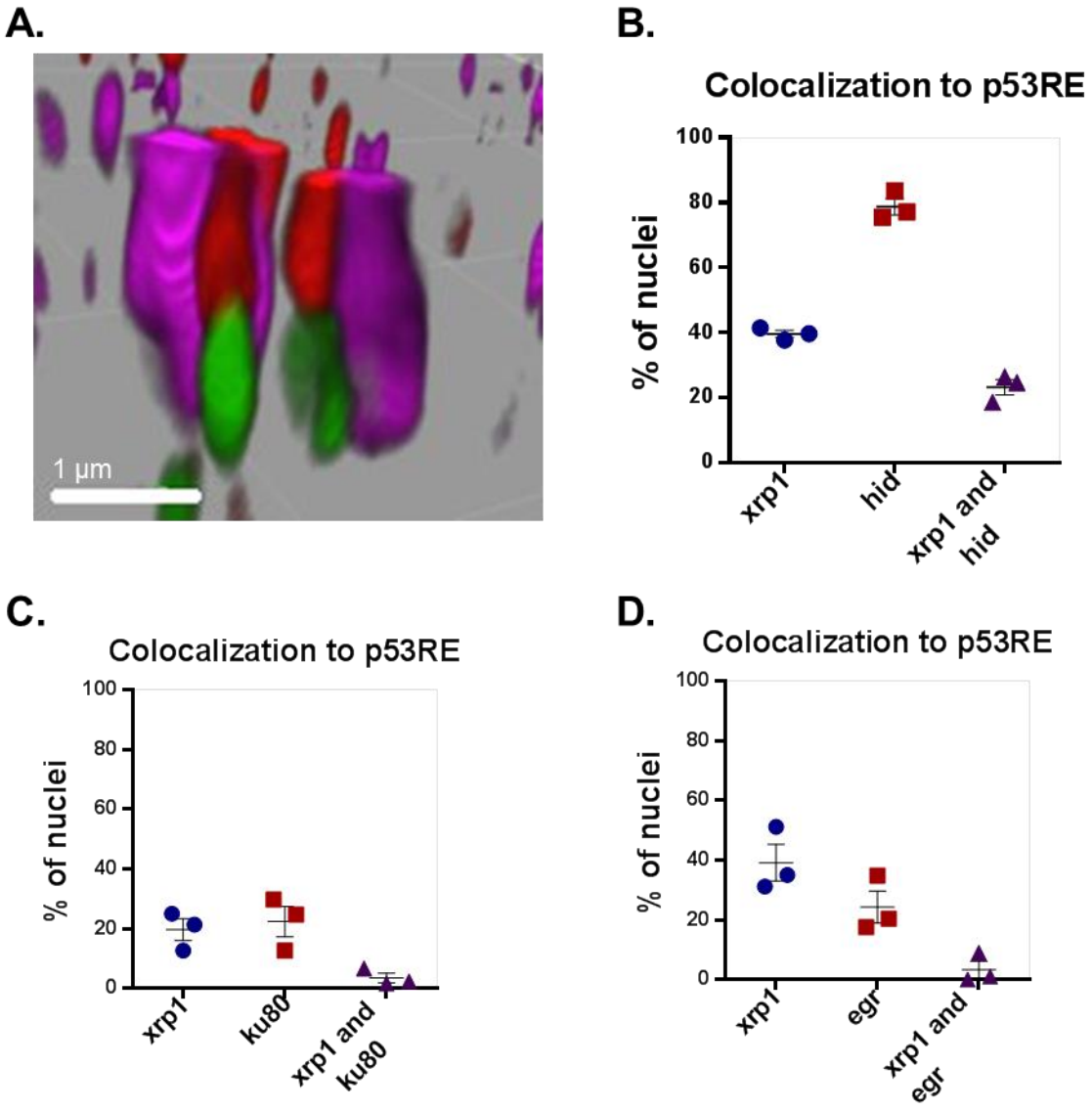

Figure 3-7: The p53RE^{rpr} can form multigenic interactions

A. Three-way interaction between p53RE^{rpr} (green), *hid* (red) and *xrp1* (pink). B-D. Quantification of three-way interactions.

DISCUSSION AND RECOMMENDATIONS

Here I examined the p53 *rpr* enhancer looping network in *Drosophila* embryos. We had previously established that this single enhancer forms chromatin loops to transmit regulatory signals to IR p53 targets (Link et al., 2013). However, many genes affected by genetic removal of this enhancer had not been tested for looping to the p53RE^{rpr} (Link, 2011). I conducted 4C-seq to determine the full extent of long-range interactions to the p53RE^{rpr}. I have identified potential p53RE^{rpr} looping targets among genes transcriptionally regulated by p53. Most of these looping interactions were not detected in the p53 mutant embryos. However, it was hard to confirm biological validity of 4C-seq datasets. Overall, the dataset appeared noisy. This high background issue was observed by others, and modifications of the 4C protocol have been published (Gao, Wei, Lu, & Wang, 2013; van de Werken et al., 2012). One problem is that unlike the simplified schematic of the protocol, the crosslinked complexes form aggregates ("hairballs") that after ligation become too large for the inverted PCR to capture. To fix this problem a second digestion step can be introduced (van de Werken et al., 2012). Another approach recently used to improve this technique replaces enzymatic digestion with sonication, however this makes bioinformatic analyses very challenging (Gao et al., 2013). Nonetheless, the potential p53RE^{rpr} novel interactors identified here can be tested by FISH protocols, and it would be interesting to confirm whether p53 is required to form interactions. Lastly, given the findings from chapter 2, that p53 genome-wide DNA binding is a poor predictor of nearby gene regulation, these genome-wide approaches to characterize p53 enhancers' three dimensional networks could determine whether most p53 binding sites are truly inactive, or simply exerting regulation in faraway genes.

At the single cell level, I determined that the p53 *rpr* enhancer can form multigenic complexes to its target genes; however these associations appear to be low frequency. This suggests that interactions between the enhancer and its targets are dynamic and could change in different contexts, such as different cell types or throughout development. It is important to point out that these experiments were performed with no

stress stimulus. In mouse, globin genes are regulated by dynamic interactions to gene promoters and preexisting transcription factories, which are defined by PolII staining (Zhou et al., 2006). Therefore, perhaps upon genotoxic stress the p53 enhancer and its targets stabilize in multigenic hubs for efficient gene activation. Furthermore, it would be interesting to test if the p53RE^{rpr} looping interactions localize to PolII nuclear foci. In addition, given the heterogeneity of cell types in embryos, this model could be used to test cell-specific looping. This could be accomplished by combining antibody staining and FISH protocols. Lastly, while examining three-way looping between the p53RE^{rpr}, *hid* and *xrp1* as seen in figure 3-7A, I often detected association of *hid* and *xrp1*. Given that p53 enrichment was detected at *hid* and *xrp1* by ChIP experiments described in chapter 2*,* it is reasonable to speculate that perhaps these p53 enhancers at *hid* and *xrp1* form looping conformations that are activated by the p53RE^{rpr}.

ACKNOWLEDGEMENTS

I would like to thank former member of the Abrams lab, Dr. Nichole Link, for great mentorship in the conception of this project as well as at the bench. Also from the Abrams lab, Dr. Amanda E. Jones for 4C-seq bioinformatics. Abhijit Budge and Kate Luby-Phelps with the University of Texas Southwestern, Live-Cell Imaging Facility, for assistance with microscopy.

CHAPTER FOUR

Developing tools to study *Drosophila* p53 protein *in vivo*

INTRODUCTION

As I started my studies in the Abrams lab, one significant barrier to studying p53 in *Drosophila* was the lack of a high quality antibody that could detect native p53 protein *in vivo*. Some success had been made to detect *Drosophila* p53 under overexpression conditions, in cell culture, and in ovaries through immunohistochemistry. However antibodies for other *in vivo* sophisticated protocols were lacking. Additionally, previous lab members have tried to generate p53 antibodies using peptides and were unsuccessful (D'Brot, 2014; W.J. Lu, 2010).

In my main project, described in chapter two, I had found that in postmitotic tissue the p53 canonical apoptotic network was unresponsive. Moreover, I had evidence that the p53 enhancer at *rpr*, which in embryos is a major regulator of p53 stress-response was not functional in heads. This opened exciting opportunities to explore p53 tissue specific programs. To directly test whether p53 engaged the *rpr* enhancer and to uncover postmitotic p53 enhancer networks, p53 chromatin immunoprecipitation studies were necessary.

In this chapter I present two strategies that I explored to detect p53 protein *in vivo*. First, I sought to produce p53 polyclonal antibodies using full length protein as antigen. Second, in collaboration with Hugo Bellen's lab, I tested an eGFP endogenously tagged unpublished strain of *Drosophila* p53 for WT function. While these efforts were taking place, two relevant publications emerged. Zhang et al. produced transgenic *Drosophila* strains which expressed a C-terminal mCherry p53 tag and the equivalent untagged BAC control (B. Zhang, Mehrotra, Ng, & Calvi, 2014). These strains were included in my functional analyses. Second, Merlo et al. published ChIP studies using a polyclonal

commercial antibody (Santa Cruz, d200, anti-Drosophilap53) (Merlo et al., 2014). This antibody had been tested by previous lab members and it did not produce high quality specific signal by western blots. However, given it is a polyclonal antibody, it is possible through time its p53 detection improved. Therefore, I tested the d200 antibody and ultimately used it for ChIP studies presented in chapter two. Nonetheless, I observed promising ChIP signal with the p53 antibodies I generated. Furthermore, I characterized the $p53^{mch}$ as a wildtype p53 allele for many of the p53 functions our lab studies. Lastly, taking advantage of the $p53^{mCh}$ I launched some pilot studies described in this chapter.

MATERIAL AND METHODS

Fly Strains

Flies were kept at 18 to 25°C and fed standard medium. Wildtype strain yw and p53 null p535A-1-4 (Xie & Golic, 2004) were used. p53mcherry and p53Bac transgenic flies (B. Zhang et al., 2014). $p53^{MI01307}$ MiMIC parental line from Bloomington Stock Center (#35102), p53EGFP from (Nagarkar-Jaiswal et al., 2015).

DNA extraction

To genotype flies I extracted DNA using PROMEGA Wizard Genomic DNA purification kit (cat#A1120). Followed by PCR using PROMEGA GoTaq (cat#M7123) and standard gel electrophoresis.

Primers:

Target	Sequence
p53 FWD	CGG AAT CGA GTA CAT CCA AAG A
p53 REV	AGC TGG AAC ATG AAG CTC TAT C
MIL-FWD	GCG TAA GCT ACC TTA ATC TCA AGA AGA G
MIL-REV	CGC GGC GTA ATG TGA TTT ACT ATC ATA C
EGFPdo-Seq-FWD	GGA TGA CGG CAC CTA CAA GAC
EGFPdo-Seq-REV	GTG GCT GTT GAA GTT GTA CTC

Production of p53 polyclonal antibodies

Full length p53 transcript A was amplified through PCR using Bio-Rad's iProof High-Fidelity PCR kit then cloned into pet30A plasmid (figure 4-1). The plasmid containing p53 was transformed into Max Efficiency DH5-alpha competent cells (Invitrogen cat#: 18258012). After selection, plasmid was grown and purified using Qiagen's QIAprep Spin Miniprep Kit. Plasmid was sequenced verified for insertion of p53 as well as sequence accuracy of the p53 transcript, using "seq" primers below. Pet30A-p53 was transformed into BL21 (DE3) (New England Biolabs cat#: C2527I) following manufacture's guidelines. After induction of p53-his expression using 400µM of IPTG,

B-PER Bacterial Protein Extraction Reagent (ThermoFisher, cat# 78243) was used following manufacturer's manual. Most of p53-his was found in the insoluble portion. p53-his was further purified using Ni-NTA agarose resin (ThermoFisher, cat# R90101). Beads were eluted with Imidazole. A lot of protein was left on beads, so a mixture of eluate and beads were sent for injection at Pocono Rabbit Farm and Laboratory. Sera were screened using embryo and head lysates of WT and $p53^{-}$ flies. Summary of strategy (figure 4-4)

Primers:

Target	Sequence
p53transcriptA FWD	GGA ATT CCA TAT GAT GTA TAT ATC ACA GCC AAT GTC GTG GC
p53transcriptA REV	CCG CTC GAG TGG CAG CTC GTA GGC ACG TTT CTT AAG
p53transcriptA seq1 FWD	CAG TGT ATA TTG TGG AAA TGC TCA GGG C
p53transcriptA seq1 REV	CAG GGG GAC TAC AAC GGA AAA ACG CT
p53transcriptA seq2 REV	GTG CCA CGA CAT TGG CTG TGA
p53transcriptA seq2 FWD	AGC CTT AAG AAA CGT GCC TAC G

Cellular lysis

For nuclear lysate, tissue was incubated in hypotonic solution for 15 minutes on ice (10mM Hepes ph 7.9, 10mM KCl, 1.5mM $MgCl_2$, 0.34M Sucrose). Then, mechanic lysis was performed with 3 strokes using loose pestle A douncer. The homogenization was repeated twice with 10 minutes rest on ice between each. Nuclei were spun down at 5,000 rpm for 5 minutes at 4°C. Next, nuclei were resuspended in RIPA buffer (140mM NaCl, 1mM EDTA, 1% Triton X-100, 0.1% SDS, 0.1% Sodium deoxycholate, 10mM Tris-HCl pH 8.0) and incubated on nutator for 10 minutes at 4°C. Lastly, debris was spun down for 5 minutes at 13,000 rpm at 4°C. Nuclear extract (supernatant) was transferred to a clean tube. For whole cell extraction, hypotonic lysis was skipped and

tissue was homogenized in RIPA buffer using an electric pestle motor and disposable pestles. Debris was spun down as described above. Protein was quantified using BIORAD Protein Assay (cat#500-0006) according to manufacturer's instructions with a BSA standard curve.

Western blot

Desired amount of protein lysate was separated by SDS-PAGE and transferred to Immobilon-P membranes (Millipore) using standard wet transfer protocol. Membrane was blocked for 1 hour at room temperature or overnight at 4°C while rocking (5% milk, 0.5% Tween-20, 1xTBS). Membrane was rinsed twice and washed once for 15minutes on rocker (0.2% milk, 0.2% Tween-20, 1xTBS). Primary antibody diluted in 1%milk, 0.2% Tween-20, 1xTBS, was incubated for 1 hour at room temperature or overnight at 4°C on rocker. Membrane was rinsed in wash buffer twice and washed once for 15 minutes on rocker at room temperature. HRP-conjugated secondary antibody diluted in 1%milk, 0.2% Tween-20, 1xTBS was incubated for 30-60minutes on rocker at room temperature. Next, membrane was rinsed twice with wash buffer and washed 3 times 10 minutes each on rocker at room temperature. HRP was detected using enhanced chemiluminescence (Amersham ECL cat#:RPN2232) according to manufacturer's protocol. Membrane signal was capture and developed in GeneMate Blue Autoradiography Film. Lastly, films were scanned and analyzed in ImageJ Software.

Antibodies:

Target	Dilution
Anti-dsRED (Clontech, cat# 632496)	1:500
Anti-GFP (Invitrogen, cat#: A-6455)	1:1,000
Anti-dp53 (Santa Cruz, C11)	1:500

ImmunoHistoChemistry (IHC)

For IR studies flies were treated with 40Gy γ-radiation. Females were fed yeast paste for 1-2 days before dissecting ovaries in 1xPBS. Ovarioles were teased apart without disrupting ovary. They were fixed in 4% formaldehyde PBST solution (1xPBS, 0.1%

Triton-X100) and 3 volumes heptane at room temperature for 15 minutes on a nutator. After fixation tissue was rinsed twice with PBST and washed 3 times with PBST at room temperature 10 minutes each on nutator. Tissue was blocked with PBSTA (PBST, 1.5% wt/vol BSA) for 1 hour at room temperature on nutator. Primary antibody diluted in PBSTA was incubated overnight at 4°C on nutator. Samples were rinsed twice with PBSTA and washed 3 times with PBSTA at room temperature 10 minutes each on nutator. Secondary antibody diluted in PBSTA was incubated for 2-4 hours or overnight at room temperature on nutator protected from light. Samples were rinsed 3 times with PBSTA and washed overnight in PBSTA at 4°C on nutator. Next, samples were stained with Hoechst stain (Life Technologies cat#: H3570, H33342, 2µg/ml in PBST) for 10 minutes at room temperature on nutator. Tissue was washed one last time with 1xPBS for 5 minutes. Lastly, all liquid was aspirated and VectaShield was added for mounting. Alternatively, Hoechst stain was skipped and samples were mounted in VectaShield with DAPI.

Antibodies:

Target	Dilution
Anti-dsRED (Clontech, cat# 632496)	1:1,000
Anti-GFP (Invitrogen, cat#: A-6455)	1:1,000
Anti-p53 25F4 (hybridoma bank)	1:500
Anti-HetA(L. Zhang, Beaucher, Cheng, & Rong, 2014)	1:500
Secondary Alexa-488 (Invitrogen,)	1:250 or 1:500
Secondary Alexa-555 (Invitrogen)	1:250 or 1:500

Microscopy

Tissue was imaged in the digital light microscope or in a Zeiss LSM 780 confocal microscope with 0.1-0.25µm z-sections.

Acridine Orange

Wandering larvae were exposed to 40Gy ionizing radiation. After four hours recovery, wing disks stained with acridine orange were imaged in the green channel of a digital light microscope. Staining was performed with 0.1µg/ml of acridine orange in 0.1 M phosphate solution for 5 minutes. One wash was performed with 1xPBS for 5 minutes after acridine orange treatment. Tissue was mounted in 1xPBS with a support so cover slip did not apply high pressure to the tissue.

RT-PCR and ChIP-PCR

As described in chapter two.

ChIP-ddPCR primers

Target	Sequence
TAHRE 1 FWD	GTT TGA ACC GCG ACG ATA CAA AC
TAHRE 1 REV	AGG TGG TCG GAC GTG GAC AT
TAHRE 2 FWD	CTA CTT CAT CCT GCT GAA GAC ACG C
TAHRE 2 REV	CAG GTA CAT TAG GTG GAA TGC AGT TC
TAHRE 3 FWD	ACT CGG TGC TTC CGT CCT TC
TAHRE 3 REV	TTG CTG GTG GAG GTA CGG AGA
Gypsy 1 FWD	ACC AAC AAT CTG AAC CCA CC
Gypsy 1 REV	GAT TGC GTC AAA GAA GTG TC
Gypsy 2 FWD	ACA AGA CAC TTC TTT GAC GC
Gypsy 2 REV	ACA CTT ATT ACG TGG CCA GA
Gypsy 3 FWD	GTG CCA ACC AAC AAC CAA TG
Gypsy 3 REV	CAG CTA TCC TCG CTT TCG TA

RESULTS

Production of p53 polyclonal antibodies

To generate polyclonal antibodies, I expressed full length his tagged p53 protein in bacteria. We reasoned that since short peptides previously did not produce a strong and specific p53 antibody, the full length protein could instigate a stronger immune response in host animals. First, I amplified full length p53 transcript A using high fidelity PCR. Primers were designed to contain appropriate restriction enzyme sites to permit cloning into pet30A plasmid (figure 4-1A). The plasmid was sequenced-verified for p53 insertion and gene accuracy. Next I transformed the p53-his plasmid into bacteria for large scale expression and protein purification. As seen in figure 4-1B, p53-his protein was efficiently inducible after IPTG in the BL21 cells. After comparing extraction from whole cells and insoluble faction, I determined p53 was enriched at the insoluble portion (inclusion bodies) (figure 4-2A). Denaturing protocols were then used to extract insoluble bacterial protein. A nickel-charged purification resin was used to further purify p53-his protein. p53-his was strongly bound to Ni-NTA beads. I tested multiple elution conditions, including low pH urea and imidazole treatment (figure 4-1B). Imidazole only partially eluted p53, therefore a mixture of eluate and beads bound by p53 was used to inject rabbits for serum production. Purified p53-his was verified by western blot (figure 4-2C). I screened pre-immune sera from guinea pig which had high background in the *Drosophila* tissue (data not shown). Next, I screened pre-immune sera from rabbits and choose two animals for injection (boxed in figure 4-3).

Full length p53-his was injected in rabbits by Pocono Rabbit Farm and Laboratory. Briefly, a 70-day protocol was used, during the first 70 days animals were injected every other week. I screened a small bleed from two rabbits (figure 4-4A-A'). No specific p53 signal was observed at the expected size by western blot. However, serum from both rabbits strongly reacted to purified p53-his. Then, rabbits were injected once a month. After a few bleeds that did not appear to detect p53 in whole cell lysates, I purified the nuclear portion and tested the seventh bleed. I detected promising signal in nuclear embryo lysate; expected size and specific to WT lysates (bleed from rabbit 21 only)

(figure 4-5A). I prepared nuclear lysate from animals expressing tagged $p53^{eGFP}$ and observed the expected shift to larger size (figure 4-5B).

Finally, I tested this bleed in ChIP experiments (protocol in chapter 2). At that time, work published by Mel Feany's laboratory with Harvard Medical School, successfully applied a commercial polyclonal antibody from Santa Cruz (d200) to *in vivo* ChIP protocols (Merlo et al., 2014). Therefore, I compared ChIP experiments with both antibodies in parallel, using their published positive and negative regions (figure 4-6). The d200 antibody pulled down p53 at higher affinity and specificity than the bleed newly generated (PK). Therefore, I used Santa Cruz antibodies in ChIP experiments in chapter two.

Lastly, taking advantage of these optimized ChIP samples and our findings that p53 represses retrotransposons in heads, I tested if p53 is bound to retroelements in *Drosophila* heads. To test this, I designed primers to two mobile elements, *TAHRE* and *Gypsy*. *TAHRE* is a non-LTR retrotransposon from a family of elements that are involved in telomere maintenance in flies (Abad et al., 2004). The last 414bp of the 3'UTR of TAHRE elements have promoter activity, making this region the top candidate for p53 direct repression (Shpiz et al., 2007). I designed primers as shown in figure 4-7A. Although, possible weak enrichment was observed with primer TAHRE 3 (figure 4-7B), later similar experiments with a tagged p53 allele resulted in no enrichment at this region. Another retrotransposon highly dysregulated after p53 loss is the LTR element *Gypsy* (figure 4-8A). Interestingly, promising high enrichment is observed with primer Gypsy 1, which decreases with adjacent primers (figure 4-8B).

p53 intragenic eGFP tag results in a hypomorph p53 allele

Another popular approach to study proteins *in vivo* consists in genetically engineering the insertion of an epitope into its gene. Therefore, the protein of interest will be translated with the addition of the chosen epitope. There are many tags available and certain tags are best suited for specific applications (e.g. live imaging, ChIP, etc.). Initially, I had planned to take advantage of a p53 rescue from our lab, and through

recombineering insert a c-terminal HA tag for ChIP experiments, which would tag all different p53 transcripts. However, the Bellen lab at Baylor College of Medicine, had generated a fly strain containing a fusion $p53^{eGFP}$ protein. Dr. Bellen kindly shared this unpublished strain for my studies.

Previously the Bellen lab generated a collection of fly strains; each containing single insertions of Minos-Mediated Integration Cassette (MiMIC) transposable elements (Venken et al., 2011). Currently, together these fly strains cover 1862 distinct genes (Nagarkar-Jaiswal et al., 2015). MiMIC elements contain a splicer acceptor (SA) sequence followed by stop codons in all three reading frames, therefore, insertions in the correct orientation result in a truncation (Venken et al., 2011). These elements also contain sequences that enable, through Recombination-Mediated Cassette Exchange (RMCE), conversion of the transposable element into an artificial exon that encodes a chosen epitope. Therefore, proteins are tagged in their original genomic locus and remain under the native regulatory sequences, maintaining expression patterns intact. Currently, many strains, generated by the Bellen lab, already containing a tag in various genes are available, as well as tools that can be used with this system; these can be found online (http://flypush.imgen.bcm.tmc.edu/pscreen/rmce/).

Before exploiting the MiMIC generated $p53^{eGFP}$ strain in our studies, I tested whether insertion of eGFP affected p53 WT function in various important contexts. Based on predicted protein structure (Khoury & Bourdon, 2010), the eGFP tag is inserted between p53's transactivation and DNA binding domains (figure 4-9A). After I PCR validated correct insertion of eGFP (figure 4-9B-C), I tested if $p53^{eGFP}$ flies promote known p53 stress-response cellular fates. Specifically, I performed acridine orange staining to detect IR-induced apoptosis in larval wing disks. As seen in figure 4-10A, $p53^{eGFP}$ protein fails to complement p53 null flies for IR-apoptosis induction. Furthermore, $p53^{eGFP}$ homozygous flies are severely defective for IR induction of cell death when compared to WT animals (figure 4-10B).

Next, I performed experiments to test if $p53^{eGFP}$ animals can upregulate canonical p53 gene targets in response to IR (figure 4-11). I measured upregulation of embryonic pro-

apoptotic genes *hid, rpr* and *skl,* as well as *xrp1* (most robust p53 embryonic target), using RT-ddPCR. As seen in figure 4-11A, at 1.5 hour after IR treatment (F. Akdemir et al., 2007), $p53^{eGFP}$ fails to induce *hid, rpr* and *skl,* similar to a p53 null. A modest upregulation of *xrp1* is observed (figure 4-11A). To test if extended recovery time after IR was necessary for $p53^{eGFP}$ mediated stress-response, I measured upregulation of the same targets 2 and 3 hours post IR (figure 4-11B). While in WT target induction is decreasing from 2-3 hours, the $p53^{eGFP}$ shows increased upregulation of *xrp1,* while cell death genes remain unresponsive. These results corroborate that the $p53^{eGFP}$ flies are severely compromised for p53 mediated apoptosis and suggest that $p53^{eGFP}$ can weakly upregulate some p53 targets.

Our lab has uncovered interesting functions of p53 in the *Drosophila* female germline (W. J. Lu et al., 2010; Wylie et al., 2016; Wylie, Lu, D'Brot, Buszczak, & Abrams, 2014). To test if $p53^{eGFP}$ protein is expressed in similar patterns as WT protein in *Drosophila* ovaries, I performed immunohistochemistry. I observed similar nuclear foci, as seen in WT ovaries (figure 4-12). However, the $p53^{eGFP}$ allele appeared stabilized (higher expression) in comparison to WT. I did not rule out that this difference was mainly due to antibody quality. Lastly, I checked if $p53^{eGFP}$ can restrain retrotransposon expression in ovaries similar to WT (Wylie et al., 2016). I observed highly expressed TAHRE transcripts in both the $p53^{eGFP}$ and the parental p53MiMIC line, similar to a p53 null allele (figure 4-13). Based on the location of the Minos transposable element, the p53MiMIC parental line is most likely a p53 truncation, lacking the DNA domain as well as the oligomerization domain. The results of these experiments establish that the $p53^{eGFP}$ is a p53 mutant allele and therefore not suited for studies of WT p53 function.

$p53^{mCh}$ fusion behaves close to WT p53 in multiple contexts

Zhang et al. generated a p53 tagged *Drosophila* strain by recombineering mCherry sequence in the c-terminus of the p53 gene in a 24Kb genomic BAC (B. Zhang et al., 2014); similar to the approach I had initiated. Both the tagged and untagged constructs were injected in flies containing a specific “landing” site in the second chromosome of the fly genome, ensuring that both transgenes would be located in the exact same

genomic region ($p53^{mCh}$ and $p53^{Bac}$). These flies were then crossed into a p53 null background and validated for functional IR induced apoptosis as well as protein binding to the $p53RE^{rpr}$ (B. Zhang et al., 2014). I confirmed that both $p53^{Bac}$ and $p53^{mCh}$ promote robust apoptosis in larval wing disks in response to IR (figure 4-14).

To establish $p53^{mCh}$ functions as WT p53 in *Drosophila* ovaries, I crossed $p53^{mCh}$ flies to our published p53 reporter strain (W. J. Lu et al., 2010; Wylie et al., 2014). The reporter contains GFP protein under the control of 150 bp spanning the known p53 response element from *rpr* ($p53RE^{rpr}$). Upon IR, I observed robust reporter activation in the germline stem cells (snake eye phenotype), as seen in WT flies (figure 4-15) (Wylie et al., 2014). To determine $p53^{mCh}$ protein localization, I again, performed immunohistochemistry in ovaries. I also included IR treated ovaries as a pilot experiment, because p53 protein expression and localization after IR is unknown in ovaries. As expected, $p53^{mCh}$ appeared to form nuclear foci similar to WT (figure 4-16A). Interestingly, at 15 minutes post IR treatment, I observed possible p53 stabilization at the stem cells, the 2A-2B region (where p53 is activated in response to meiotic recombination DSB) and randomly throughout the ovarioles (figure 4-16B).

Next, to confirm $p53^{mCh}$ forms robust nuclear foci in the female germline, I stained again ovaries with dsRED and performed confocal microscopy. This time as a pilot experiment, I included an antibody to the retrotransposon Het-A, which is highly upregulated in p53 null ovaries. $p53^{mCh}$ exhibits robust WT-like nuclear foci in ovaries (figure 4-17A). Although Het-A antibody staining appeared noisy, as shown in figure 4-17A, a nuclear containing high Het-A signal correlated with increased p53 protein foci. This association needs to be quantified and validated with cleaner Het-A staining. Note that in later egg chambers (figure 4-17B), $p53^{mCh}$ is expressed in nurse cells as well as in the presumptive oocyte, at similar levels. Finally to test $p53^{mCh}$ for retrotransposon repression, I performed RT-PCR in ovaries and heads. Both $p53^{mCh}$ and $p53^{Bac}$ rescue p53 retroelement repression close to WT levels in ovaries and heads (figure 4-18A-B).

In chapter two, I explored novel functions of p53 in postmitotic tissue (heads). To perform ChIP-seq studies I had to overcome two barriers, first, I had to obtain a high

quality antibody, and second, I had to optimize ChIP protocols in the head tissue, which proved to be a challenging tissue to work with (in part because of the fly cuticle). While ChIP protocols appeared to not work with both my antibody and the published d200 antibody, I decided to check my ChIP protocol using the $p53^{mCh}$ flies, which were validated by Zhang et al. for binding to the $p53RE^{rpr}$ in embryos (B. Zhang et al., 2014). Working with this validated strain and the dsRED ChIP-published antibody enabled me to adjust my ChIP protocols. By "ChIPing" $p53^{mCh}$ flies I arrived in a working protocol, seen in figure 4-19A, I detected p53 binding to a published positive region (p53 gene promoter) and no signal at a negative region (p53 gene 3'UTR). Furthermore, I had the first indication that p53 binding to the $p53RE^{rpr}$ is lost in *Drosophila* heads. Given that $p53^{mCh}$ flies repress TAHRE retrotransposons in heads, I tested $p53^{mCh}$ enrichment at TAHRE. As observed in later experiments with native antibodies (described in the first part of these results), I did not detect robust $p53^{mCh}$ binding to TAHRE. *Gypsy* repression and binding was not checked in the $p53^{mCh}$ flies.

As described in chapter two, the *Drosophila* head is a promising system to study postmitotic function of p53. In mammalian systems upon stress p53 protein is stabilized accumulating at high levels, and the basal expression is very low/undetectable. In flies, little is known about how p53 protein levels are regulated, basally or in response to IR. To determine p53 expression patterns in heads, basally and upon IR, I performed western blots and immunohistochemistry (figure 4-20A-B). I was able to detect p53 basally both by western and IHC, and upon IR protein levels appeared to increase. However protein loading was not similar enough to determine if p53 protein is upregulated upon IR.

To test $p53^{mCh}$ potential for live cell tracing, I imaged $p53^{mCh}$ embryos live in the confocal microscope (figure 4-19). Highly specific mCherry signal was observed both in mid-stage embryos, as well as early embryos (including the pole plasm). Note that signal from the red channel is completely absent in embryos from $p53^{Bac}$ control.

Lastly, also in Zhang et al., it was demonstrated that a monoclonal commercial antibody from Santa Cruz (c11) detected native p53 in western blots. To confirm the specificity

and further explore p53 basal and IR protein levels, I performed western blots in heads and embryos (figure 4-22A-B). In both tissues, the c11 antibody produces robust, specific signal (validated by loss of signal in the p53null). Interestingly, at the corresponding time points when p53 target activation is observed in each tissue, p53 protein appears to be more abundant than in lysates from animals not treated with IR. These studies should be repeated with biological replicates and a time course after IR to definitively answer this question.

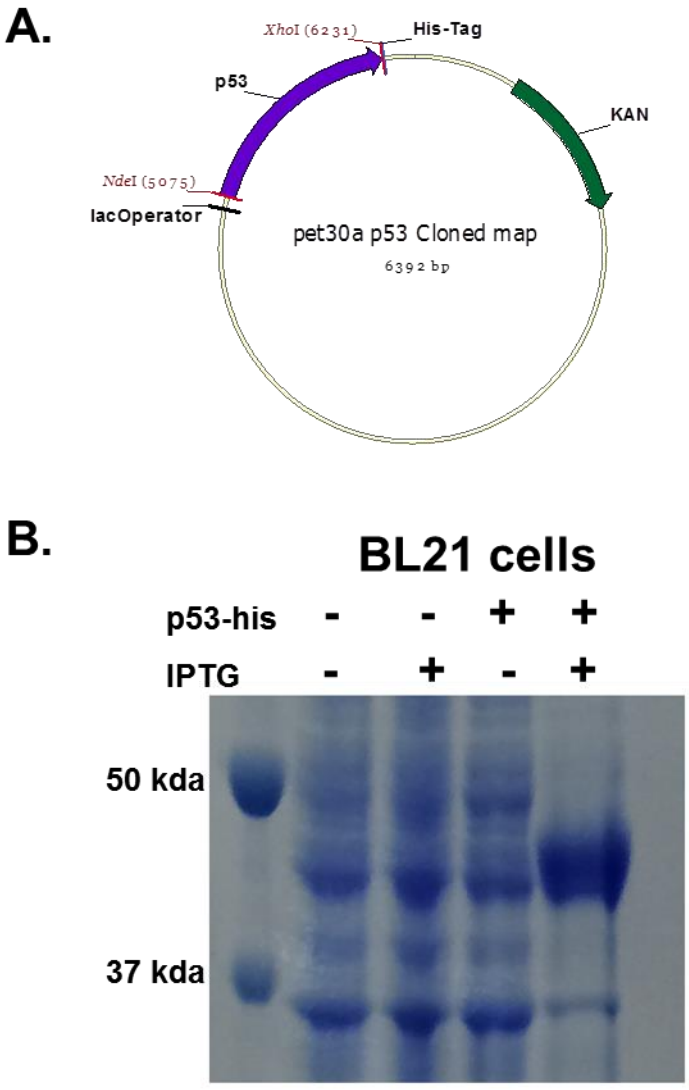

Figure 4-1: *Drosophila* p53 in bacterial expression system

A. p53 transcript A was cloned into pet30A vector, lac operator allows inducible expression in bacteria. Kanamycin resistance for selection. p53 is expressed tagged with his for purification. B. SDS-PAGE stained with coomassie blue confirms p53-his is well inducible in BL21 cells upon IPTG treatment.

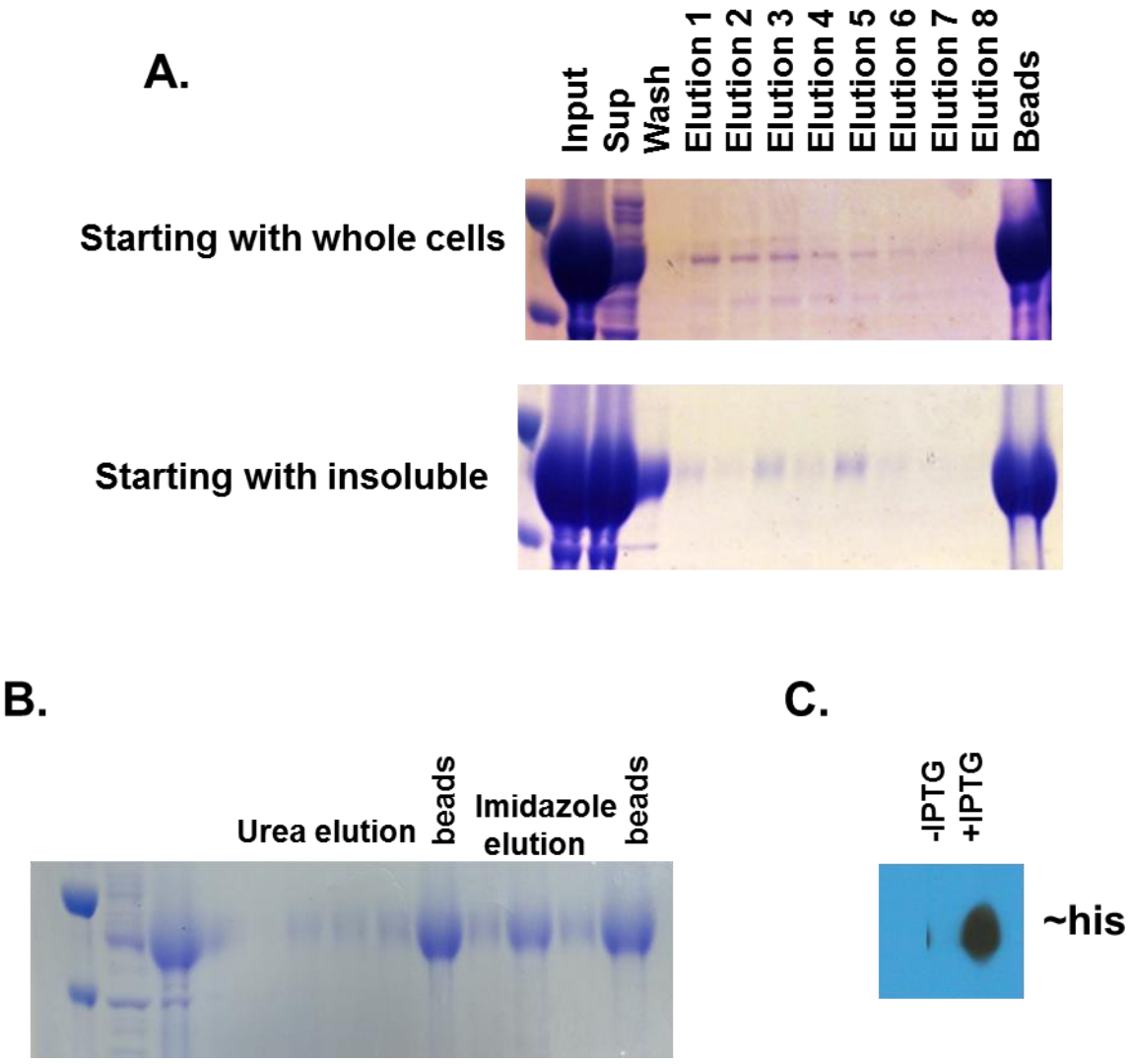

Figure 4-2: p53-his purification

A. p53-his highly enriched in inclusion bodies (insoluble). B. p53-his is tightly bound in Ni-NTA beads; imidazole elutes beads more efficiently than urea. C. Western blots with anti-his antibody confirms p53-his purification.

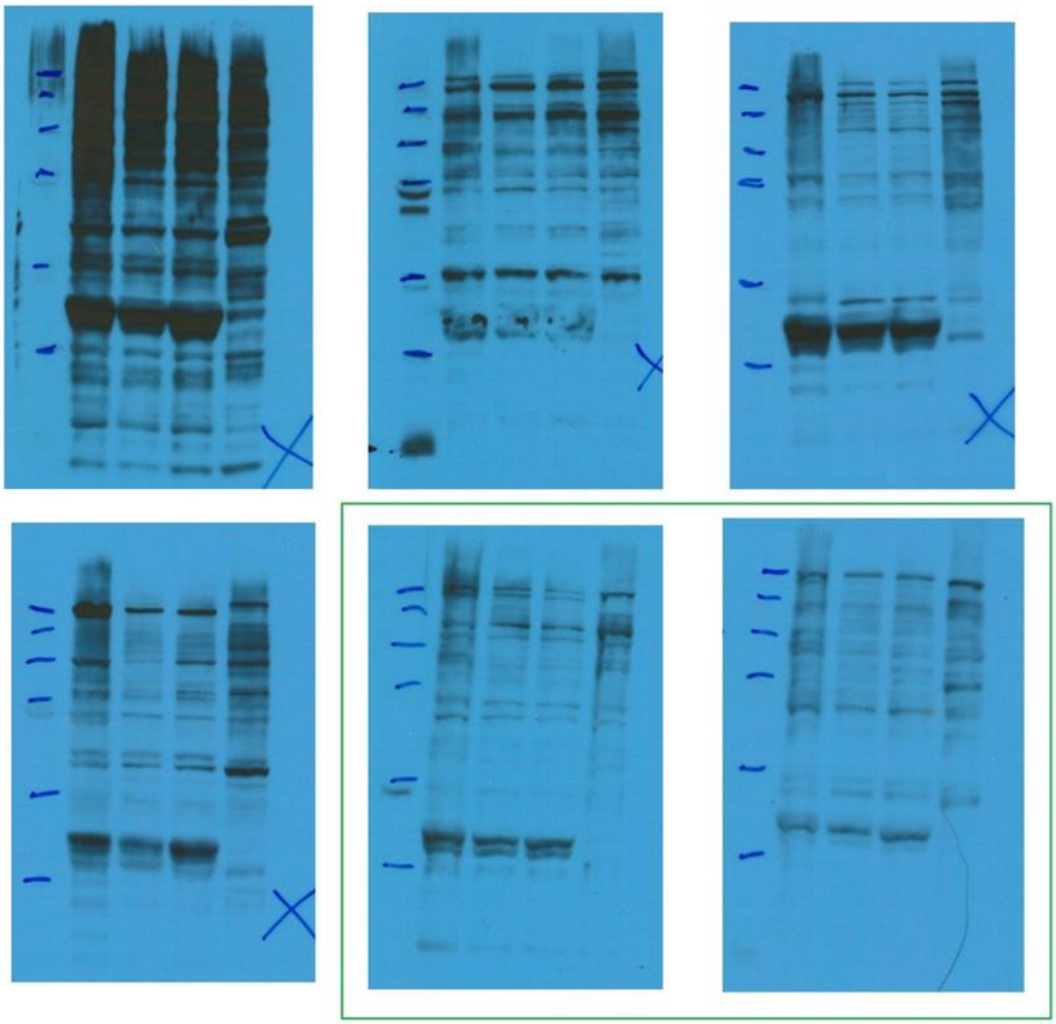

Figure 4-3: Pre-immune screening of six rabbits

Western blots using pre-immune sera from six rabbits on *Drosophila* whole cell protein extracts (lane 1-embryos, lane 2-3-heads, lane 4 -Kc Cells). Boxed in green are the selected rabbits, 21 and 22.

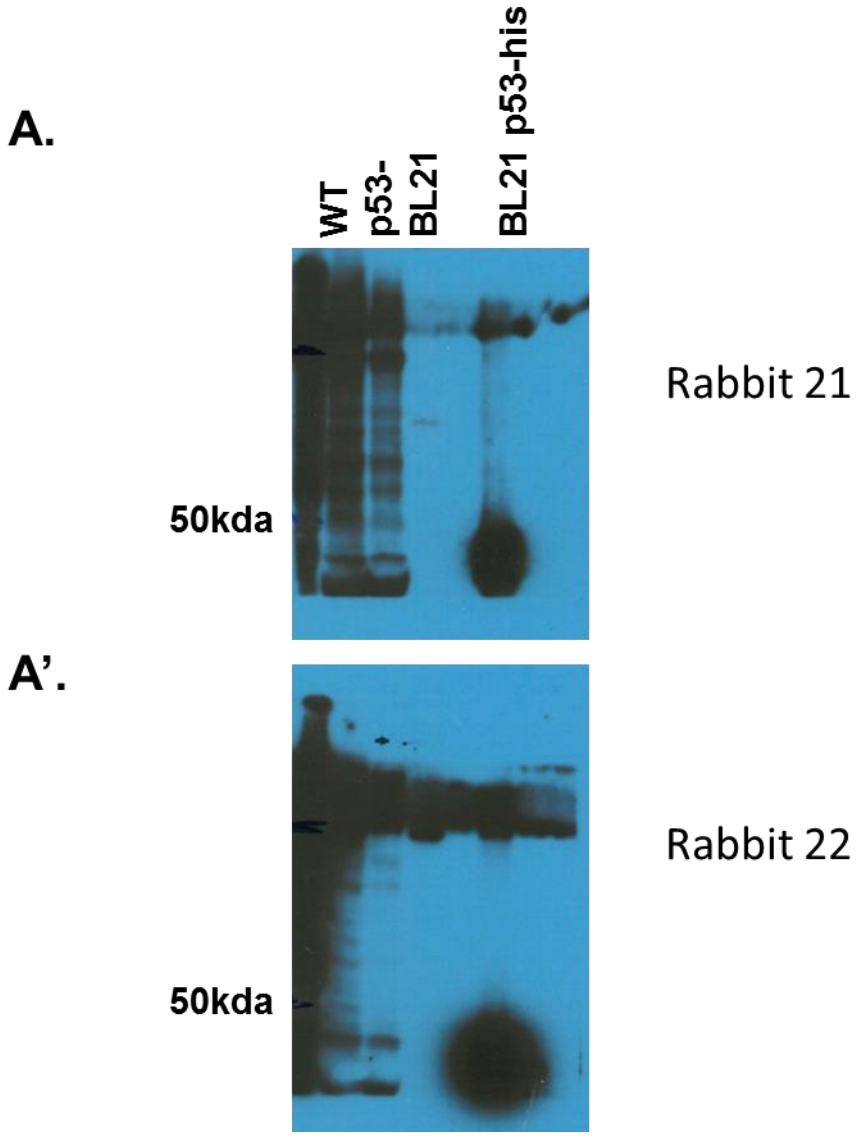

Figure 4-4: First bleeds from both rabbits detect purified p53-his

A.A'. First bleeds from both rabbits detect purified p53-his. No apparent p53 detection in lysates from *Drosophila* embryos, lane 1 and 2.

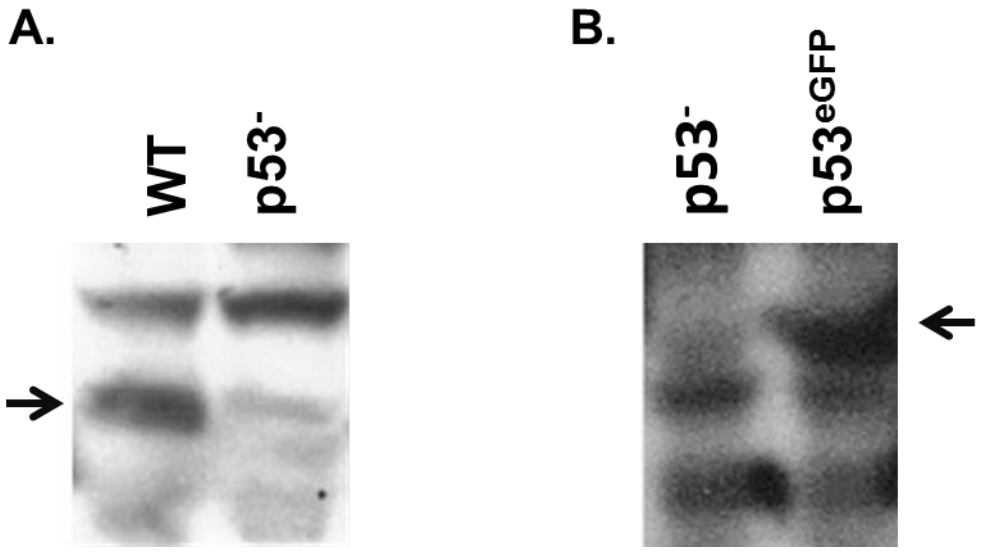

Figure 4-5: Seventh bleed detects p53 in nuclear lysates

A. Western blot using seventh bleed from rabbit 21 detects specific protein at p53 expected size. B. Same bleed from A, detects larger expected size for the $p53^{eGFP}$ fusion protein.

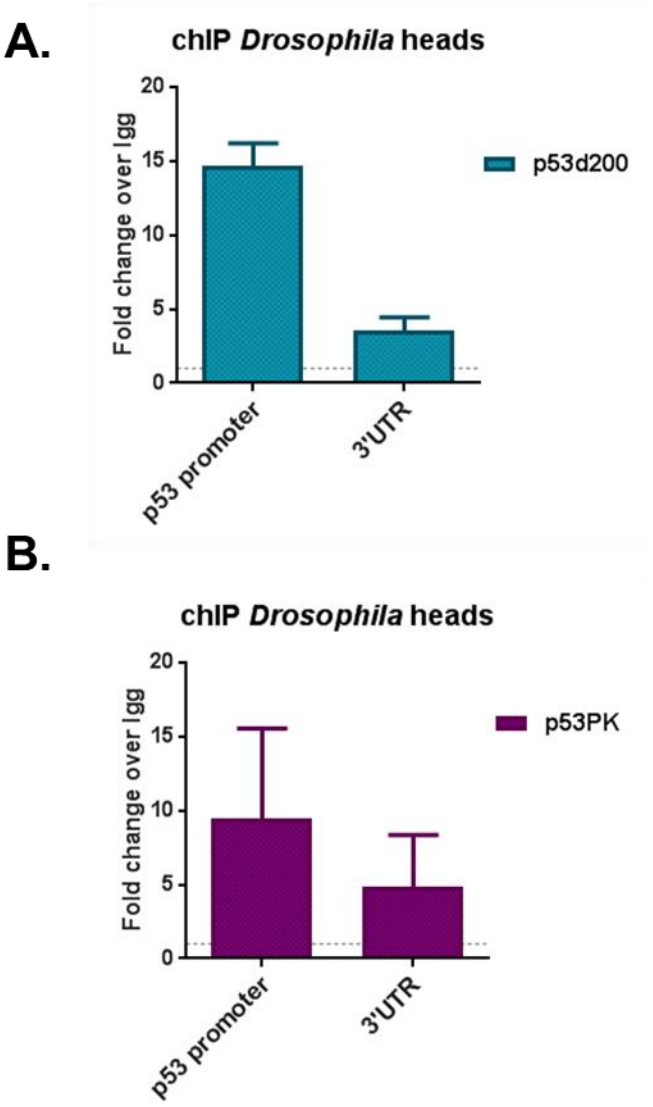

Figure 4-6: Comparison of Santa Cruz d200 and rabbit 21 seventh bleed in ChIP experiments

A. High and specific p53 enrichment at expected genomic binding site detected with d200. B. Rabbit 21 bleed gives modest enrichment at positive p53 binding site (p53 promoter) compared to negative region (3'UTR).

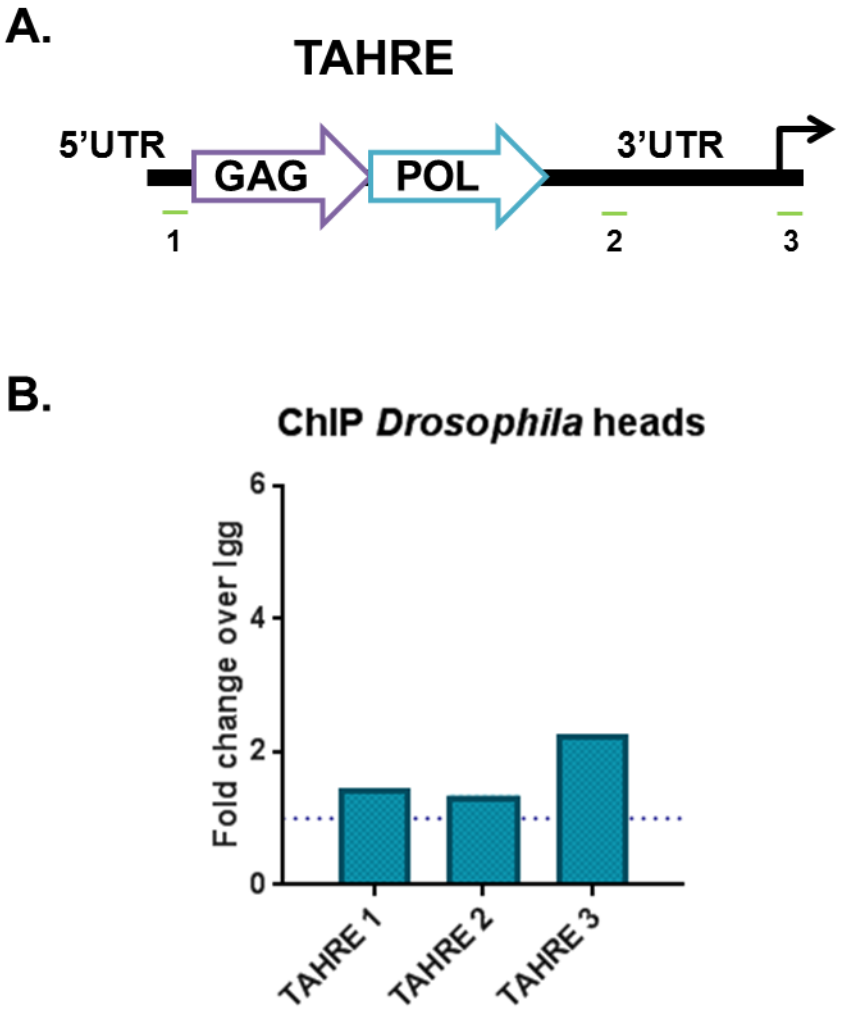

Figure 4-7: p53 does not bind selected regions of TAHRE

A. Schematic of full length TAHRE retrotransposon and ChIP primer locations (green lines numbered 1, 2 and 3). Reported promoter region indicated at end of 3'UTR with arrow. B. p53 is not significantly enriched in probed regions of TAHRE elements.

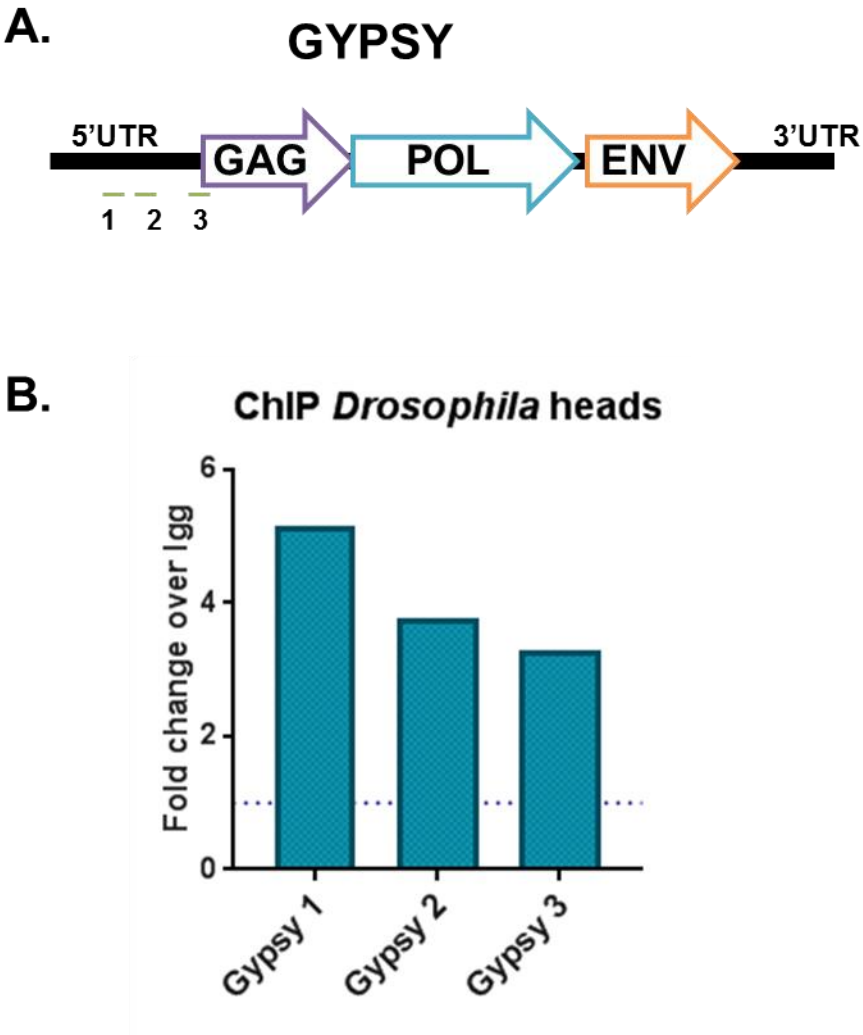

Figure 4-8: p53 enrichment at Gypsy 5'UTR

A. Schematic of full length *Gypsy* retrotransposon and ChIP primer locations (green lines numbered 1, 2 and 3). LTRs are not displayed in the cartoon. B. ChIP-ddPCR detected p53 enrichment in 5'UTR of *Gypsy* retroelement.

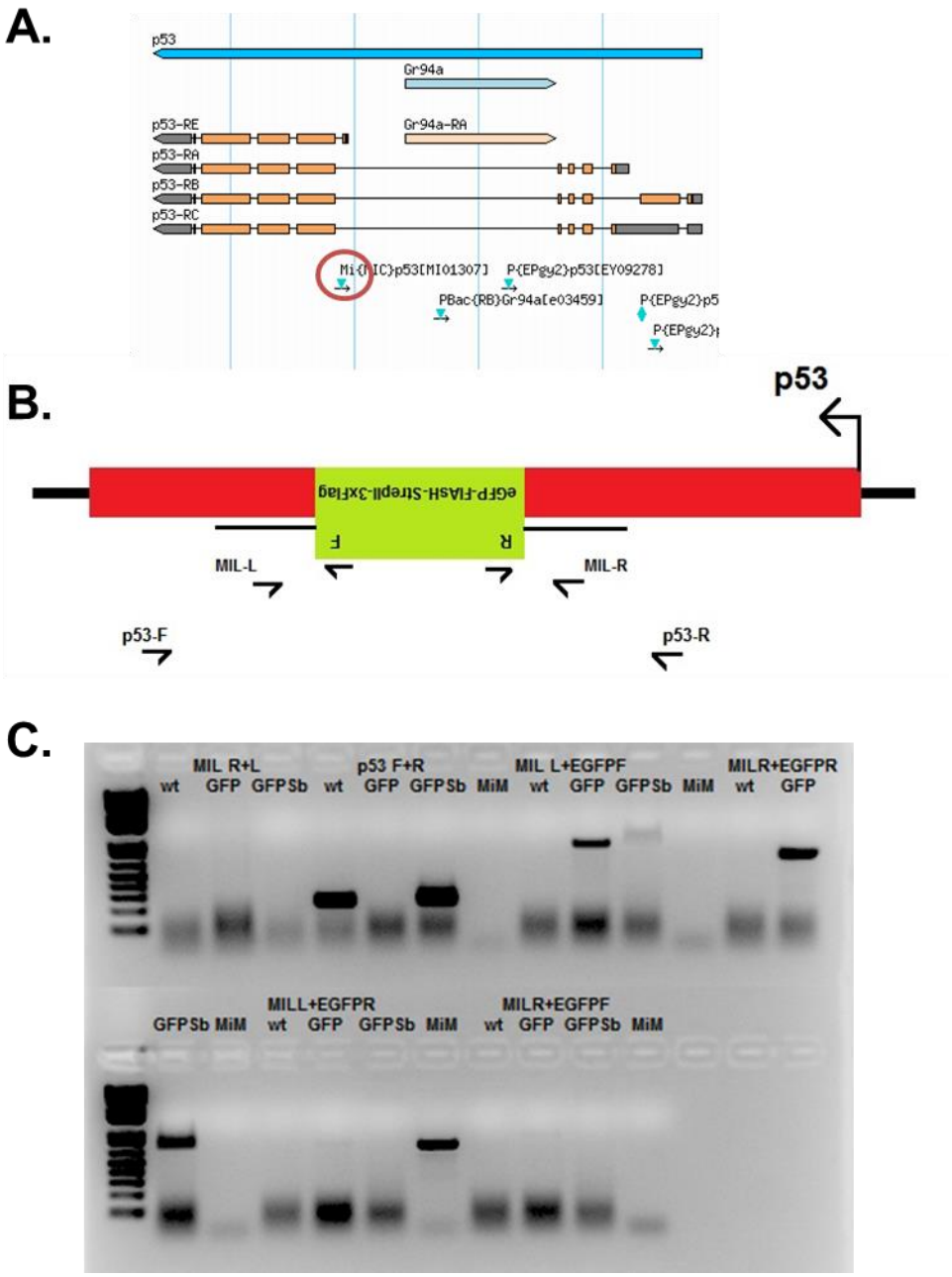

Figure 4-9: p53^{eGFP} flies validation

A. p53 gene region (from Flybase). MiMIC transposable element insertion circled. MiMIC TE was converted into eGFP tag by the Bellen lab. B. PCR primer scheme for validation of eGFP insertion and correct orientation. C. Gel electrophoresis of PCR products confirms p53^{eGFP} homozygous flies were correctly tagged.

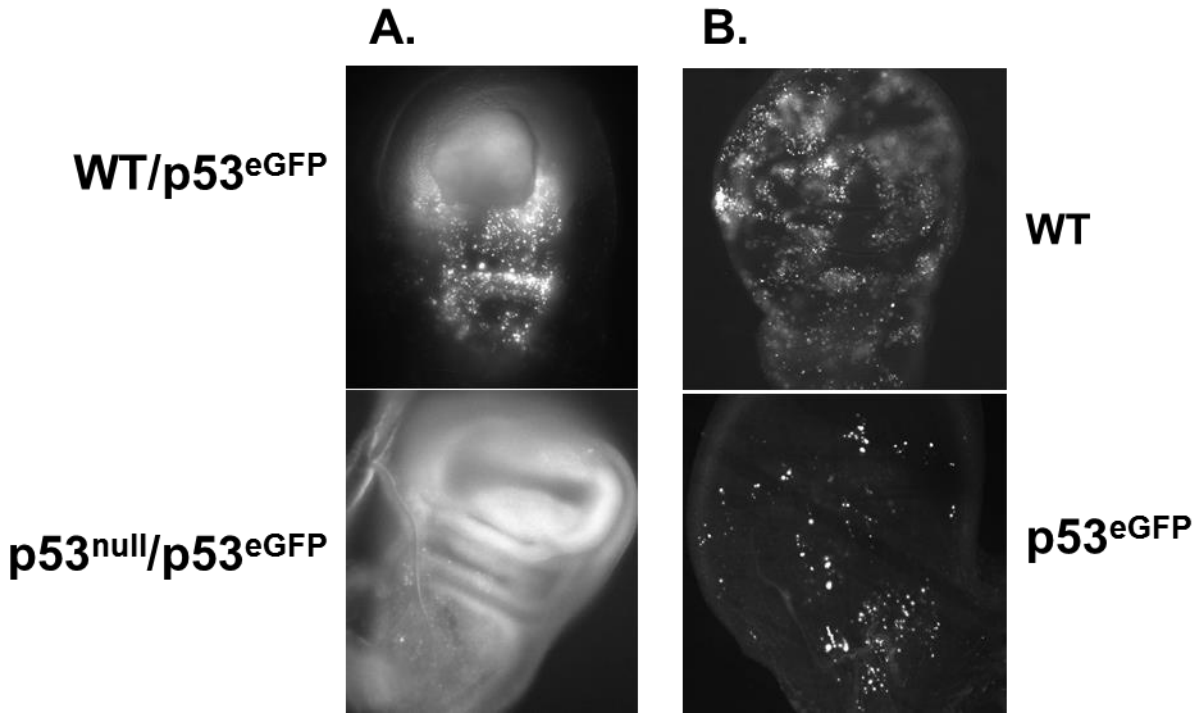

Figure 4-10: p53^{eGFP} allele does not complement defective apoptosis in p53null animals

A. Acridine orange staining for dying cells in irradiated larval wing disks in transheterozygous of p53^{eGFP} allele and either WT or a p53null allele. B. Apoptosis staining in WT and p53^{eGFP} homozygous larvae.

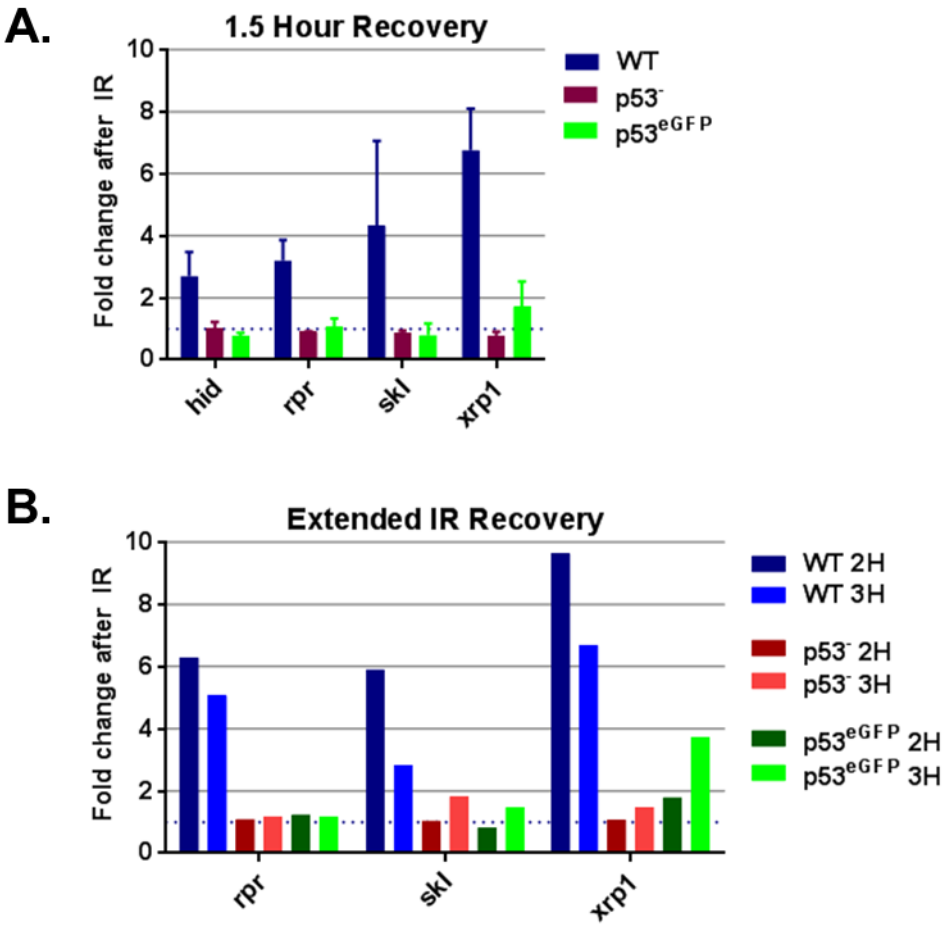

Figure 4-11: p53^{eGFP} fails to induce canonical p53 IR targets in embryos

A. RT-ddPCR for embryonic p53 IR targets using published recovery time. B. RT-ddPCR extended IR recovery. Modest induction of *xrp1* is observed in p53^{eGFP} embryos at 3 hours.

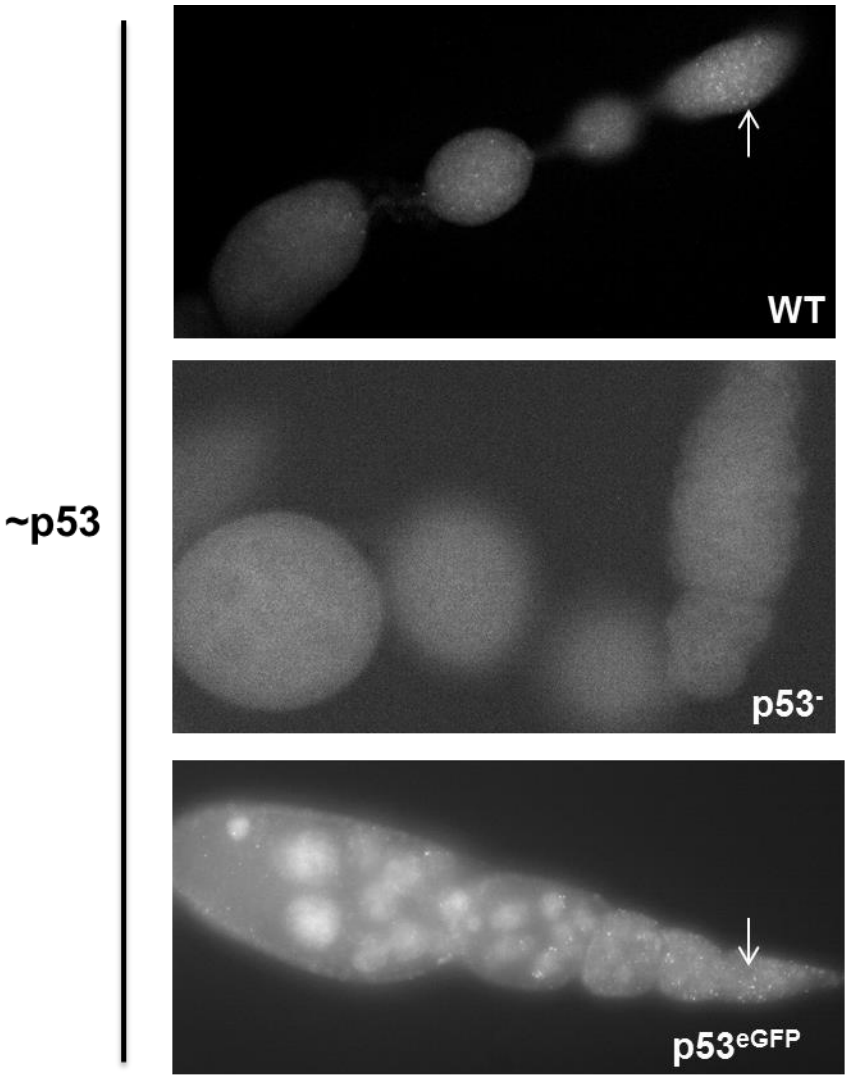

Figure 4-12: p53^{eGFP} forms nuclear foci in *Dosophila* ovaries.

Similar to WT, p53^{eGFP} forms nuclear foci in the *Drosophila* female germline.

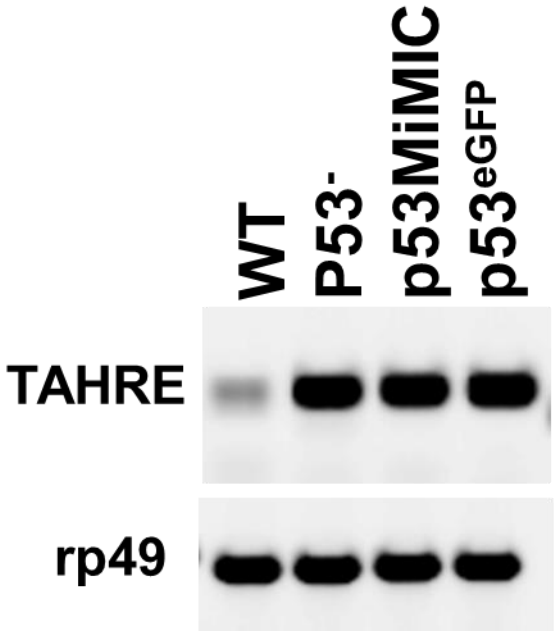

Figure 4-13: High TAHRE transcript expression in p53^{eGFP}

RT-PCR for TAHRE transcripts in p53MiMIC (parental line) and p53^{eGFP}. TAHRE transcript levels in both p53MiMIC and p53^{eGFP} ovaries are similar to p53null ovaries.

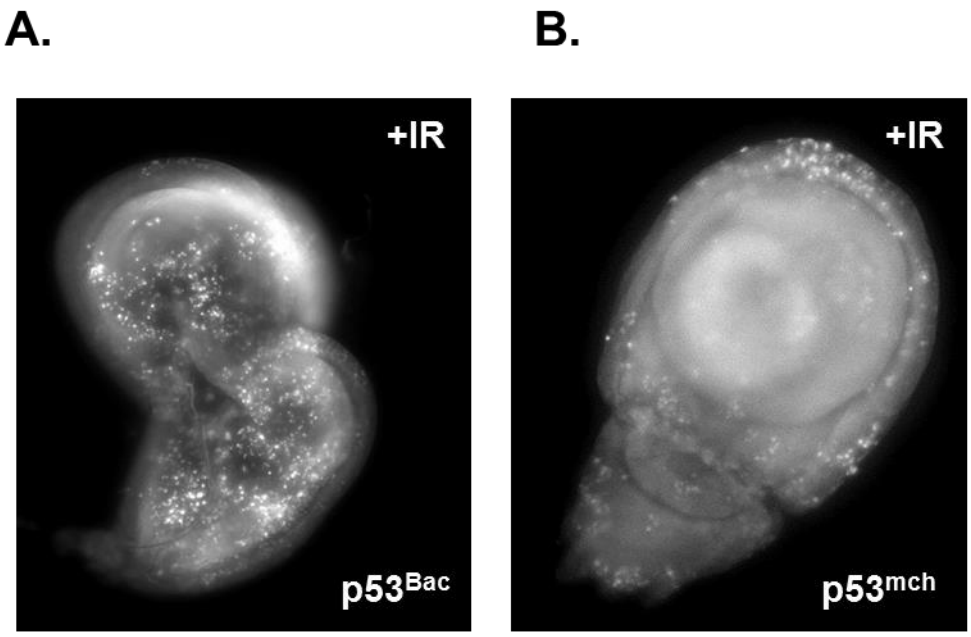

Figure 4-14: $p53^{mCh}$ fusion does not affect p53 mediated apoptosis

A. High number of apoptotic cells are detected by acridine orange in irradiated larval wing disks from untagged $p53^{Bac}$ control and $p53^{mCh}$ in B.

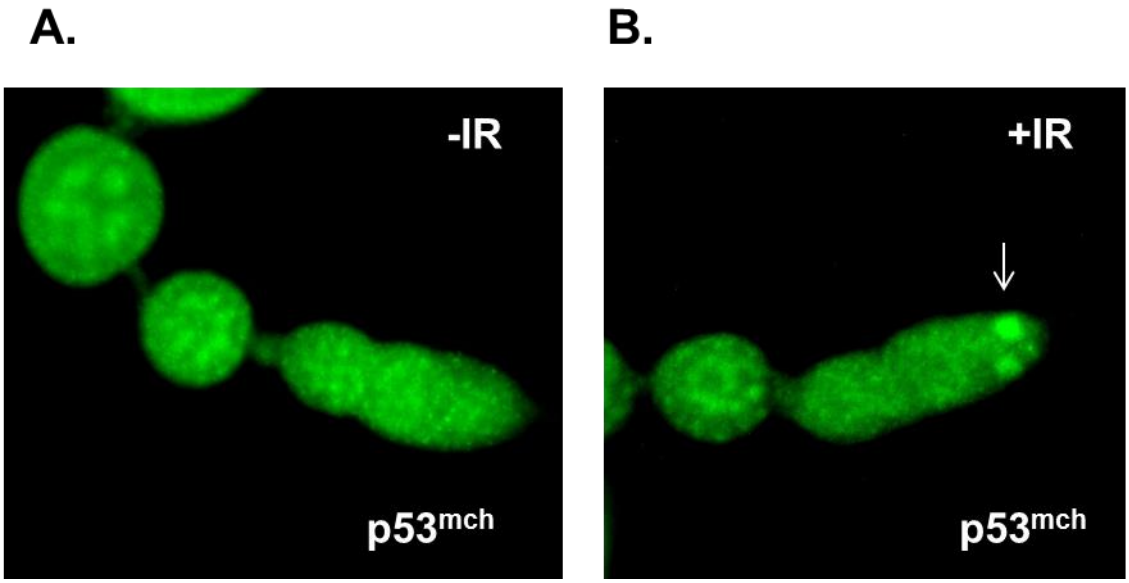

Figure 4-15: p53^{mCh} activates p53-*rpr* GFP reporter

Activation of GFP p53-*rpr* reporter was observed in stem cells following IR treatment similar to previously reported in WT ovaries (Wylie et al., 2014).

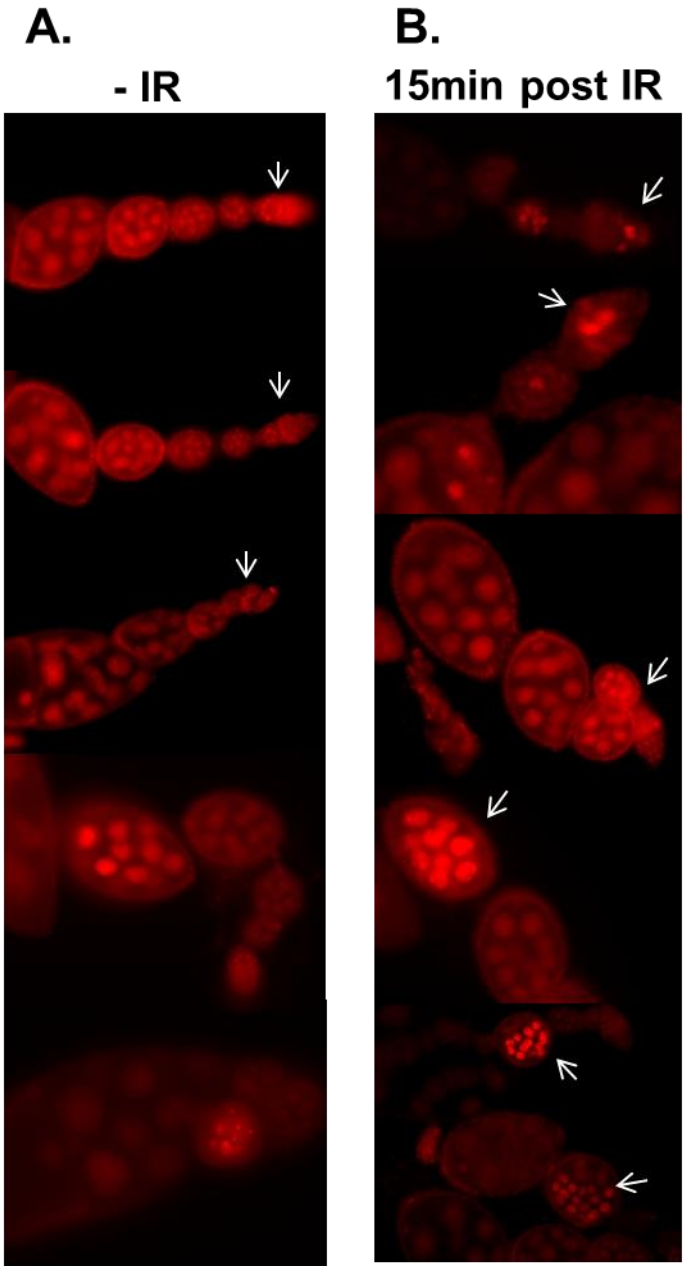

Figure 4-16: p53^{mCh} expression in ovaries before and after IR

A-B. *Drosophila* ovaries before and after IR, stained with dsRED antibody for p53^{mCh}

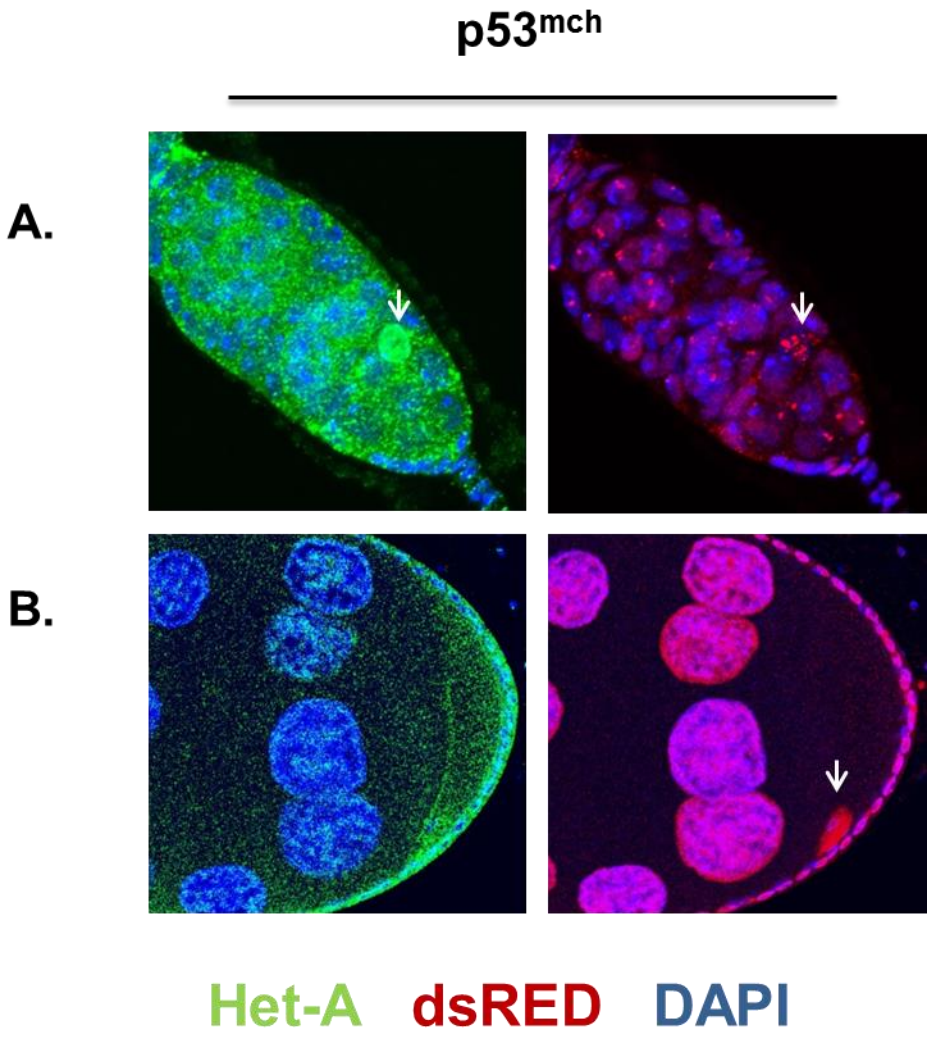

Figure 4-17: p53^{mCh} co-stained with Het-A retrotransposon protein

A. p53^{mCh} forms robust nuclear foci. B. p53^{mCh} is expressed throughout the ovarioles including the oocyte (arrow).

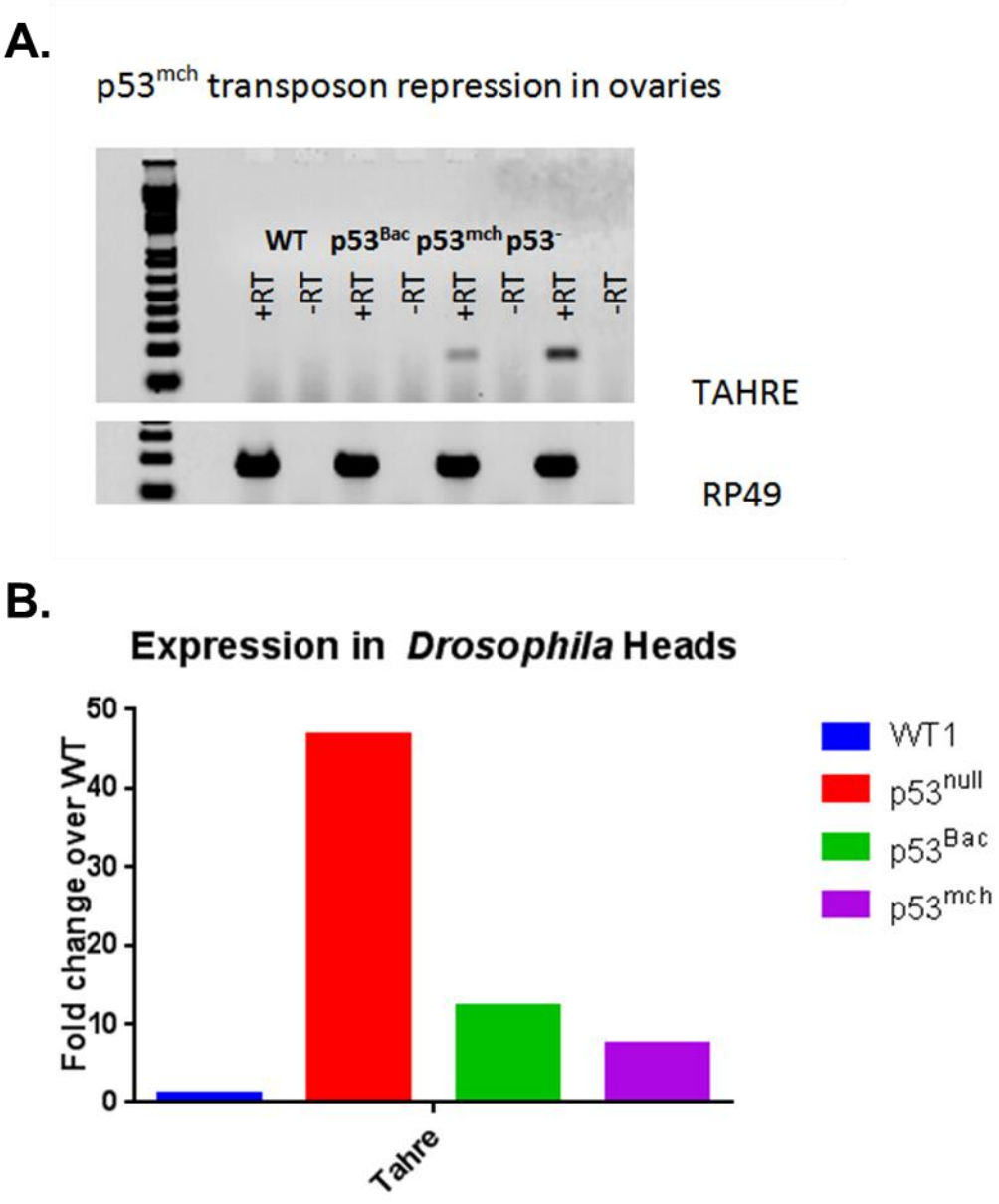

Figure 4-18: p53^{mCh} represses retrotransposon TAHRE

A. RT-PCR detects low levels of TAHRE transcripts in ovaries of p53^{mCh} and p53^{Bac} similar to WT. B. RT-ddPCR quantification of TAHRE transcripts in heads of p53^{mCh} and p53^{Bac} at similar levels to WT.

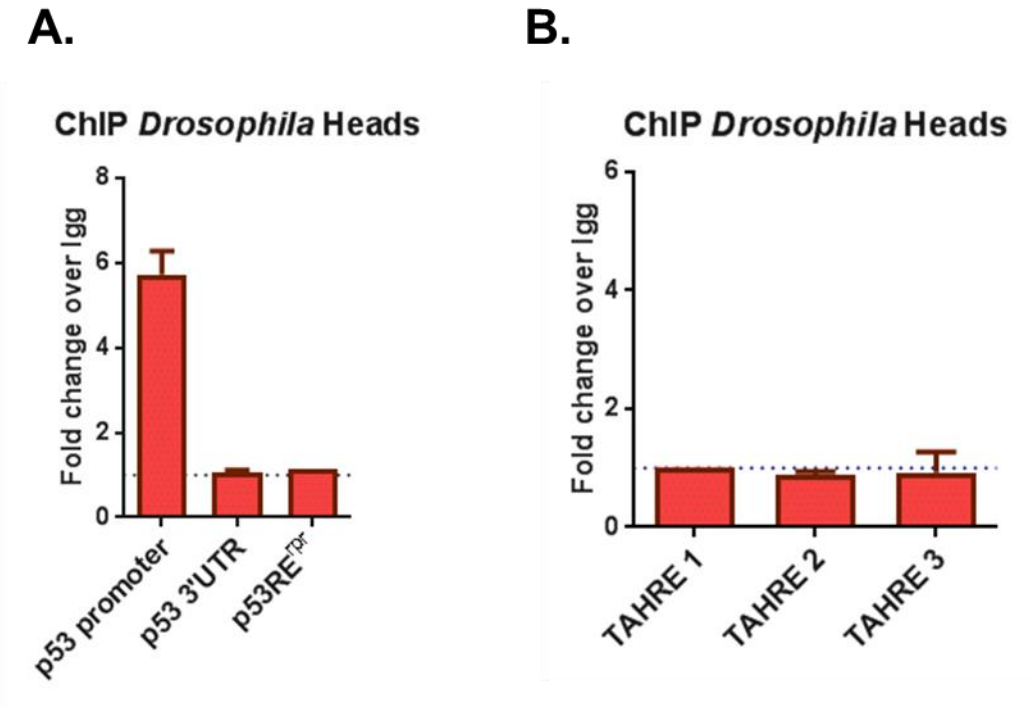

Figure 4-19: p53^{mCh} ChIP

A. In *Drosophila* heads, p53^{mCh} is enriched in expected positive region (p53 promoter), no signal in negative control region (3'UTR) or the p53RE^{rpr}. B. No p53 enrichment is detected in TAHRE retrotransposons.

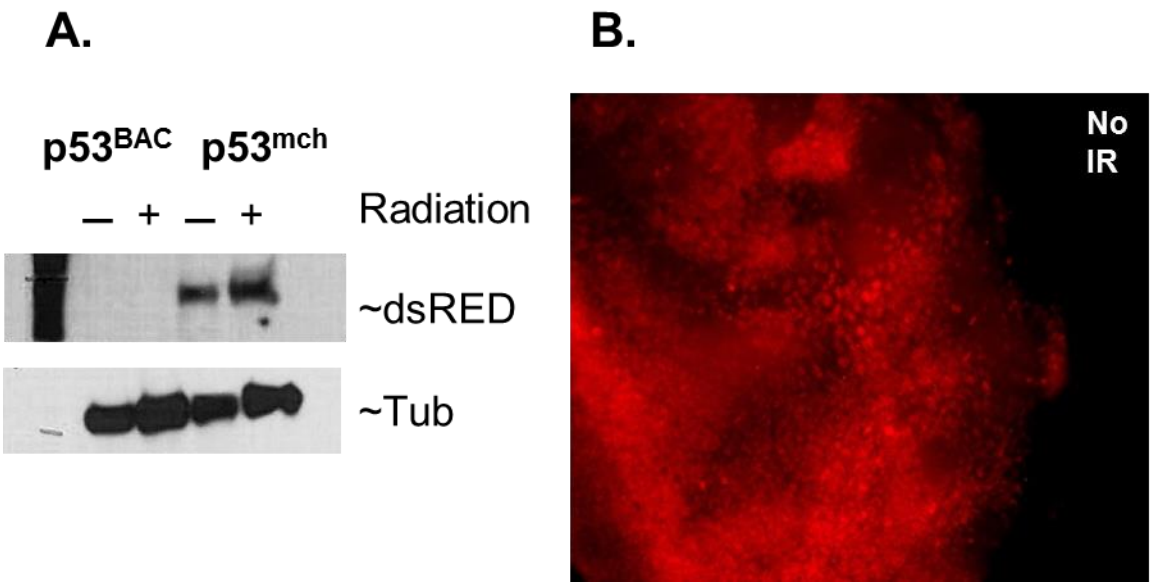

Figure 4-20: p53^{mCh} is basally expressed in *Drosophila* heads.

A. Western blots detecting p53^{mCh} in head lysates. B. Immunohistochemistry in brains of p53^{mCh} flies.

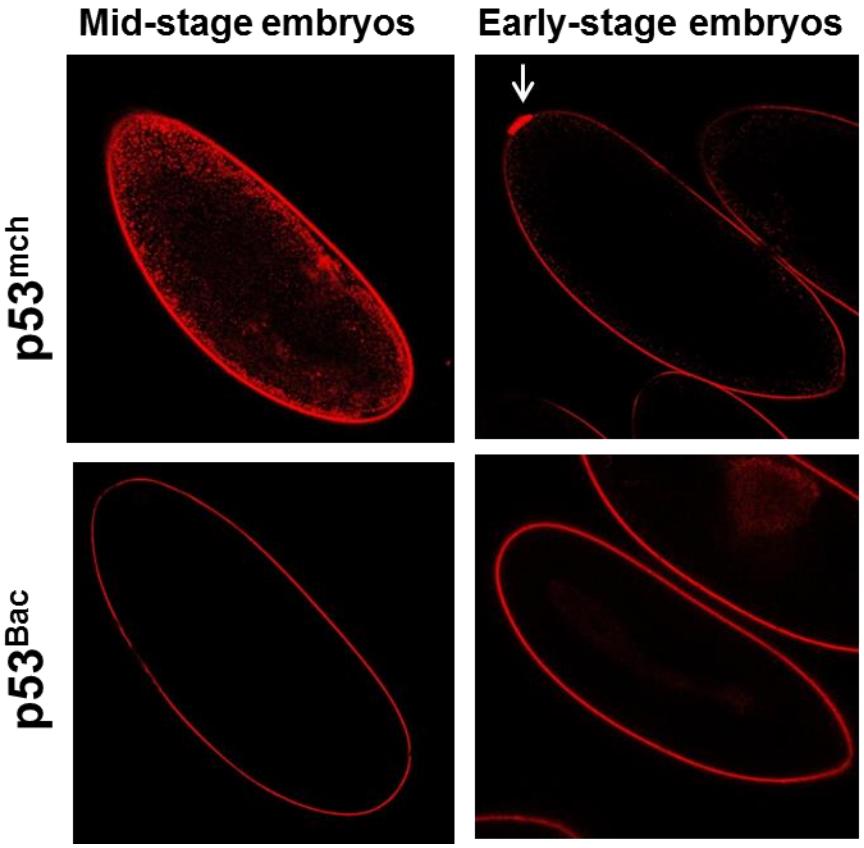

Figure 4-21: p53^{mCh} is detected live in *Drosophila* embryos.

p53^{mCh} signal can be detected by confocal microscopy in embryos. Interestingly in early embryos p53^{mCh} is seen at the pole plasm.

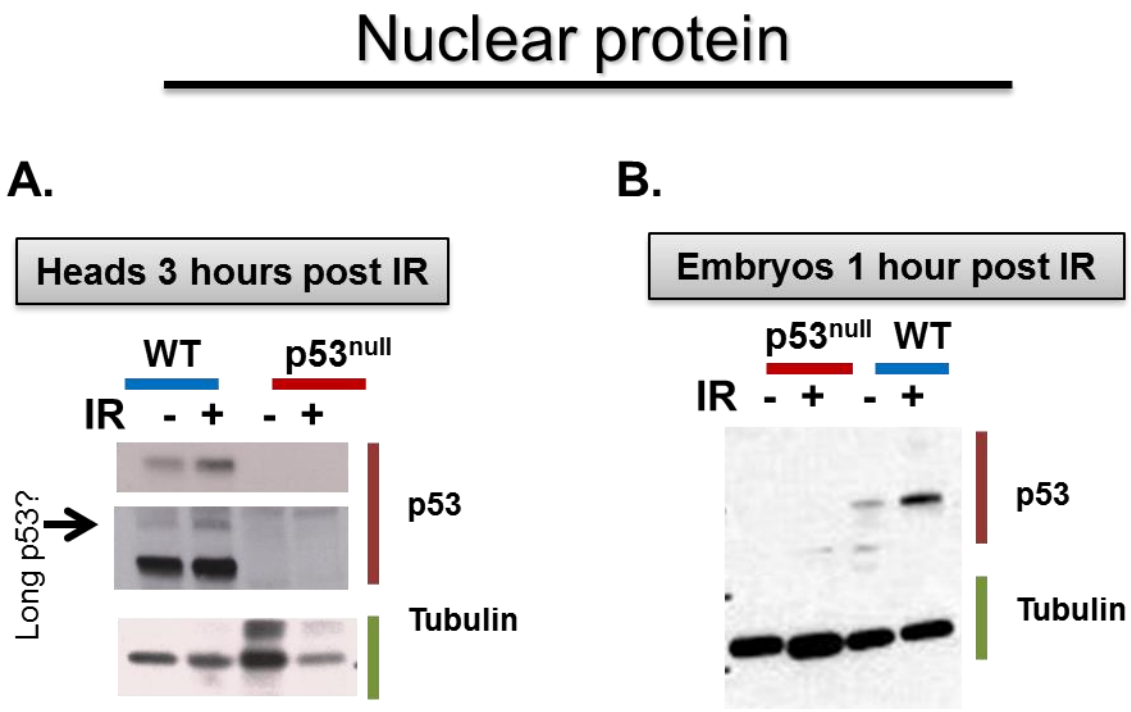

Figure 4-22: Native p53 expression before and after IR

Native p53 is basally expressed in heads and embryos. IR sample appears to have higher levels of p53 protein. Time points were chosen to match p53 target induction in each tissue.

	Santa Cruz d200	Santa Cruz C11	Hybridoma bank 25F4	Rabbit 21 Bleeds (PK)
Western Blot	Not tested	Good quality	Not tested	High background
IHC	Not tested	Not tested	Acceptable	Not tested
ChIP	Good quality	Not tested	Not tested	High background

Table 4-1: Summary of antibodies tested

DISCUSSION AND RECOMMENDATIONS

Through exploring different tools, I was able to implement challenging ChIP experiments in both embryo and head tissues. While generating p53 antibodies I found that raw bleeds from a rabbit immune-stimulated by *Drosophila* p53 protein appear to contain antibodies reactive to p53. These bleeds displayed promising signal in westerns and ChIP experiments. However, current Santa Cruz polyclonal p53 antibody d200 provided best results in ChIP experiments. Therefore, I chose to use d200 for ChIP-seq studies in chapter two.

Unfortunately, Santa Cruz has recently lost its license to produce and sell some antibodies, and the d200 polyclonal was discontinued. Therefore, it might be worth performing affinity purification in the bleeds I generated here in order to improve anti-p53 signal strength and specificity. Additionally, bacterial lines I created to express and purify p53 can be used to acquire p53 full length protein for re-injection in other animals. I did not check homology between *Drosophila* p53 and rabbit p53 (if this data is available), but alignment between human and fly p53 proteins shows modest sequence conservation outside the DNA binding domain, and therefore we have not seen cross reactivity of human p53 antibodies in fly protein. p53 homology should be checked if possible when choosing the host animal for antibody production. It is also worth noting that other bleeds before the seventh bleed used in results presented here, might have p53 reactivity. After negative results in the six bleeds with whole cell lysates, I decided to try nuclear protein extracts which resulted in p53 detection in bleed 7. The first six bleeds were tested in whole cell extracts only.

The bacterial p53 expression system could also be used to generate purified p53 protein for *in vitro* studies. This will require optimization of IPTG induction to avoid p53 accumulation in inclusion bodies. If this cannot be avoided, then after denaturing purification protocols, it is possible to apply the purified protein in re-folding assays. In addition, the p53 containing pet30A vector could be used in different expression systems.

I also have demonstrated that the intragenic natively tagged $p53^{eGFP}$ allele is severely compromised for p53 WT function in stress-response gene activation, apoptosis induction and retrotransposon repression. Interestingly, other translated p53 alleles that have p53 loss of function, tested by our lab, are not able to form nuclear foci in the female germline. The $p53^{eGFP}$ strains form robust foci in ovaries. It is unclear if these foci are protein aggregation or the original structure that native p53 forms. Nonetheless, in ovaries $p53^{eGFP}$ does not function to restrain retroelement TAHRE as WT p53. I also validated that the parental line p53MiMIC loses ability to restrain TAHRE. Based on the location of the MiMIC insertion, the p53MiMIC should lack the DNA binding and oligaremization domains, therefore confirming the importance of these domains for proper retrotransposon repression.

Finally, I have extended characterization of the published $p53^{mCh}$ fusion transgene (B. Zhang et al., 2014). I have shown that the $p53^{mCh}$ allele can activate our published p53-*rpr* GFP reporter in ovary stem cells, following similar pattern as the WT p53 reporter activation in this same tissue (Wylie et al., 2014). These results suggest that $p53^{mCh}$ can, not only trans-activate p53 canonical targets, but also $p53^{mCh}$ action is likely spatially regulated through similar factors as the WT p53. I also have established the $p53^{mCh}$ as an ideal allele to study p53 function in retrotransposon repression. In both ovaries and heads, $p53^{mCh}$ restrains TAHRE transcripts to similar levels found in WT animals. The opportunity to learn WT p53 function using the $p53^{mCh}$, established by my experiments, has already led to advances in other lab member projects. Additionally, I confirmed the dsRED clontech antibody can be used in many applications to detect the $p53^{mCh}$ lines (ChIP, westerns, and IHC). The contrast between the eGFP and mCherry alleles illustrates the importance of fully validating proteins tagged with exogenous epitopes, and that the location of the epitope insertion can determine successful retention of WT functions.

ACKNOWLEDGEMENTS

From the Fontoura lab, I would like to thank Dr. Beatriz Fontoura and Dr. Ke Zhang, for assistance with strategy and plasmids for p53 antibody production. Dr. Hugo Bellen with Baylor College of Medicine, for providing the unpublished strain of $p53^{eGFP}$. Dr. Brian R. Calvi with Indiana University, for gifting his recently published $p53^{mCh}$ and $p53^{BAC}$ flies.

APPENDIX A

Radiation Induced p53 Dependent genes in *Drosophila* heads

Gene	GO BIOLOGICAL PROCESS	H SAPIENS ORTHOLOGS
CG14645	chitin metabolic process | inferred from electronic annotation with InterPro:IPR002557	-
CG34212	biological_process | no biological data available	-
CG16826	biological_process | no biological data available	-
CG3906	-	-
CG14125	chitin metabolic process | inferred from electronic annotation with InterPro:IPR002557	-
Jon65Aiv	proteolysis | inferred from electronic annotation with InterPro:IPR001254, InterPro:IPR001314, InterPro:IPR018114	Hsap\CELA2A
	proteolysis | inferred from sequence model	
CG45080	biological_process | no biological data available	-
Jon65Aiii	proteolysis | inferred from sequence model	Hsap\CTRB1
	proteolysis | inferred from electronic annotation with InterPro:IPR001254, InterPro:IPR001314, InterPro:IPR018114	
betaTry	proteolysis | inferred from electronic annotation with InterPro:IPR001254, InterPro:IPR001314, InterPro:IPR018114	Hsap\PRSS36
	proteolysis | inferred from sequence model	Hsap\PRSS22
		Hsap\PRSS33
		Hsap\PRSS45
		Hsap\PRSS53
		Hsap\PRSS3
		Hsap\PRSS8
		Hsap\KLK15
		Hsap\PRSS27
		Hsap\TPSG1

		Hsap\PRSS38
		Hsap\PRSS1
Muc68D	chitin metabolic process | inferred from electronic annotation with InterPro:IPR002557	-
yip7	proteolysis | inferred from sequence model	Hsap\KLK3
	proteolysis | inferred from electronic annotation with InterPro:IPR001254, InterPro:IPR001314, InterPro:IPR018114	
epsilonTry	proteolysis | inferred from electronic annotation with InterPro:IPR001254, InterPro:IPR001314, InterPro:IPR018114	Hsap\PRSS36
	proteolysis | inferred from sequence model	Hsap\PRSS53
		Hsap\ELANE
		Hsap\PRSS1
		Hsap\PRSS3
CG13323	-	-
CG15043	-	-
CG10912	cold acclimation | inferred from expression pattern	-
CG7298	chitin metabolic process | inferred from electronic annotation with InterPro:IPR002557	-
CG4734	biological_process | no biological data available	-
CG5506	-	-
CG11672	-	-
CG34324	chitin metabolic process | inferred from electronic annotation with InterPro:IPR002557	-
CG15818	-	Hsap\COLEC11
		Hsap\CLEC4A
		Hsap\MBL2
		Hsap\CLEC1B
		Hsap\SFTPD
		Hsap\SFTPA1
		Hsap\SFTPA2

		Hsap\CLEC7A
		Hsap\COLEC10
LysD	-	Hsap\SPACA4
		Hsap\SPACA1
		Hsap\SPACA5B
		Hsap\SPACA5
		Hsap\LYZL2
		Hsap\LYZ
		Hsap\LYZL1
		Hsap\SPACA7
		Hsap\LALBA
		Hsap\LYZL6
		Hsap\LYZL4
		Hsap\SPACA3
alphaTry	proteolysis | inferred from electronic annotation with InterPro:IPR001254, InterPro:IPR001314, InterPro:IPR018114	Hsap\TPSG1
	proteolysis | inferred from sequence model	Hsap\PRSS45
		Hsap\PRSS36
		Hsap\PRSS3
		Hsap\PRSS38
		Hsap\PRSS53
		Hsap\KLK2
		Hsap\PRSS33
		Hsap\PRSS48
		Hsap\CMA1

		Hsap\KLK1
		Hsap\PRSS27
		Hsap\PRSS1
		Hsap\PRSS22
		Hsap\PRSS8
CG43680	biological_process | no biological data available	-
CG10911	biological_process | no biological data available	-
CG3819	apoptotic DNA fragmentation | inferred from biological aspect of ancestor with PANTHER:PTN000359601	Hsap\ENDOG
CG34220	chitin metabolic process | inferred from electronic annotation with InterPro:IPR002557	-
Bace	protein autoprocessing | inferred from electronic annotation with InterPro:IPR033145	Hsap\NAPSA
	protein catabolic process | inferred from biological aspect of ancestor with PANTHER:PTN000342793	Hsap\PGA4
	proteolysis | inferred from biological aspect of ancestor with PANTHER:PTN000342793	Hsap\PGA5
		Hsap\PGA3
		Hsap\PGC
		Hsap\CTSD
		Hsap\REN
		Hsap\BACE1
		Hsap\CTSE
		Hsap\BACE2
CG6295	lipid catabolic process | inferred from sequence or structural similarity with MGI:MGI:96820	Hsap\LIPC
		Hsap\LIPH
		Hsap\PNLIPRP3
		Hsap\PNLIPRP2
		Hsap\PLA1A
		Hsap\LIPI
		Hsap\PNLIP
		Hsap\PNLIPRP1
		Hsap\LIPG
		Hsap\LPL

Ag5r	biological_process | no biological data available	Hsap\CRISP2
		Hsap\CLEC18A
		Hsap\CLEC18B
		Hsap\GLIPR1L2
		Hsap\R3HDML
		Hsap\PI15
		Hsap\PI16
		Hsap\CRISPLD1
		Hsap\CRISP1
		Hsap\CRISPLD2
		Hsap\GLIPR1L1
		Hsap\GLIPR1
		Hsap\CLEC18C
		Hsap\GLIPR2
CG33109	-	-
CG43673	chitin metabolic process | inferred from electronic annotation with InterPro:IPR002557	-
Jon25Bi	proteolysis | inferred from electronic annotation with InterPro:IPR001254, InterPro:IPR001314, InterPro:IPR018114	Hsap\KLK3
	proteolysis | inferred from sequence model	
CG7953	-	-
CG4783	-	-
CG34026	biological_process | no biological data available	-
CG13324	-	-
CG18180	proteolysis | inferred from electronic annotation with InterPro:IPR001254, InterPro:IPR001314, InterPro:IPR018114	Hsap\PROC
	proteolysis | inferred from sequence model	Hsap\C1S
LysP	-	Hsap\LALBA
		Hsap\SPACA4

		Hsap\SPACA7
		Hsap\LYZL6
		Hsap\SPACA3
		Hsap\LYZL4
		Hsap\LYZL1
		Hsap\SPACA1
		Hsap\LYZ
		Hsap\SPACA5
		Hsap\SPACA5B
		Hsap\LYZL2
Scp1	-	-
CG42680	biological_process | no biological data available	-
CG1678	-	-
CG17633	proteolysis | inferred from electronic annotation with InterPro:IPR000834, InterPro:IPR003146	Hsap\CPB1
		Hsap\CPB2
		Hsap\CPA5
		Hsap\CPA4
		Hsap\CPO
		Hsap\CPA1
		Hsap\CPA2
		Hsap\CPA3
		Hsap\CPA6
CG8997	biological_process | no biological data available	-
CG42397	chitin metabolic process | inferred from electronic annotation with InterPro:IPR002557	-
TpnC4	flight | inferred from mutant phenotype	Hsap\TNNC2
		Hsap\CALN1
		Hsap\CALB1
		Hsap\EFCAB7
		Hsap\CABP5
		Hsap\CALM1
		Hsap\CALM2
		Hsap\RHBDL3

		Hsap\EFCAB11
		Hsap\CABP2
		Hsap\CABP7
		Hsap\EFCAB9
		Hsap\EFCAB3
		Hsap\SPATA21
		Hsap\CALM3
		Hsap\CALML5
		Hsap\CALML4
		Hsap\PVALB
		Hsap\OCM
		Hsap\CABP1
		Hsap\TNNC1
		Hsap\EFCAB6
		Hsap\OCM2
		Hsap\CALML3
		Hsap\CABP4
		Hsap\CALB2
		Hsap\CALML6
		Hsap\EFCAB13
		Hsap\EFCAB2
		Hsap\SCGN
CG6839	apoptotic DNA fragmentation | inferred from biological aspect of ancestor with PANTHER:PTN000359601	Hsap\ENDOG
CG7567	-	-
CG43166	biological_process | no biological data available	-
Jon25Bii	proteolysis | inferred from electronic annotation with InterPro:IPR001254, InterPro:IPR001314, InterPro:IPR018114	-

	proteolysis | inferred from sequence model	
Npc2e	sterol transport | inferred from sequence or structural similarity with Npc2a	Hsap\NPC2
	peptidoglycan recognition protein signaling pathway | inferred from mutant phenotype	
Kaz-m1	regulation of proteolysis | inferred by curator from GO:0004867	-
CG10659	nitrogen compound metabolic process | inferred from biological aspect of ancestor with PANTHER:PTN001463139	-
CG31077	chitin metabolic process | inferred from electronic annotation with InterPro:IPR002557	Hsap\MATN2
CG4363	-	Hsap\LYNX1
		Hsap\LY6D
CG10910	-	Hsap\CDA
		Hsap\MAGED4
		Hsap\MAGED2
		Hsap\MAGED1
		Hsap\MAGED4B
		Hsap\TRO
CG14499	biological_process | no biological data available	-
lcs	biological_process | no biological data available	-
Peritrophin-15a	chitin metabolic process | inferred from electronic annotation with InterPro:IPR002557	-
CG34176	-	-
Jon74E	proteolysis | inferred from sequence model	Hsap\C1S
	proteolysis | inferred from electronic annotation with InterPro:IPR001254, InterPro:IPR001314, InterPro:IPR018114	Hsap\PROC
		Hsap\F9
Akh	lipid homeostasis | inferred from mutant phenotype	-
	response to starvation | inferred from mutant phenotype	
	carbohydrate homeostasis | inferred from mutant phenotype	
	neuropeptide signaling pathway | inferred from expression pattern	
	neuropeptide signaling pathway | traceable	

	author statement	
	regulation of glucose metabolic process | inferred from mutant phenotype	
CG3868	-	-
lectin-37Db	calcium-dependent cell-cell adhesion via plasma membrane cell adhesion molecules | inferred from direct assay	Hsap\COLEC10
		Hsap\CLEC3A
		Hsap\CLEC11A
		Hsap\ASGR2
Phae2	proteolysis | inferred from electronic annotation with InterPro:IPR001254, InterPro:IPR001314, InterPro:IPR018114	Hsap\PRSS36
	proteolysis | inferred from sequence model	Hsap\PRSS57
		Hsap\PRSS53
		Hsap\PRSS33
CG42538	-	Hsap\CRISPLD2
		Hsap\SPINT4
		Hsap\CRISPLD1
		Hsap\GLIPR2
		Hsap\AMBP
		Hsap\PI15
		Hsap\CLEC18C
		Hsap\GLIPR1
		Hsap\TFPI
		Hsap\CLEC18A
		Hsap\R3HDML
		Hsap\GLIPR1L1
		Hsap\GLIPR1L2
		Hsap\CRISP2

		Hsap\CRISP1
		Hsap\PI16
		Hsap\CLEC18B
CG13482	-	-
CG13704	-	-
Mal-A6	carbohydrate metabolic process | inferred from electronic annotation with InterPro:IPR006047, InterPro:IPR006589, InterPro:IPR013781	Hsap\SLC3A1
		Hsap\SLC3A2
RnrL	activation of cysteine-type endopeptidase activity involved in apoptotic process | inferred from mutant phenotype	Hsap\RRM1
	deoxyribonucleotide biosynthetic process | inferred from sequence or structural similarity with UniProtKB:P07742	
	tissue regeneration | inferred from mutant phenotype	
	oxidation-reduction process | inferred from electronic annotation with InterPro:IPR000788, InterPro:IPR013346, InterPro:IPR013509	
	DNA replication | inferred from electronic annotation with InterPro:IPR000788, InterPro:IPR013509	
CG44000	-	-
Mal-A1	carbohydrate metabolic process | inferred from electronic annotation with InterPro:IPR006047, InterPro:IPR006589, InterPro:IPR013781	Hsap\SLC3A2
		Hsap\SLC3A1
CG33469	biological_process | no biological data available	-
CG43131	biological_process | no biological data available	-
CG3344	proteolysis involved in cellular protein catabolic process | inferred from biological aspect of ancestor with PANTHER:PTN000210642	Hsap\SCPEP1
		Hsap\CTSA
CG5399	biological_process | no biological data available	-
Cht8	chitin metabolic process | inferred from electronic annotation with InterPro:IPR002557	Hsap\CHI3L1
	carbohydrate metabolic process | inferred from electronic annotation with InterPro:IPR001223, InterPro:IPR001579, InterPro:IPR013781	Hsap\CHI3L2
	ecdysis, chitin-based cuticle | inferred from mutant phenotype	Hsap\CHIA
		Hsap\CHIT1

		Hsap\SRL
		Hsap\OVGP1
CheA7a	sensory perception of chemical stimulus | inferred from sequence or structural similarity with CheA29a	-
CG3448	DNA recombination | inferred from electronic annotation with InterPro:IPR010585, InterPro:IPR014751	-
	double-strand break repair | inferred from electronic annotation with InterPro:IPR010585, InterPro:IPR014751	
CG43999	regulation of lipid metabolic process | inferred from biological aspect of ancestor with PANTHER:PTN000281649	Hsap\OPA3
Ku80	telomere maintenance | inferred from mutant phenotype	Hsap\XRCC6
	DNA recombination | inferred from electronic annotation with InterPro:IPR024193	Hsap\XRCC5
	cellular response to gamma radiation | inferred from mutant phenotype	
	response to ethanol | inferred from mutant phenotype	
	double-strand break repair via nonhomologous end joining | inferred from mutant phenotype	
Irbp	double-strand break repair via nonhomologous end joining | inferred from mutant phenotype	Hsap\XRCC6
	telomere maintenance | inferred from mutant phenotype	
CG5892	-	-
CG15456	-	Hsap\MIEN1
		Hsap\SELENOW
dgt4	regulation of mitotic nuclear division | inferred from mutant phenotype	-
	mitotic spindle organization | inferred from mutant phenotype	
CG42363	biological_process | no biological data available	-
CG11878	sensory perception of pain | inferred from mutant phenotype	-
CG31104	-	-
CG16888	-	-
Ote	positive regulation of BMP signaling pathway | inferred from genetic interaction with tkv	-
	oogenesis | inferred from mutant phenotype	

	negative regulation of transcription, DNA-templated | inferred from mutant phenotype	
	nuclear envelope reassembly | inferred from direct assay	
	germ-line stem cell population maintenance | inferred from mutant phenotype	
	female germ-line stem cell asymmetric division | inferred from mutant phenotype	
	germ-line stem-cell niche homeostasis | inferred from mutant phenotype	
Obp8a	sensory perception of smell | inferred from biological aspect of ancestor with PANTHER:PTN000220814	-
	sensory perception of chemical stimulus | inferred from sequence alignment with UniProtKB:P34174	
	sensory perception of chemical stimulus | inferred from sequence or structural similarity with lush	
CG8952	proteolysis | inferred from electronic annotation with InterPro:IPR001254, InterPro:IPR001314, InterPro:IPR018114	-
	proteolysis | inferred from sequence model	

APPENDIX B

p53 direct target genes uncovered by integrated ChIP and RNA-seq

Head p53 direct targets

Activated basally by p53 and bound within 5kb			
SUBMITTED ID	**GO BIOLOGICAL PROCESS**	**GO MOLECULAR FUNCTION**	**H SAPIENS ORTHOLOGS**
CG3987	mesoderm development | inferred from expression pattern	-	-
CG6912	-	-	-
CG3984	-	-	Hsap\ACRV1
IntS12	snRNA 3'-end processing | inferred from direct assay	zinc ion binding | inferred from electronic annotation with InterPro:IPR001965	Hsap\INTS12
	snRNA processing | inferred from sequence or structural similarity with HGNC:25067		Hsap\PHF19
	neurogenesis | inferred from mutant phenotype		Hsap\MTF2
			Hsap\PHF1
phr	photoreactive repair | inferred from biological aspect of ancestor with	deoxyribodipyrimidine photo-lyase activity | inferred from biological aspect of ancestor with	Hsap\CRY2
			Hsap\CRY1

	PANTHER:PTN000025285	PANTHER:PTN000025285	
Cyp311a1	oxidation-reduction process | inferred from electronic annotation with InterPro:IPR001128, InterPro:IPR002401, InterPro:IPR017972	oxidoreductase activity, acting on paired donors, with incorporation or reduction of molecular oxygen | inferred from electronic annotation with InterPro:IPR001128, InterPro:IPR002401, InterPro:IPR017972	Hsap\CYP46A1
		heme binding | inferred from electronic annotation with InterPro:IPR001128, InterPro:IPR002401	Hsap\CYP4A11
		iron ion binding | inferred from electronic annotation with InterPro:IPR001128, InterPro:IPR002401	Hsap\CYP3A4
			Hsap\CYP4Z1
			Hsap\CYP4X1
			Hsap\CYP26C1
			Hsap\CYP4F2
			Hsap\CYP19A1
			Hsap\CYP4F12
			Hsap\CYP26B1
			Hsap\CYP4F8
			Hsap\CYP20A1

			Hsap\CYP4V2
			Hsap\CYP4F11
			Hsap\CYP3A43
			Hsap\CYP3A7
			Hsap\CYP4F3
			Hsap\CYP4F22
			Hsap\CYP4A22
			Hsap\CYP4B1
			Hsap\CYP3A5
			Hsap\CYP26A1
CG32750	nitrogen compound metabolic process | inferred from electronic annotation with InterPro:IPR003010	hydrolase activity, acting on carbon-nitrogen (but not peptide) bonds, in linear amides | inferred from electronic annotation with InterPro:IPR012101	Hsap\VNN1
	biological_process | no biological data available	hydrolase activity, acting on carbon-nitrogen (but not peptide) bonds | inferred from biological aspect of ancestor with PANTHER:PTN000064607	Hsap\VNN2
			Hsap\VNN3
			Hsap\BTD

			Hsap\NIT2
kat80	dorsal appendage formation | inferred from mutant phenotype	microtubule binding | inferred from electronic annotation with InterPro:IPR026962	Hsap\KATNBL1
	microtubule severing | inferred from sequence or structural similarity with NCBI_gi:3005599	microtubule binding | inferred from sequence or structural similarity	Hsap\KATNB1
	microtubule-based process | inferred from sequence or structural similarity		
CG44303	biological_process | no biological data available	molecular_function | no biological data available	-
CG4174	oxidation-reduction process | inferred from electronic annotation with InterPro:IPR006620, InterPro:IPR013547	procollagen-proline 4-dioxygenase activity | inferred from electronic annotation with InterPro:IPR013547	Hsap\P4HA2
		L-ascorbic acid binding | inferred from electronic annotation with InterPro:IPR006620	Hsap\P4HTM
		oxidoreductase activity, acting on single donors with incorporation of molecular oxygen, incorporation of two atoms of oxygen | inferred from electronic annotation with InterPro:IPR013547	Hsap\P4HA3
		iron ion binding | inferred from electronic annotation with InterPro:IPR006620	Hsap\P4HA1

CG9377	proteolysis | inferred from electronic annotation with InterPro:IPR001254	serine-type endopeptidase activity | NOT inferred from key residues	Hsap\F9
			Hsap\F10
Repressed basally by p53 and bound within 5kb			
SUBMITTED ID	**GO BIOLOGICAL PROCESS**	**GO MOLECULAR FUNCTION**	**H SAPIENS ORTHOLOGS**
CG17119	amino acid transmembrane transport | inferred from sequence or structural similarity with Eaat1	amino acid transmembrane transporter activity | inferred from sequence or structural similarity with Eaat1	Hsap\CTNS
	L-cystine transport | inferred from biological aspect of ancestor with PANTHER:PTN000319849	L-cystine transmembrane transporter activity | inferred from biological aspect of ancestor with PANTHER:PTN000319849	
CG2962	-	-	Hsap\POU2AF1
GstE8	glutathione metabolic process | inferred from sequence or structural similarity with GstE1	glutathione transferase activity | inferred from sequence or structural similarity with GstE1	Hsap\MARS
			Hsap\VARS
			Hsap\EEF1E1
			Hsap\GSTT2
			Hsap\GSTT2B
			Hsap\EEF1G
			Hsap\GSTT1

CG43175	biological_process | no biological data available	molecular_function | no biological data available	-
Rh5	visual perception | inferred from electronic annotation with InterPro:IPR000856	G-protein coupled photoreceptor activity | inferred from sequence or structural similarity	Hsap\OR12D3
	G-protein coupled receptor signaling pathway | inferred from electronic annotation with InterPro:IPR000276, InterPro:IPR000856	G-protein coupled photoreceptor activity | inferred from genetic interaction with ninaE	Hsap\RHO
	thermotaxis | inferred from mutant phenotype	G-protein coupled photoreceptor activity | inferred from sequence or structural similarity with ninaE inferred from sequence or structural similarity with Rh3 inferred from sequence or structural similarity with Rh4	Hsap\OPN1MW
	phototransduction | inferred from sequence or structural similarity with Rh3 inferred from sequence or structural similarity with Rh4 inferred from sequence or structural similarity with protein_id:CAA56378.1	G-protein coupled photoreceptor activity | non-traceable author statement	Hsap\OPN4
	G-protein coupled receptor signaling pathway | inferred from sequence or structural similarity	G-protein coupled photoreceptor activity | inferred from sequence or structural similarity with Rh3 inferred from sequence or structural similarity with Rh4 inferred from sequence or structural similarity with protein_id:CAA56378.1	Hsap\OPN1MW3

	sensory perception of sound | inferred from mutant phenotype		Hsap\RGR
	phototransduction | inferred from sequence or structural similarity with ninaE inferred from sequence or structural similarity with Rh3 inferred from sequence or structural similarity with Rh4 inferred from genetic interaction with ninaE		Hsap\RRH
	phototransduction | non-traceable author statement		Hsap\OPN1MW2
	response to light stimulus | inferred from direct assay		Hsap\OPN5
	absorption of visible light | inferred from mutant phenotype		Hsap\OPN1SW
	entrainment of circadian clock by photoperiod | inferred from genetic interaction with Rh6, cry inferred from genetic interaction with Rh6, cry, norpA inferred from genetic interaction with cry, norpA		Hsap\OPN3
	phototransduction | inferred from genetic interaction with ninaE		Hsap\OPN1LW
	UV-A, blue light phototransduction | non-traceable author statement		

nxf2	poly(A)+ mRNA export from nucleus | inferred from biological aspect of ancestor with PANTHER:PTN000070434	-	Hsap\NXF1
			Hsap\NXF2
			Hsap\NXF3
			Hsap\NXF2B
			Hsap\NXF5
Diedel	defense response to virus | inferred from mutant phenotype	cytokine activity | inferred from mutant phenotype	-
	response to bacterium | inferred from expression pattern		
	negative regulation of JAK-STAT cascade | traceable author statement		
pen	regulation of translation | inferred from biological aspect of ancestor with PANTHER:PTN000333308	mRNA binding | inferred from biological aspect of ancestor with PANTHER:PTN000333308	Hsap\PUM3
	apposition of dorsal and ventral imaginal disc-derived wing surfaces | inferred from mutant phenotype		

IR upregulated by p53 and bound within 5kb

SUBMITTED ID	GO BIOLOGICAL PROCESS	GO MOLECULAR FUNCTION	H SAPIENS ORTHOLOGS

CG15456	-	-	Hsap\MIEN1
			Hsap\SELENOW

Embryo p53 direct targets

Activated basally by p53 and bound within 5kb			
SUBMITTED ID	**GO BIOLOGICAL PROCESS**	**GO MOLECULAR FUNCTION**	**H SAPIENS ORTHOLOGS**
CG8272	SCF-dependent proteasomal ubiquitin-dependent protein catabolic process | inferred from sequence model	ubiquitin-protein transferase activity | contributes_to inferred from sequence model	Hsap\LRRC29
			Hsap\AK8
			Hsap\USP29
			Hsap\USP26
Sirup	biological_process | no biological data available	molecular_function | no biological data available	Hsap\SDHAF4
Repressed basally by p53 and bound within 5kb			
SUBMITTED ID	**GO BIOLOGICAL PROCESS**	**GO MOLECULAR FUNCTION**	**H SAPIENS ORTHOLOGS**
GstE9	glutathione metabolic process | inferred from direct assay	glutathione transferase activity | inferred from direct assay	Hsap\GSTT2
			Hsap\VARS
			Hsap\MARS
			Hsap\GSTT2B

			Hsap\EEF1G
			Hsap\GSTO1
			Hsap\GSTT1
			Hsap\EEF1E1
Prosalpha1	proteasome-mediated ubiquitin-dependent protein catabolic process | inferred by curator from GO:0005839	threonine-type endopeptidase activity | inferred from electronic annotation with InterPro:IPR001353, InterPro:IPR023332	Hsap\PSMA6
	cellular response to DNA damage stimulus | inferred from mutant phenotype	endopeptidase activity | contributes_to inferred by curator from GO:0005839	
	proteasome-mediated ubiquitin-dependent protein catabolic process | inferred from mutant phenotype		
fal	-	-	Hsap\SAMHD1
nAChRalpha4	ion transport | inferred from electronic annotation with InterPro:IPR002394, InterPro:IPR006029, InterPro:IPR006201	acetylcholine-gated cation channel activity | inferred from electronic annotation with InterPro:IPR002394	Hsap\HTR3E
	sleep | inferred from mutant phenotype	acetylcholine receptor activity | contributes_to inferred from direct assay	Hsap\CHRNA3
		acetylcholine-gated cation channel activity | inferred from sequence or structural similarity	Hsap\CHRNG

			Hsap\CHRNB1
			Hsap\CHRNB3
			Hsap\CHRNA2
			Hsap\CHRNA10
			Hsap\CHRNA5
			Hsap\CHRNB2
			Hsap\CHRNB4
			Hsap\HTR3A
			Hsap\CHRNA1
			Hsap\HTR3D
			Hsap\CHRNA9
			Hsap\CHRNA7
			Hsap\HTR3C
			Hsap\CHRND
			Hsap\CHRFAM7A
			Hsap\HTR3B
			Hsap\CHRNA4
			Hsap\CHRNA6

			Hsap\CHRNE
Prosalpha4	ubiquitin-dependent protein catabolic process | inferred from electronic annotation with InterPro:IPR000426	threonine-type endopeptidase activity | inferred from electronic annotation with InterPro:IPR001353, InterPro:IPR023332	Hsap\PSMA2
	cellular response to DNA damage stimulus | inferred from mutant phenotype	endopeptidase activity | contributes_to inferred by curator from GO:0005839	Hsap\PSMA7
	proteasome-mediated ubiquitin-dependent protein catabolic process | inferred by curator from GO:0005839		Hsap\PSMA8
			Hsap\PSMA4
			Hsap\PSMA5
CG31705	-	-	-
wech	instar larval development | inferred from mutant phenotype	zinc ion binding | inferred from electronic annotation with InterPro:IPR000315	Hsap\TRIM71
	regulation of cell-cell adhesion mediated by integrin | inferred from physical interaction with rhea	protein binding, bridging | inferred from physical interaction with Ilk, rhea	Hsap\TRIM42
	muscle attachment | inferred from mutant phenotype		Hsap\TRIM3

Cyp6a13	oxidation-reduction process | inferred from electronic annotation with InterPro:IPR001128, InterPro:IPR002401, InterPro:IPR017972	oxidoreductase activity, acting on paired donors, with incorporation or reduction of molecular oxygen | inferred from electronic annotation with InterPro:IPR001128, InterPro:IPR002401, InterPro:IPR017972	Hsap\CYP3A7-CYP3A51P
	defense response to bacterium | inferred from mutant phenotype	heme binding | inferred from electronic annotation with InterPro:IPR001128, InterPro:IPR002401	Hsap\TBXAS1
		iron ion binding | inferred from electronic annotation with InterPro:IPR001128, InterPro:IPR002401	Hsap\CYP3A43
		oxidoreductase activity | inferred from biological aspect of ancestor with PANTHER:PTN001209891	Hsap\CYP3A5
			Hsap\CYP3A7
			Hsap\CYP3A4

IR downregulated by p53 and bound within 5kb

SUBMITTED ID	GO BIOLOGICAL PROCESS	GO MOLECULAR FUNCTION	H SAPIENS ORTHOLOGS
CG8272	SCF-dependent proteasomal ubiquitin-dependent protein catabolic process | inferred	ubiquitin-protein transferase activity | contributes_to inferred from sequence model	Hsap\LRRC29

	from sequence model		
			Hsap\AK8
			Hsap\USP29
			Hsap\USP26
pkaap	protein localization | inferred from biological aspect of ancestor with PANTHER:PTN000322519	-	Hsap\AKAP10

IR upregulated by p53 and bound within 5kb

SUBMITTED ID	GO BIOLOGICAL PROCESS	GO MOLECULAR FUNCTION	H SAPIENS ORTHOLOGS
be	neuromuscular synaptic transmission | inferred from mutant phenotype	molecular_function | no biological data available	-
	long-term memory | inferred from mutant phenotype		
egr	JNK cascade | inferred from mutant phenotype inferred from genetic interaction with bsk inferred from genetic interaction with hep inferred from genetic interaction with msn inferred from genetic interaction with Tak1	tumor necrosis factor receptor binding | inferred from electronic annotation with InterPro:IPR006052	Hsap\TNFSF13

	apoptotic process | inferred from mutant phenotype	tumor necrosis factor receptor superfamily binding | inferred from mutant phenotype	Hsap\TNFSF12
	melanization defense response | inferred from mutant phenotype	protein binding | inferred from physical interaction with wgn	Hsap\TNFSF12-TNFSF13
	neuron cellular homeostasis | inferred from genetic interaction with Ank2	tumor necrosis factor receptor binding | non-traceable author statement	Hsap\TNFSF13B
	extrinsic apoptotic signaling pathway | inferred from mutant phenotype	tumor necrosis factor receptor binding | traceable author statement	Hsap\EDA
	asymmetric protein localization involved in cell fate determination | inferred from mutant phenotype	receptor binding | inferred from direct assay	
	apical protein localization | inferred from mutant phenotype	tumor necrosis factor receptor superfamily binding | inferred from sequence or structural similarity with HGNC:11892	
	negative regulation of neuromuscular synaptic transmission | inferred from genetic interaction with Ank2		
	innate immune response | inferred from mutant phenotype		
	glial cell proliferation | inferred from mutant		

	phenotype		
	defense response to Gram-negative bacterium | inferred from mutant phenotype		
	engulfment of apoptotic cell | inferred from mutant phenotype		
	apoptotic process | non-traceable author statement		
	apoptotic process | inferred from direct assay		
	immune response | inferred from mutant phenotype		
	positive regulation of sensory perception of pain | inferred from mutant phenotype		
rpr	larval midgut cell programmed cell death | inferred from genetic interaction with hid	ubiquitin conjugating enzyme binding | inferred from physical interaction with Bruce	Hsap\TSC1
	apoptotic process | inferred from mutant phenotype	ubiquitin protein ligase binding | inferred from physical interaction with Diap1	Hsap\RIN1
	positive regulation of cysteine-type endopeptidase activity | inferred from direct assay	ubiquitin protein ligase binding | inferred from physical interaction with Diap2	

	intrinsic apoptotic signaling pathway in response to osmotic stress | traceable author statement	protein homodimerization activity | inferred from direct assay	
	programmed cell death | traceable author statement	phospholipid binding | inferred from direct assay	
	larval central nervous system remodeling | traceable author statement		
	apoptotic process | inferred from expression pattern inferred from mutant phenotype		
	ecdysone-mediated induction of salivary gland cell autophagic cell death | inferred from expression pattern		
	cellular response to ionizing radiation | inferred from direct assay		
	regulation of protein catabolic process | inferred from direct assay		
	nurse cell apoptotic process | NOT traceable author statement		
	apoptotic process | inferred from direct assay		
	apoptotic signaling pathway | inferred from mutant phenotype		

	apoptotic process | traceable author statement		
	intrinsic apoptotic signaling pathway in response to DNA damage | inferred from mutant phenotype		
	positive regulation of cysteine-type endopeptidase activity involved in execution phase of apoptosis | inferred from direct assay		
	imaginal disc-derived male genitalia morphogenesis | inferred from mutant phenotype		
	positive regulation of protein ubiquitination | inferred from direct assay		
	salivary gland cell autophagic cell death | inferred from genetic interaction with hid		
	negative regulation of neuron apoptotic process | inferred from mutant phenotype		
	apoptotic signaling pathway | inferred from genetic interaction with Diap1		
	programmed cell death | inferred from mutant phenotype		

	apoptotic process | non-traceable author statement		
	cellular response to gamma radiation | inferred from mutant phenotype		
	positive regulation of protein ubiquitination involved in ubiquitin-dependent protein catabolic process | inferred from genetic interaction with eff		
	cell death | inferred from mutant phenotype		
Xrp1	double-strand break repair | inferred from mutant phenotype	P-element binding | inferred from direct assay	-
	olfactory behavior | inferred from mutant phenotype	protein dimerization activity | inferred from sequence or structural similarity	
	chromosome organization | inferred from mutant phenotype		
	imaginal disc-derived wing morphogenesis | inferred from mutant phenotype		
	negative regulation of cell proliferation | inferred from direct assay		
	cellular process | inferred from mutant phenotype		

hid	salivary gland cell autophagic cell death | inferred from mutant phenotype inferred from genetic interaction with rpr	protein binding | inferred from physical interaction with Diap1	-
	positive regulation of apoptotic process | inferred from mutant phenotype	BIR domain binding | inferred from physical interaction with Diap2 inferred from physical interaction with Diap1	
	nurse cell apoptotic process | NOT traceable author statement	ubiquitin protein ligase binding | inferred from physical interaction with Diap1	
	sex differentiation | inferred from mutant phenotype		
	antennal morphogenesis | inferred from mutant phenotype		
	programmed cell death | inferred from mutant phenotype		
	entrainment of circadian clock by photoperiod | inferred from mutant phenotype		
	cellular response to gamma radiation | inferred from mutant phenotype		
	apoptotic signaling pathway | inferred from direct assay		

	ecdysone-mediated induction of salivary gland cell autophagic cell death | inferred from expression pattern		
	cell death | inferred from mutant phenotype		
	head involution | inferred from mutant phenotype		
	apoptotic process | traceable author statement		
	compound eye retinal cell programmed cell death | traceable author statement		
	programmed cell death | traceable author statement		
	positive regulation of apoptotic process | inferred from direct assay		
	response to red light | inferred from mutant phenotype		
	regulation of organ growth | inferred from mutant phenotype		
	dendrite morphogenesis | inferred from mutant phenotype		
	larval midgut cell programmed cell death | inferred from genetic		

	interaction with rpr		
	cellular response to starvation | inferred from mutant phenotype		
	apoptotic signaling pathway | inferred from mutant phenotype		
	regulation of cysteine-type endopeptidase activity involved in apoptotic process | inferred from genetic interaction with Drice inferred from genetic interaction with Dronc inferred from genetic interaction with Decay inferred from genetic interaction with Strica inferred from genetic interaction with Dark		
	regulation of retinal cell programmed cell death | non-traceable author statement		
	positive regulation of cellular response to X-ray | inferred from mutant phenotype		
	programmed cell death | inferred from mutant phenotype inferred from genetic interaction with rpr		
	positive regulation of macroautophagy | inferred from mutant phenotype		

	positive regulation of cysteine-type endopeptidase activity involved in execution phase of apoptosis | inferred from direct assay		
	apoptotic process | non-traceable author statement		
	open tracheal system development | inferred from mutant phenotype		
	apoptotic process | inferred from mutant phenotype		
	apoptotic signaling pathway | inferred from genetic interaction with Diap1		
	positive regulation of cysteine-type endopeptidase activity | inferred from direct assay		
	intrinsic apoptotic signaling pathway in response to DNA damage | inferred from mutant phenotype		
	instar larval or pupal development | inferred from mutant phenotype		
CG9065	mitochondrial respiratory chain complex IV assembly | inferred from biological aspect of ancestor with PANTHER:PTN000423137	copper chaperone activity | inferred from biological aspect of ancestor with PANTHER:PTN000423136	Hsap\COX17

	copper ion transport | inferred from biological aspect of ancestor with PANTHER:PTN000423136	copper chaperone activity | inferred from sequence or structural similarity with UniProtKB:Q14061	
	respiratory chain complex IV assembly | inferred from sequence or structural similarity with UniProtKB:Q14061		
Corp	negative regulation of intrinsic apoptotic signaling pathway in response to DNA damage by p53 class mediator | inferred from genetic interaction with p53	p53 binding | inferred from physical interaction with p53	-
	negative regulation of intrinsic apoptotic signaling pathway in response to DNA damage | inferred from mutant phenotype		

BIBLIOGRAPHY

Abad, J. P., De Pablos, B., Osoegawa, K., De Jong, P. J., Martin-Gallardo, A., & Villasante, A. (2004). TAHRE, a novel telomeric retrotransposon from Drosophila melanogaster, reveals the origin of Drosophila telomeres. *Mol Biol Evol, 21*(9), 1620-1624. doi: 10.1093/molbev/msh180

Afgan, E., Baker, D., van den Beek, M., Blankenberg, D., Bouvier, D., Cech, M., . . . Goecks, J. (2016). The Galaxy platform for accessible, reproducible and collaborative biomedical analyses: 2016 update. *Nucleic Acids Res, 44*(W1), W3-W10. doi: 10.1093/nar/gkw343

Akdemir, F., Christich, A., Sogame, N., Chapo, J., & Abrams, J. M. (2007). p53 directs focused genomic responses in Drosophila. *Oncogene, 26*(36), 5184-5193. doi: 10.1038/sj.onc.1210328

Akdemir, K. C., Jain, A. K., Allton, K., Aronow, B., Xu, X., Cooney, A. J., . . . Barton, M. C. (2014). Genome-wide profiling reveals stimulus-specific functions of p53 during differentiation and DNA damage of human embryonic stem cells. *Nucleic Acids Res, 42*(1), 205-223. doi: 10.1093/nar/gkt866

Andrysik, Z., Kim, J., Tan, A. C., & Espinosa, J. M. (2013). A genetic screen identifies TCF3/E2A and TRIAP1 as pathway-specific regulators of the cellular response to p53 activation. *Cell Rep, 3*(5), 1346-1354. doi: 10.1016/j.celrep.2013.04.014

Baker, S. J., Fearon, E. R., Nigro, J. M., Hamilton, S. R., Preisinger, A. C., Jessup, J. M., . . . Vogelstein, B. (1989). Chromosome 17 deletions and p53 gene mutations in colorectal carcinomas. *Science, 244*(4901), 217-221.

Bandele, O. J., Wang, X., Campbell, M. R., Pittman, G. S., & Bell, D. A. (2011). Human single-nucleotide polymorphisms alter p53 sequence-specific binding at gene regulatory elements. *Nucleic Acids Res, 39*(1), 178-189. doi: 10.1093/nar/gkq764

Barbalat, R., Ewald, S. E., Mouchess, M. L., & Barton, G. M. (2011). Nucleic acid recognition by the innate immune system. *Annu Rev Immunol, 29*, 185-214. doi: 10.1146/annurev-immunol-031210-101340

Belyi, V. A., & Levine, A. J. (2009). One billion years of p53/p63/p73 evolution. *Proc Natl Acad Sci U S A, 106*(42), 17609-17610. doi: 10.1073/pnas.0910634106

Bieging, K. T., Mello, S. S., & Attardi, L. D. (2014). Unravelling mechanisms of p53-mediated tumour suppression. *Nat Rev Cancer, 14*(5), 359-370. doi: 10.1038/nrc3711

Bolzer, A., Kreth, G., Solovei, I., Koehler, D., Saracoglu, K., Fauth, C., . . . Cremer, T. (2005). Three-dimensional maps of all chromosomes in human male fibroblast nuclei and prometaphase rosettes. *PLoS Biol, 3*(5), e157. doi: 10.1371/journal.pbio.0030157

Botcheva, K., & McCorkle, S. R. (2014). Cell context dependent p53 genome-wide binding patterns and enrichment at repeats. *PLoS One, 9*(11), e113492. doi: 10.1371/journal.pone.0113492

Botcheva, K., McCorkle, S. R., McCombie, W. R., Dunn, J. J., & Anderson, C. W. (2011). Distinct p53 genomic binding patterns in normal and cancer-derived human cells. *Cell Cycle, 10*(24), 4237-4249. doi: 10.4161/cc.10.24.18383

Brodsky, M. H., Nordstrom, W., Tsang, G., Kwan, E., Rubin, G. M., & Abrams, J. M. (2000). Drosophila p53 binds a damage response element at the reaper locus. *Cell, 101*(1), 103-113. doi: 10.1016/S0092-8674(00)80627-3

Brodsky, M. H., Weinert, B. T., Tsang, G., Rong, Y. S., McGinnis, N. M., Golic, K. G., . . . Rubin, G. M. (2004). Drosophila melanogaster MNK/Chk2 and p53 regulate multiple DNA repair and apoptotic pathways following DNA damage. *Mol Cell Biol, 24*(3), 1219-1231.

Ceribelli, M., Alcalay, M., Vigano, M. A., & Mantovani, R. (2006). Repression of new p53 targets revealed by ChIP on chip experiments. *Cell Cycle, 5*(10), 1102-1110. doi: 10.4161/cc.5.10.2777

Chakraborty, R., Li, Y., Zhou, L., & Golic, K. G. (2015). Corp Regulates P53 in Drosophila melanogaster via a Negative Feedback Loop. *PLoS Genet, 11*(7), e1005400. doi: 10.1371/journal.pgen.1005400

Chambeyron, S., & Bickmore, W. A. (2004). Chromatin decondensation and nuclear reorganization of the HoxB locus upon induction of transcription. *Genes Dev, 18*(10), 1119-1130. doi: 10.1101/gad.292104

Chanas, G., Lavrov, S., Iral, F., Cavalli, G., & Maschat, F. (2004). Engrailed and polyhomeotic maintain posterior cell identity through cubitus-interruptus regulation. *Dev Biol, 272*(2), 522-535. doi: 10.1016/j.ydbio.2004.05.020

Chang, G. S., Chen, X. A., Park, B., Rhee, H. S., Li, P., Han, K. H., . . . Pugh, B. F. (2014). A comprehensive and high-resolution genome-wide response of p53 to stress. *Cell Rep, 8*(2), 514-527. doi: 10.1016/j.celrep.2014.06.030

Chang, T. C., Wentzel, E. A., Kent, O. A., Ramachandran, K., Mullendore, M., Lee, K. H., . . . Mendell, J. T. (2007). Transactivation of miR-34a by p53 broadly influences gene expression and promotes apoptosis. *Mol Cell, 26*(5), 745-752. doi: 10.1016/j.molcel.2007.05.010

Chaudhary, R., & Lal, A. (2017). Long noncoding RNAs in the p53 network. *Wiley Interdiscip Rev RNA, 8*(3). doi: 10.1002/wrna.1410

Cremer, T., & Cremer, C. (2006a). Rise, fall and resurrection of chromosome territories: a historical perspective. Part I. The rise of chromosome territories. *Eur J Histochem, 50*(3), 161-176.

Cremer, T., & Cremer, C. (2006b). Rise, fall and resurrection of chromosome territories: a historical perspective. Part II. Fall and resurrection of chromosome territories during the 1950s to 1980s. Part III. Chromosome territories and the functional nuclear architecture: experiments and models from the 1990s to the present. *Eur J Histochem, 50*(4), 223-272.

Czech, B., Malone, C. D., Zhou, R., Stark, A., Schlingeheyde, C., Dus, M., . . . Brennecke, J. (2008). An endogenous small interfering RNA pathway in Drosophila. *Nature, 453*(7196), 798-802. doi: 10.1038/nature07007

D'Brot, A. (2014). *OF APOPTOSOMES AND ONCOGENES: REPURPOSING A DEATH MACHINE & DECONSTRUCTING THE ACTION OF P53 MUTATIONS.* (Ph.D.), The University of Texas Southwestern Medical Center at Dallas, Dallas, TX.

de Laat, W., Klous, P., Kooren, J., Noordermeer, D., Palstra, R. J., Simonis, M., . . . Grosveld, F. (2008). Three-dimensional organization of gene expression in erythroid cells. *Curr Top Dev Biol, 82*, 117-139. doi: 10.1016/S0070-2153(07)00005-1

de Wit, E., & de Laat, W. (2012). A decade of 3C technologies: insights into nuclear organization. *Genes Dev, 26*(1), 11-24. doi: 10.1101/gad.179804.111

Dekker, J. (2006). The three 'C' s of chromosome conformation capture: controls, controls, controls. *Nat Methods, 3*(1), 17-21. doi: 10.1038/nmeth823

Dekker, J., Rippe, K., Dekker, M., & Kleckner, N. (2002). Capturing chromosome conformation. *Science, 295*(5558), 1306-1311. doi: 10.1126/science.1067799

DeLeo, A. B., Jay, G., Appella, E., Dubois, G. C., Law, L. W., & Old, L. J. (1979). Detection of a transformation-related antigen in chemically induced sarcomas and other transformed cells of the mouse. *Proc Natl Acad Sci U S A, 76*(5), 2420-2424.

Donehower, L. A., Harvey, M., Slagle, B. L., McArthur, M. J., Montgomery, C. A., Jr., Butel, J. S., & Bradley, A. (1992). Mice deficient for p53 are developmentally normal but susceptible to spontaneous tumours. *Nature, 356*(6366), 215-221. doi: 10.1038/356215a0

Dong, X., Huang, Y., Kong, L., Li, J., Kou, J., Yin, L., & Yang, J. (2015). C35 is overexpressed in colorectal cancer and is associated tumor invasion and metastasis. *Biosci Trends, 9*(2), 117-121. doi: 10.5582/bst.2015.01057

Eden, E., Navon, R., Steinfeld, I., Lipson, D., & Yakhini, Z. (2009). GOrilla: a tool for discovery and visualization of enriched GO terms in ranked gene lists. *BMC Bioinformatics, 10*, 48. doi: 10.1186/1471-2105-10-48

el-Deiry, W. S., Kern, S. E., Pietenpol, J. A., Kinzler, K. W., & Vogelstein, B. (1992). Definition of a consensus binding site for p53. *Nat Genet, 1*(1), 45-49. doi: 10.1038/ng0492-45

Eliyahu, D., Raz, A., Gruss, P., Givol, D., & Oren, M. (1984). Participation of p53 cellular tumour antigen in transformation of normal embryonic cells. *Nature, 312*(5995), 646-649.

Fei, P., Bernhard, E. J., & El-Deiry, W. S. (2002). Tissue-specific induction of p53 targets in vivo. *Cancer Res, 62*(24), 7316-7327.

Ferrai, C., Xie, S. Q., Luraghi, P., Munari, D., Ramirez, F., Branco, M. R., . . . Crippa, M. P. (2010). Poised transcription factories prime silent uPA gene prior to activation. *PLoS Biol, 8*(1), e1000270. doi: 10.1371/journal.pbio.1000270

Filippou, P. S., Karagiannis, G. S., Musrap, N., & Diamandis, E. P. (2016). Kallikrein-related peptidases (KLKs) and the hallmarks of cancer. *Critical Reviews in Clinical Laboratory Sciences, 53*(4), 277-291. doi: 10.3109/10408363.2016.1154643

Finlay, C. A., Hinds, P. W., & Levine, A. J. (1989). The p53 proto-oncogene can act as a suppressor of transformation. *Cell, 57*(7), 1083-1093.

Funk, W. D., Pak, D. T., Karas, R. H., Wright, W. E., & Shay, J. W. (1992). A transcriptionally active DNA-binding site for human p53 protein complexes. *Mol Cell Biol, 12*(6), 2866-2871.

Galikova, M., Diesner, M., Klepsatel, P., Hehlert, P., Xu, Y., Bickmeyer, I., . . . Kuhnlein, R. P. (2015). Energy Homeostasis Control in Drosophila Adipokinetic Hormone Mutants. *Genetics, 201*(2), 665-683. doi: 10.1534/genetics.115.178897

Ganesan, S., Aggarwal, K., Paquette, N., & Silverman, N. (2011). NF-κB/Rel Proteins and the Humoral Immune Responses of Drosophila melanogaster. *Curr Top Microbiol Immunol, 349*, 25-60.

Gao, F., Wei, Z., Lu, W., & Wang, K. (2013). Comparative analysis of 4C-Seq data generated from enzyme-based and sonication-based methods. *BMC Genomics, 14*, 345. doi: 10.1186/1471-2164-14-345

Ghildiyal, M., Seitz, H., Horwich, M. D., Li, C., Du, T., Lee, S., . . . Zamore, P. D. (2008). Endogenous siRNAs derived from transposons and mRNAs in Drosophila somatic cells. *Science, 320*(5879), 1077-1081. doi: 10.1126/science.1157396

Goldstein, I., & Rotter, V. (2012). Regulation of lipid metabolism by p53 - fighting two villains with one sword. *Trends Endocrinol Metab, 23*(11), 567-575. doi: 10.1016/j.tem.2012.06.007

Gomes, N. P., & Espinosa, J. M. (2010). Disparate chromatin landscapes and kinetics of inactivation impact differential regulation of p53 target genes. *Cell Cycle, 9*(17), 3428-3437. doi: 10.4161/cc.9.17.12998

Gondor, A., Rougier, C., & Ohlsson, R. (2008). High-resolution circular chromosome conformation capture assay. *Nat Protoc, 3*(2), 303-313. doi: 10.1038/nprot.2007.540

Gramates, L. S., Marygold, S. J., Santos, G. D., Urbano, J. M., Antonazzo, G., Matthews, B. B., . . . the FlyBase, C. (2017). FlyBase at 25: looking to the future. *Nucleic Acids Res, 45*(D1), D663-D671. doi: 10.1093/nar/gkw1016

Gu, B., & Zhu, W. G. (2012). Surf the post-translational modification network of p53 regulation. *Int J Biol Sci, 8*(5), 672-684. doi: 10.7150/ijbs.4283

Hainaut, P., & Hollstein, M. (2000). p53 and human cancer: the first ten thousand mutations. *Adv Cancer Res, 77*, 81-137.

Heinz, S., Benner, C., Spann, N., Bertolino, E., Lin, Y. C., Laslo, P., . . . Glass, C. K. (2010). Simple combinations of lineage-determining transcription factors prime cis-regulatory elements required for macrophage and B cell identities. *Mol Cell, 38*(4), 576-589. doi: 10.1016/j.molcel.2010.05.004

Hermeking, H. (2012). MicroRNAs in the p53 network: micromanagement of tumour suppression. *Nat Rev Cancer, 12*(9), 613-626. doi: 10.1038/nrc3318

Hinds, P., Finlay, C., & Levine, A. J. (1989). Mutation is required to activate the p53 gene for cooperation with the ras oncogene and transformation. *J Virol, 63*(2), 739-746.

Hultmark, D. (2003). Drosophila immunity: paths and patterns. *Curr Opin Immunol, 15*(1), 12-19.

Idogawa, M., Ohashi, T., Sasaki, Y., Maruyama, R., Kashima, L., Suzuki, H., & Tokino, T. (2014). Identification and analysis of large intergenic non-coding RNAs regulated by p53 family members through a genome-wide analysis of p53-binding sites. *Hum Mol Genet, 23*(11), 2847-2857. doi: 10.1093/hmg/ddt673

Jacks, T., Remington, L., Williams, B. O., Schmitt, E. M., Halachmi, S., Bronson, R. T., & Weinberg, R. A. (1994). Tumor spectrum analysis in p53-mutant mice. *Curr Biol, 4*(1), 1-7.

Janky, R., Verfaillie, A., Imrichova, H., Van de Sande, B., Standaert, L., Christiaens, V., . . . Aerts, S. (2014). iRegulon: from a gene list to a gene regulatory network using large motif and track collections. *PLoS Comput Biol, 10*(7), e1003731. doi: 10.1371/journal.pcbi.1003731

Jay, G., DeLeo, A. B., Appella, E., Dubois, G. C., Law, L. W., Khoury, G., & Old, L. J. (1980). A common transformation-related protein in murine sarcomas and leukemias. *Cold Spring Harb Symp Quant Biol, 44 Pt 1*, 659-664.

Jen, K. Y., & Cheung, V. G. (2005). Identification of novel p53 target genes in ionizing radiation response. *Cancer Res, 65*(17), 7666-7673. doi: 10.1158/0008-5472.can-05-1039

Jenkins, J. R., Rudge, K., & Currie, G. A. (1984). Cellular immortalization by a cDNA clone encoding the transformation-associated phosphoprotein p53. *Nature, 312*(5995), 651-654.

Joerger, A. C., & Fersht, A. R. (2010). The tumor suppressor p53: from structures to drug discovery. *Cold Spring Harb Perspect Biol, 2*(6), a000919. doi: 10.1101/cshperspect.a000919

Jones, B. C., Wood, J. G., Chang, C., Tam, A. D., Franklin, M. J., Siegel, E. R., & Helfand, S. L. (2016). A somatic piRNA pathway in the Drosophila fat body ensures metabolic homeostasis and normal lifespan. *Nat Commun, 7*, 13856. doi: 10.1038/ncomms13856

Katz, E., Dubois-Marshall, S., Sims, A. H., Faratian, D., Li, J., Smith, E. S., . . . Harrison, D. J. (2010). A gene on the HER2 amplicon, C35, is an oncogene in breast cancer whose actions are prevented by inhibition of Syk. *Br J Cancer, 103*(3), 401-410. doi: http://www.nature.com/bjc/journal/v103/n3/suppinfo/6605763s1.html

Kenzelmann Broz, D., & Attardi, L. D. (2010). In vivo analysis of p53 tumor suppressor function using genetically engineered mouse models. *Carcinogenesis, 31*(8), 1311-1318. doi: 10.1093/carcin/bgp331

Kenzelmann Broz, D., Spano Mello, S., Bieging, K. T., Jiang, D., Dusek, R. L., Brady, C. A., . . . Attardi, L. D. (2013). Global genomic profiling reveals an extensive p53-regulated autophagy program contributing to key p53 responses. *Genes Dev, 27*(9), 1016-1031. doi: 10.1101/gad.212282.112

Khoury, M. P., & Bourdon, J. C. (2010). The isoforms of the p53 protein. *Cold Spring Harb Perspect Biol, 2*(3), a000927. doi: 10.1101/cshperspect.a000927

Kim, D., Pertea, G., Trapnell, C., Pimentel, H., Kelley, R., & Salzberg, S. L. (2013). TopHat2: accurate alignment of transcriptomes in the presence of insertions, deletions and gene fusions. *Genome Biol, 14*(4), R36. doi: 10.1186/gb-2013-14-4-r36

Kirschner, K., Samarajiwa, S. A., Cairns, J. M., Menon, S., Perez-Mancera, P. A., Tomimatsu, K., . . . Narita, M. (2015). Phenotype specific analyses reveal distinct regulatory mechanism for chronically activated p53. *PLoS Genet, 11*(3), e1005053. doi: 10.1371/journal.pgen.1005053

Knights, C. D., Catania, J., Di Giovanni, S., Muratoglu, S., Perez, R., Swartzbeck, A., . . . Avantaggiati, M. L. (2006). Distinct p53 acetylation cassettes differentially influence gene-expression patterns and cell fate. *J Cell Biol, 173*(4), 533-544. doi: 10.1083/jcb.200512059

Kress, M., May, E., Cassingena, R., & May, P. (1979). Simian virus 40-transformed cells express new species of proteins precipitable by anti-simian virus 40 tumor serum. *J Virol, 31*(2), 472-483.

Kryza, T., Silva, M. L., Loessner, D., Heuzé-Vourc'h, N., & Clements, J. A. (2016). The kallikrein-related peptidase family: Dysregulation and functions during cancer progression. *Biochimie, 122*, 283-299. doi: http://dx.doi.org/10.1016/j.biochi.2015.09.002

Lakin, N. D., & Jackson, S. P. (1999). Regulation of p53 in response to DNA damage. *Oncogene, 18*(53), 7644-7655. doi: 10.1038/sj.onc.1203015

Lane, D. P., & Crawford, L. V. (1979). T antigen is bound to a host protein in SV40-transformed cells. *Nature, 278*(5701), 261-263.

Langmead, B., & Salzberg, S. L. (2012). Fast gapped-read alignment with Bowtie 2. *Nat Meth, 9*(4), 357-359. doi: 10.1038/nmeth.1923

http://www.nature.com/nmeth/journal/v9/n4/abs/nmeth.1923.html#supplementary-information
Lee, J. H., Lee, E., Park, J., Kim, E., Kim, J., & Chung, J. (2003). In vivo p53 function is indispensable for DNA damage-induced apoptotic signaling in Drosophila. *FEBS Letters, 550*(1), 5-10. doi: http://dx.doi.org/10.1016/S0014-5793(03)00771-3
Lee, K. H., Li, M., Michalowski, A. M., Zhang, X., Liao, H., Chen, L., . . . Huang, J. (2010). A genomewide study identifies the Wnt signaling pathway as a major target of p53 in murine embryonic stem cells. *Proc Natl Acad Sci U S A, 107*(1), 69-74. doi: 10.1073/pnas.0909734107
Leonova, K. I., Brodsky, L., Lipchick, B., Pal, M., Novototskaya, L., Chenchik, A. A., . . . Gudkov, A. V. (2013). p53 cooperates with DNA methylation and a suicidal interferon response to maintain epigenetic silencing of repeats and noncoding RNAs. *Proc Natl Acad Sci U S A, 110*(1), E89-98. doi: 10.1073/pnas.1216922110
Li, F. P., Fraumeni, J. F., Jr., Mulvihill, J. J., Blattner, W. A., Dreyfus, M. G., Tucker, M. A., & Miller, R. W. (1988). A cancer family syndrome in twenty-four kindreds. *Cancer Res, 48*(18), 5358-5362.
Li, H., Handsaker, B., Wysoker, A., Fennell, T., Ruan, J., Homer, N., . . . Durbin, R. (2009). The Sequence Alignment/Map format and SAMtools. *Bioinformatics, 25*(16), 2078-2079. doi: 10.1093/bioinformatics/btp352
Li, M., He, Y., Dubois, W., Wu, X., Shi, J., & Huang, J. (2012). Distinct regulatory mechanisms and functions for p53-activated and p53-repressed DNA damage response genes in embryonic stem cells. *Mol Cell, 46*(1), 30-42. doi: 10.1016/j.molcel.2012.01.020
Li, T., Kon, N., Jiang, L., Tan, M., Ludwig, T., Zhao, Y., . . . Gu, W. (2012). Tumor suppression in the absence of p53-mediated cell-cycle arrest, apoptosis, and senescence. *Cell, 149*(6), 1269-1283. doi: 10.1016/j.cell.2012.04.026
Li, Y., Liu, J., McLaughlin, N., Bachvarov, D., Saifudeen, Z., & El-Dahr, S. S. (2013). Genome-wide analysis of the p53 gene regulatory network in the developing mouse kidney. *Physiol Genomics, 45*(20), 948-964. doi: 10.1152/physiolgenomics.00113.2013
Liang, K., & Keleş, S. (2012). Normalization of ChIP-seq data with control. *BMC Bioinformatics, 13*(1), 199. doi: 10.1186/1471-2105-13-199
Lidor Nili, E., Field, Y., Lubling, Y., Widom, J., Oren, M., & Segal, E. (2010). p53 binds preferentially to genomic regions with high DNA-encoded nucleosome occupancy. *Genome Res, 20*(10), 1361-1368. doi: 10.1101/gr.103945.109
Lill, N. L., Grossman, S. R., Ginsberg, D., DeCaprio, J., & Livingston, D. M. (1997). Binding and modulation of p53 by p300/CBP coactivators. *Nature, 387*(6635), 823-827. doi: 10.1038/42981
Link, N. (2011). *Communal cell death and p53 mediated transcriptional control in Drosophila melanogaster*. (PhD PhD), University of Texas Southwestern Medical Center, Dallas, TX.
Link, N., Kurtz, P., O'Neal, M., Garcia-Hughes, G., & Abrams, J. M. (2013). A p53 enhancer region regulates target genes through chromatin conformations in cis and in trans. *Genes Dev, 27*(22), 2433-2438. doi: 10.1101/gad.225565.113
Linzer, D. I., & Levine, A. J. (1979). Characterization of a 54K dalton cellular SV40 tumor antigen present in SV40-transformed cells and uninfected embryonal carcinoma cells. *Cell, 17*(1), 43-52.

Liu, Z., & Kraus, W. L. (2017). Catalytic-Independent Functions of PARP-1 Determine Sox2 Pioneer Activity at Intractable Genomic Loci. *Mol Cell, 65*(4), 589-603 e589. doi: 10.1016/j.molcel.2017.01.017

Lu, W. J. (2010). *ILLUMINATING THE P53 REGULATORY NETWORK IN GENETIC MODELS.* (Ph.D.), The University of Texas Southwestern Medical Center at Dallas, Dallas, TX.

Lu, W. J., Amatruda, J. F., & Abrams, J. M. (2009). p53 ancestry: gazing through an evolutionary lens. *Nat Rev Cancer, 9*(10), 758-762. doi: 10.1038/nrc2732

Lu, W. J., Chapo, J., Roig, I., & Abrams, J. M. (2010). Meiotic recombination provokes functional activation of the p53 regulatory network. *Science, 328*(5983), 1278-1281. doi: 10.1126/science.1185640

Lunardi, A., Di Minin, G., Provero, P., Dal Ferro, M., Carotti, M., Del Sal, G., & Collavin, L. (2010). A genome-scale protein interaction profile of Drosophila p53 uncovers additional nodes of the human p53 network. *Proc Natl Acad Sci U S A, 107*(14), 6322-6327. doi: 10.1073/pnas.1002447107

Martin, M. (2011). Cutadapt removes adapter sequences from high-throughput sequencing reads. *2011, 17*(1). doi: 10.14806/ej.17.1.200

pp. 10-12

Masuda, H., Miller, C., Koeffler, H. P., Battifora, H., & Cline, M. J. (1987). Rearrangement of the p53 gene in human osteogenic sarcomas. *Proc Natl Acad Sci U S A, 84*(21), 7716-7719.

Matsui, T., Katsuno, Y., Inoue, T., Fujita, F., Joh, T., Niida, H., . . . Nakanishi, M. (2004). Negative regulation of Chk2 expression by p53 is dependent on the CCAAT-binding transcription factor NF-Y. *J Biol Chem, 279*(24), 25093-25100. doi: 10.1074/jbc.M403232200

McDade, S. S., Patel, D., Moran, M., Campbell, J., Fenwick, K., Kozarewa, I., . . . McCance, D. J. (2014). Genome-wide characterization reveals complex interplay between TP53 and TP63 in response to genotoxic stress. *Nucleic Acids Res, 42*(10), 6270-6285. doi: 10.1093/nar/gku299

Melero, J. A., Stitt, D. T., Mangel, W. F., & Carroll, R. B. (1979). Identification of new polypeptide species (48-55K) immunoprecipitable by antiserum to purified large T antigen and present in SV40-infected and -transformed cells. *Virology, 93*(2), 466-480.

Mellert, H., & Espinosa, J. M. (2013). Tumor suppression by p53: is apoptosis important or not? *Cell Rep, 3*(5), 1335-1336. doi: 10.1016/j.celrep.2013.05.011

Melo, C. A., Drost, J., Wijchers, P. J., van de Werken, H., de Wit, E., Oude Vrielink, J. A., . . . Agami, R. (2013). eRNAs are required for p53-dependent enhancer activity and gene transcription. *Mol Cell, 49*(3), 524-535. doi: 10.1016/j.molcel.2012.11.021

Menendez, D., Nguyen, T. A., Freudenberg, J. M., Mathew, V. J., Anderson, C. W., Jothi, R., & Resnick, M. A. (2013). Diverse stresses dramatically alter genome-wide p53 binding and transactivation landscape in human cancer cells. *Nucleic Acids Res, 41*(15), 7286-7301. doi: 10.1093/nar/gkt504

Merlo, P., Frost, B., Peng, S., Yang, Y. J., Park, P. J., & Feany, M. (2014). p53 prevents neurodegeneration by regulating synaptic genes. *Proc Natl Acad Sci U S A, 111*(50), 18055-18060. doi: 10.1073/pnas.1419083111

Millau, J. F., Mai, S., Bastien, N., & Drouin, R. (2010). p53 functions and cell lines: have we learned the lessons from the past? *Bioessays, 32*(5), 392-400. doi: 10.1002/bies.200900160

Momand, J., Zambetti, G. P., Olson, D. C., George, D., & Levine, A. J. (1992). The mdm-2 oncogene product forms a complex with the p53 protein and inhibits p53-mediated transactivation. *Cell, 69*(7), 1237-1245.

Mowat, M., Cheng, A., Kimura, N., Bernstein, A., & Benchimol, S. (1985). Rearrangements of the cellular p53 gene in erythroleukaemic cells transformed by Friend virus. *Nature, 314*(6012), 633-636.

Mu, X., Ahmad, S., & Hur, S. (2016). Endogenous Retroelements and the Host Innate Immune Sensors. *Adv Immunol, 132*, 47-69. doi: 10.1016/bs.ai.2016.07.001

Nagarkar-Jaiswal, S., Lee, P. T., Campbell, M. E., Chen, K., Anguiano-Zarate, S., Gutierrez, M. C., . . . Bellen, H. J. (2015). A library of MiMICs allows tagging of genes and reversible, spatial and temporal knockdown of proteins in Drosophila. *Elife, 4*. doi: 10.7554/eLife.05338

Negre, N., Hennetin, J., Sun, L. V., Lavrov, S., Bellis, M., White, K. P., & Cavalli, G. (2006). Chromosomal distribution of PcG proteins during Drosophila development. *PLoS Biol, 4*(6), e170. doi: 10.1371/journal.pbio.0040170

Nigro, J. M., Baker, S. J., Preisinger, A. C., Jessup, J. M., Hostetter, R., Cleary, K., . . . et al. (1989). Mutations in the p53 gene occur in diverse human tumour types. *Nature, 342*(6250), 705-708. doi: 10.1038/342705a0

Nikulenkov, F., Spinnler, C., Li, H., Tonelli, C., Shi, Y., Turunen, M., . . . Selivanova, G. (2012). Insights into p53 transcriptional function via genome-wide chromatin occupancy and gene expression analysis. *Cell Death Differ, 19*(12), 1992-2002. doi: 10.1038/cdd.2012.89

Niu, Y., Yeh, S., Miyamoto, H., Li, G., Altuwaijri, S., Yuan, J., . . . Chang, C. (2008). Tissue prostate specific antigen (PSA) facilitates refractory prostate tumor progression via enhancing ARA70-regulated androgen receptor transactivation. *Cancer Res, 68*(17), 7110-7119.

Oda, K., Arakawa, H., Tanaka, T., Matsuda, K., Tanikawa, C., Mori, T., . . . Taya, Y. (2000). p53AIP1, a potential mediator of p53-dependent apoptosis, and its regulation by Ser-46-phosphorylated p53. *Cell, 102*(6), 849-862.

Oliner, J. D., Pietenpol, J. A., Thiagalingam, S., Gyuris, J., Kinzler, K. W., & Vogelstein, B. (1993). Oncoprotein MDM2 conceals the activation domain of tumour suppressor p53. *Nature, 362*(6423), 857-860.

Olivier, M., Goldgar, D. E., Sodha, N., Ohgaki, H., Kleihues, P., Hainaut, P., & Eeles, R. A. (2003). Li-Fraumeni and related syndromes: correlation between tumor type, family structure, and TP53 genotype. *Cancer Res, 63*(20), 6643-6650.

Olsson, A., Manzl, C., Strasser, A., & Villunger, A. (2007). How important are post-translational modifications in p53 for selectivity in target-gene transcription and tumour suppression? *Cell Death Differ, 14*(9), 1561-1575. doi: 10.1038/sj.cdd.4402196

Parada, L. F., Land, H., Weinberg, R. A., Wolf, D., & Rotter, V. (1984). Cooperation between gene encoding p53 tumour antigen and ras in cellular transformation. *Nature, 312*(5995), 649-651.

Pennica, D., Goeddel, D. V., Hayflick, J. S., Reich, N. C., Anderson, C. W., & Levine, A. J. (1984). The amino acid sequence of murine p53 determined from a c-DNA clone. *Virology, 134*(2), 477-482. doi: http://dx.doi.org/10.1016/0042-6822(84)90316-7

Perrat, P. N., DasGupta, S., Wang, J., Theurkauf, W., Weng, Z., Rosbash, M., & Waddell, S. (2013). Transposition-driven genomic heterogeneity in the Drosophila brain. *Science, 340*(6128), 91-95. doi: 10.1126/science.1231965

Picard. (2017). Picard ToolKit. from http://broadinstitute.github.io/picard

Prokesch, A., Graef, F. A., Madl, T., Kahlhofer, J., Heidenreich, S., Schumann, A., . . . Schupp, M. (2017). Liver p53 is stabilized upon starvation and required for amino acid catabolism and gluconeogenesis. *FASEB J, 31*(2), 732-742. doi: 10.1096/fj.201600845R

Quail, M. A., Kozarewa, I., Smith, F., Scally, A., Stephens, P. J., Durbin, R., . . . Turner, D. J. (2008). A large genome center's improvements to the Illumina sequencing system. *Nat Methods, 5*(12), 1005-1010. doi: 10.1038/nmeth.1270

Quinlan, A. R., & Hall, I. M. (2010). BEDTools: a flexible suite of utilities for comparing genomic features. *Bioinformatics, 26*(6), 841-842.

R Core Team. (2017). R: A Language and Environment for Statistical Computing. Vienna, Austria: R Foundation for Statistical Computing. Retrieved from https://www.R-project.org

Rajendiran, S., Kpetemey, M., Maji, S., Gibbs, L. D., Dasgupta, S., Mantsch, R., . . . Vishwanatha, J. K. (2015). MIEN1 promotes oral cancer progression and implicates poor overall survival. *Cancer Biol Ther, 16*(6), 876-885. doi: 10.1080/15384047.2015.1040962

Rashi-Elkeles, S., Warnatz, H. J., Elkon, R., Kupershtein, A., Chobod, Y., Paz, A., . . . Shiloh, Y. (2014). Parallel profiling of the transcriptome, cistrome, and epigenome in the cellular response to ionizing radiation. *Sci Signal, 7*(325), rs3. doi: 10.1126/scisignal.2005032

Rotter, V. (1983). p53, a transformation-related cellular-encoded protein, can be used as a biochemical marker for the detection of primary mouse tumor cells. *Proc Natl Acad Sci U S A, 80*(9), 2613-2617.

Rotter, V., Witte, O. N., Coffman, R., & Baltimore, D. (1980). Abelson murine leukemia virus-induced tumors elicit antibodies against a host cell protein, P50. *J Virol, 36*(2), 547-555.

Rowan, S., Ludwig, R. L., Haupt, Y., Bates, S., Lu, X., Oren, M., & Vousden, K. H. (1996). Specific loss of apoptotic but not cell-cycle arrest function in a human tumor derived p53 mutant. *EMBO J, 15*(4), 827-838.

Sammons, M. A., Zhu, J., Drake, A. M., & Berger, S. L. (2015). TP53 engagement with the genome occurs in distinct local chromatin environments via pioneer factor activity. *Genome Res, 25*(2), 179-188. doi: 10.1101/gr.181883.114

Sanchez, Y., Segura, V., Marin-Bejar, O., Athie, A., Marchese, F. P., Gonzalez, J., . . . Huarte, M. (2014). Genome-wide analysis of the human p53 transcriptional network unveils a lncRNA tumour suppressor signature. *Nat Commun, 5*, 5812. doi: 10.1038/ncomms6812

Schlereth, K., Heyl, C., Krampitz, A. M., Mernberger, M., Finkernagel, F., Scharfe, M., . . . Stiewe, T. (2013). Characterization of the p53 cistrome--DNA binding cooperativity dissects p53's tumor suppressor functions. *PLoS Genet, 9*(8), e1003726. doi: 10.1371/journal.pgen.1003726

Schmieder, R., & Edwards, R. (2011). Quality control and preprocessing of metagenomic datasets. *Bioinformatics, 27*(6), 863-864. doi: 10.1093/bioinformatics/btr026

Shaked, H., Shiff, I., Kott-Gutkowski, M., Siegfried, Z., Haupt, Y., & Simon, I. (2008). Chromatin immunoprecipitation-on-chip reveals stress-dependent p53 occupancy in primary normal cells but not in established cell lines. *Cancer Res, 68*(23), 9671-9677. doi: 10.1158/0008-5472.can-08-0865

Shieh, S.-Y., Ikeda, M., Taya, Y., & Prives, C. (1997). DNA Damage-Induced Phosphorylation of p53 Alleviates Inhibition by MDM2. *Cell, 91*(3), 325-334. doi: http://dx.doi.org/10.1016/S0092-8674(00)80416-X

Shpiz, S., Kwon, D., Uneva, A., Kim, M., Klenov, M., Rozovsky, Y., . . . Kalmykova, A. (2007). Characterization of Drosophila telomeric retroelement TAHRE: transcription, transpositions, and RNAi-based regulation of expression. *Mol Biol Evol, 24*(11), 2535-2545. doi: 10.1093/molbev/msm205

Smeenk, L., van Heeringen, S. J., Koeppel, M., Gilbert, B., Janssen-Megens, E., Stunnenberg, H. G., & Lohrum, M. (2011). Role of p53 serine 46 in p53 target gene regulation. *PLoS One, 6*(3), e17574. doi: 10.1371/journal.pone.0017574

Smeenk, L., van Heeringen, S. J., Koeppel, M., van Driel, M. A., Bartels, S. J., Akkers, R. C., . . . Lohrum, M. (2008). Characterization of genome-wide p53-binding sites upon stress response. *Nucleic Acids Res, 36*(11), 3639-3654. doi: 10.1093/nar/gkn232

Sogame, N., Kim, M., & Abrams, J. M. (2003). Drosophila p53 preserves genomic stability by regulating cell death. *Proc Natl Acad Sci U S A, 100*(8), 4696-4701. doi: 10.1073/pnas.0736384100

Su, D., Wang, X., Campbell, M. R., Song, L., Safi, A., Crawford, G. E., & Bell, D. A. (2015). Interactions of chromatin context, binding site sequence content, and sequence evolution in stress-induced p53 occupancy and transactivation. *PLoS Genet, 11*(1), e1004885. doi: 10.1371/journal.pgen.1004885

Sullivan, W., Ashburner, M., Hawley, R.S. (2000). *Drosophila Protocols*. Cold Sring Harbor, New York: Cold Spring Harbor Laboratory Press.

Sutcliffe, J. E., & Brehm, A. (2004). Of flies and men; p53, a tumour suppressor. *FEBS Lett, 567*(1), 86-91. doi: 10.1016/j.febslet.2004.03.122

Tedeschi, A., & Di Giovanni, S. (2009). The non-apoptotic role of p53 in neuronal biology: enlightening the dark side of the moon. *EMBO Rep, 10*(6), 576-583. doi: 10.1038/embor.2009.89

Teufel, D. P., Freund, S. M., Bycroft, M., & Fersht, A. R. (2007). Four domains of p300 each bind tightly to a sequence spanning both transactivation subdomains of p53. *Proc Natl Acad Sci U S A, 104*(17), 7009-7014. doi: 10.1073/pnas.0702010104

Thut, C. J., Chen, J. L., Klemm, R., & Tjian, R. (1995). p53 transcriptional activation mediated by coactivators TAFII40 and TAFII60. *Science, 267*(5194), 100-104.

Tominaga, K., Morisaki, H., Kaneko, Y., Fujimoto, A., Tanaka, T., Ohtsubo, M., . . . Nakanishi, M. (1999). Role of human Cds1 (Chk2) kinase in DNA damage checkpoint and its regulation by p53. *J Biol Chem, 274*(44), 31463-31467.

Tonelli, C., Morelli, M. J., Bianchi, S., Rotta, L., Capra, T., Sabo, A., . . . Amati, B. (2015). Genome-wide analysis of p53 transcriptional programs in B cells upon exposure to genotoxic stress in vivo. *Oncotarget, 6*(28), 24611-24626. doi: 10.18632/oncotarget.5232

Trapnell, C., Williams, B. A., Pertea, G., Mortazavi, A., Kwan, G., van Baren, M. J., . . . Pachter, L. (2010). Transcript assembly and quantification by RNA-Seq reveals unannotated transcripts and isoform switching during cell differentiation. *Nat Biotechnol, 28*(5), 511-515. doi: 10.1038/nbt.1621

Valanne, S., Kallio, J., Kleino, A., & Rämet, M. (2012). Large-scale RNAi screens add both clarity and complexity to Drosophila NF-κB signaling. *Developmental & Comparative Immunology, 37*(1), 9-18. doi: http://dx.doi.org/10.1016/j.dci.2011.09.001

Valente, L. J., Gray, D. H., Michalak, E. M., Pinon-Hofbauer, J., Egle, A., Scott, C. L., . . . Strasser, A. (2013). p53 efficiently suppresses tumor development in the complete absence of its cell-cycle inhibitory and proapoptotic effectors p21, Puma, and Noxa. *Cell Rep, 3*(5), 1339-1345. doi: 10.1016/j.celrep.2013.04.012

van de Werken, H. J., Landan, G., Holwerda, S. J., Hoichman, M., Klous, P., Chachik, R., . . . de Laat, W. (2012). Robust 4C-seq data analysis to screen for regulatory DNA interactions. *Nat Methods, 9*(10), 969-972. doi: 10.1038/nmeth.2173

Venken, K. J., Schulze, K. L., Haelterman, N. A., Pan, H., He, Y., Evans-Holm, M., . . . Bellen, H. J. (2011). MiMIC: a highly versatile transposon insertion resource for engineering Drosophila melanogaster genes. *Nat Methods, 8*(9), 737-743.

Volkman, H. E., & Stetson, D. B. (2014). The enemy within: endogenous retroelements and autoimmune disease. *Nat Immunol, 15*(5), 415-422. doi: 10.1038/ni.2872

Vousden, K. H., & Prives, C. (2009). Blinded by the Light: The Growing Complexity of p53. *Cell, 137*(3), 413-431. doi: 10.1016/j.cell.2009.04.037

Wei, C. L., Wu, Q., Vega, V. B., Chiu, K. P., Ng, P., Zhang, T., . . . Ruan, Y. (2006). A global map of p53 transcription-factor binding sites in the human genome. *Cell, 124*(1), 207-219. doi: 10.1016/j.cell.2005.10.043

Weinberg, R. L., Veprintsev, D. B., & Fersht, A. R. (2004). Cooperative binding of tetrameric p53 to DNA. *J Mol Biol, 341*(5), 1145-1159. doi: 10.1016/j.jmb.2004.06.071

White, K., Grether, M. E., Abrams, J. M., Young, L., Farrell, K., & Steller, H. (1994). Genetic control of programmed cell death in Drosophila. *Science, 264*(5159), 677-683.

Williams, R. L., Jr., Starmer, J., Mugford, J. W., Calabrese, J. M., Mieczkowski, P., Yee, D., & Magnuson, T. (2014). fourSig: a method for determining chromosomal interactions in 4C-Seq data. *Nucleic Acids Res, 42*(8), e68. doi: 10.1093/nar/gku156

Wu, X., Bayle, J. H., Olson, D., & Levine, A. J. (1993). The p53-mdm-2 autoregulatory feedback loop. *Genes Dev, 7*(7A), 1126-1132.

Wylie, A., Jones, A. E., D'Brot, A., Lu, W. J., Kurtz, P., Moran, J. V., . . . Abrams, J. M. (2016). p53 genes function to restrain mobile elements. *Genes Dev, 30*(1), 64-77. doi: 10.1101/gad.266098.115

Wylie, A., Lu, W. J., D'Brot, A., Buszczak, M., & Abrams, J. M. (2014). p53 activity is selectively licensed in the Drosophila stem cell compartment. *Elife, 3*, e01530. doi: 10.7554/eLife.01530

Xie, H. B., & Golic, K. G. (2004). Gene deletions by ends-in targeting in Drosophila melanogaster. *Genetics, 168*(3), 1477-1489. doi: 10.1534/genetics.104.030882

Yan, C. T., Kaushal, D., Murphy, M., Zhang, Y., Datta, A., Chen, C., . . . Alt, F. W. (2006). XRCC4 suppresses medulloblastomas with recurrent translocations in p53-deficient mice. *Proc Natl Acad Sci U S A, 103*(19), 7378-7383. doi: 10.1073/pnas.0601938103

Younger, S. T., Kenzelmann-Broz, D., Jung, H., Attardi, L. D., & Rinn, J. L. (2015). Integrative genomic analysis reveals widespread enhancer regulation by p53 in response to DNA damage. *Nucleic Acids Res, 43*(9), 4447-4462. doi: 10.1093/nar/gkv284

Zeron-Medina, J., Wang, X., Repapi, E., Campbell, M. R., Su, D., Castro-Giner, F., . . . Bond, G. L. (2013). A polymorphic p53 response element in KIT ligand influences cancer risk and has undergone natural selection. *Cell, 155*(2), 410-422. doi: 10.1016/j.cell.2013.09.017

Zhang, B., Mehrotra, S., Ng, W. L., & Calvi, B. R. (2014). Low levels of p53 protein and chromatin silencing of p53 target genes repress apoptosis in Drosophila endocycling cells. *PLoS Genet, 10*(9), e1004581. doi: 10.1371/journal.pgen.1004581

Zhang, L., Beaucher, M., Cheng, Y., & Rong, Y. S. (2014). Coordination of transposon expression with DNA replication in the targeting of telomeric retrotransposons in Drosophila. *EMBO J, 33*(10), 1148-1158. doi: 10.1002/embj.201386940

Zhang, Y., Liu, T., Meyer, C. A., Eeckhoute, J., Johnson, D. S., Bernstein, B. E., . . . Liu, X. S. (2008). Model-based analysis of ChIP-Seq (MACS). *Genome Biol, 9*(9), R137. doi: 10.1186/gb-2008-9-9-r137

Zhao, R., Gish, K., Murphy, M., Yin, Y., Notterman, D., Hoffman, W. H., . . . Levine, A. J. (2000). Analysis of p53-regulated gene expression patterns using oligonucleotide arrays. *Genes Dev, 14*(8), 981-993.

Zhou, G. L., Xin, L., Song, W., Di, L. J., Liu, G., Wu, X. S., . . . Liang, C. C. (2006). Active chromatin hub of the mouse alpha-globin locus forms in a transcription factory of clustered housekeeping genes. *Mol Cell Biol, 26*(13), 5096-5105. doi: 10.1128/MCB.02454-05